Arabidopsis GLK transcription factors interact with ABI4 to modulate cotyledon greening in light-exposed etiolated seedlings

Inaugural-Dissertation

zur

Erlangung des Doktorgrades

der Mathematisch-Naturwissenschaftlichen

Fakultät

der Universität zu Köln

vorgelegt von

Pengxin Yu

angenommen im Jahr 2025

Table of Contents

List of Figures

List of Tables

Abbreviations

At	*Arabidopsis thaliana*
35Spro	35S promoter of the cauliflower mosaic virus
ANOVA	analysis of variance
bp	base pairs
cDNA	complementary DNA
CDS	coding sequence
DNA	deoxyribonucleic acid
RNA	ribonucleic acid
dNTP	deoxynucleoside triphosphate
EDTA	ethylenediaminetetraacetic acid
gDNA	genomic DNA
GFP	green fluorescent protein
YFP	yellow fluorescent protein
OD	optical density
ONPG	2-Nitrophenyl β-D-galactopyranoside
SD	synthetic dropout

Nomenclature

Nomenclature of genes and proteins

GLK1	Gene, locus, wild-type allele
glk1	Mutant allele
GLK1	Protein

Abstract

The sessile lifestyle of plants necessitates complex molecular signalling networks that tightly adjust growth, development and metabolism to the ambient environment. During seedling etiolation in darkness, the biosynthesis of protochlorophyllide (Pchlide) and the development of etioplasts must be strictly controlled to prevent photooxidative damage upon light exposure. In this process, the transcription factors GLK1 and GLK2 are central regulators of Pchlide biosynthesis and chloroplast biogenesis. Here, we show that GLK1 and GLK2 interact with ABSCISIC ACID INSENSITIVE 4 (ABI4). We reveal that GLKs and ABI4 have antagonistic functions in cotyledon greening of etiolated seedlings: *abi4* mutants, similar to a transgenic line overexpressing GLK2, accumulated more Pchlide than the wild type in dark-grown seedlings, while *glk1 glk2* mutants exhibited lower Pchlide levels than the wild type. These high Pchlide levels in etiolated *abi4* mutants and GLK2 overexpressors were inefficiently photoreduced upon light exposure, leading to a significant accumulation of $^1O_2$ in the cotyledons after the dark-to-light transition. This corresponded to low cotyledon greening rates and low seedling survival. Additionally, we identified eight *PhANG*s involved in Pchlide biosynthesis and etioplast development, whose transcript accumulation patterns may contribute to the photobleaching of etiolated *abi4* mutants and GLK2 overexpressors. Importantly, the high Pchlide content, low cotyledon greening rate, high $^1O_2$ level and high *PhANG* induction in *abi4* mutant seedlings were fully dependent on *GLK1* and *GLK2*, indicating that *ABI4* acts upstream of *GLKs.* We found that *GLK1* and *GLK2* transcript levels are not changed in etiolated *abi4* mutant seedlings; therefore, ABI4 likely inhibits the activities of the GLK1 and GLK2 proteins through direct protein-protein interactions. Although transactivation assays in tobacco did not show this inhibitory effect of ABI4, a similar assay in yeast demonstrated the possibility that ABI4 reduces the transactivational capacity of GLK1. Together, these data suggest that ABI4 inhibits GLK1 and GLK2 activities in etiolated seedlings to prevent high Pchlide accumulation, which would lead to high $^1O_2$ levels and seedling death upon exposure to light.

1 Introduction

1.1 Chlorophyll biosynthesis and chloroplast biogenesis in plants

Chloroplasts are best known as the photosynthesis compartments that produce 80% of biomass on earth (Bar-On et al., 2018), but they are also involved in nitrogen and sulfur assimilation (Cao et al., 2013; Zhao et al., 2021), biosynthesis of various compounds (Rolland et al., 2012), abiotic stress responses (Y. Song et al., 2021), immunity (Kachroo et al., 2021), and leaf senescence (Mayta et al., 2019). Both chlorophyll biosynthesis and chloroplast biogenesis are crucial steps in plant development, and these two processes are controlled by complex molecular regulatory networks through external and endogenous signals that have been described in recent reviews (Cackett et al., 2022; Y. Li et al., 2025).

Light is one of the most important environmental signals for plants. Already as seedlings, plants adjust their developmental programs in response to ambient light conditions. When seeds germinate under the soil, the seedlings grow in darkness in a process termed etiolation (or skotomorphogenesis), during which specialised chloroplast precursors, known as etioplasts, initiate their development (Figure 1a). Within the etioplasts, the enzyme protochlorophyllide oxidoreductase (POR) accumulates along with the chlorophyll precursor protochlorophyllide (Pchlide). Pchlide forms a ternary complex with PORs and nicotinamide adenine dinucleotide phosphate (NADPH) within a para-crystalline etioplast compartment called the prolamellar body (PLB). Pchlide in the model plant Arabidopsis can be divided into two categories: the photoactive Pchlide is bound within the ternary complex, whereas the non-photoactive Pchlide is not bound in the PLB (Klein & Schiff, 1972; Lebedev & Timko, 1999; Y. Li et al., 2025).

Etiolated seedlings grow upwards through the soil by sensing gravity (Kawamoto & Morita, 2022; K. Kim et al., 2011), and they are immediately exposed to light when they reach the soil surface. This is a critical moment that impacts seedling survival and health, during which the seedlings respond to light in a process termed de-etiolation or photomorphogenesis. Two key photomorphogenic traits are chlorophyll biosynthesis and chloroplast biogenesis (overall termed greening). Chlorophyll biosynthesis (Figure 1b) refers to the enzymatic processes where the PORs convert photoactive Pchlide into chlorophyllide (Chlide) in a reaction termed photoreduction,

and subsequently Chlide is converted into chlorophyll (Apel et al., 1980; Armstrong et al., 1995). Pchlide reduction in angiosperms is strictly light-dependent (J. Yang & Cheng, 2004), which means dark-grown seedlings of the model plant Arabidopsis are not green. This is different in other taxa, such as gymnosperms (Demko et al., 2009) and mosses (Yamamoto et al., 2011), where light-independent POR enzymes exist. In contrast to the rapid enzymatic reaction that produces chlorophyll, chloroplast biogenesis (Figure 1b) is represented by structural changes in the plastid, where etioplasts differentiate into chloroplasts by expanding the thylakoid surface area while integrating and arranging photosynthetic complexes into the thylakoids (Pipitone et al., 2021). Chlorophyll is synthesized in Arabidopsis cotyledons within the first four hours of illumination, while the assembly of a fully photosynthetic chloroplast takes more than ten hours during de-etiolation (Pipitone et al., 2021).

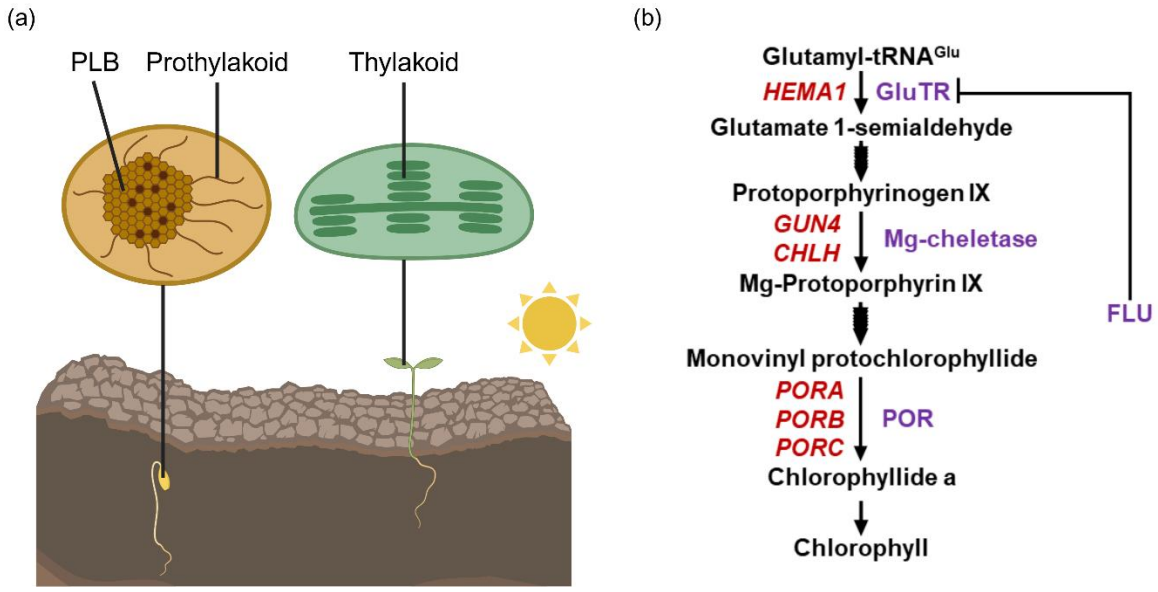

Figure 1. Chloroplast biogenesis and the chlorophyll biosynthetic pathway
(a) Exposure to light triggers the greening process, where etioplasts (left) differentiate into chloroplasts (right). PLB: prolamellar body. Figure was generated with BioRender. **(b)** A simplified scheme of the chlorophyll biosynthetic pathway. Only the genes (in brown) and the corresponding proteins (in purple) mentioned in the present thesis are shown. GluTR: GLUTAMYL-TRNA REDUCTASE; FLU: FLUORESCENT IN BLUE LIGHT; POR: PROTOCHLOROPHYLLIDE OXIDOREDUCTASE

1.2 The process of greening requires a balancing act

The maximization of photosynthetic rate requires fully developed chloroplasts with appropriately placed chlorophyll molecules to perform light harvesting and charge separation. Consequently, having a low chlorophyll content and less differentiated chloroplasts can both reduce photosynthetic performance and yield (Frangedakis et al., 2024; N. Kim et al., 2023). On the other hand, the non-photoactive Pchlide formed during etiolation can absorb light energy (termed photosensitization) and transfer this energy to atmospheric oxygen, generating potentially toxic reactive oxygen species (ROS). The detrimental effect of Pchlide photosensitization can be seen in the Arabidopsis *fluorescent in blue light* (*flu*) mutant. Seedlings of this mutant develop green cotyledons and show normal growth in continuous white light. However, when these seedlings first go through an etiolated growth phase in darkness, they show only white cotyledons and die quickly upon exposure to white light. This conditional-lethal phenotype is caused by excessive Pchlide accumulation and subsequent photobleaching upon the dark-to-light transition (Meskauskiene et al., 2001). Additionally, Liu et al. (2018) showed that a precocious etioplast-to-chloroplast differentiation in darkness also causes photobleaching in light-exposed etiolated seedlings. Hence, plastid activity needs to be appropriately repressed in darkness and activated in light to ensure plant health.

Plastid development and activity depend on the transcriptional states of both photosynthesis-associated nuclear genes (*PhANG*s) and plastid genes (*PhAPG*s). 95% of chloroplastic proteins are encoded by *PhANG*s, and the other 5% are encoded by *PhAPG*s (W. Martin et al., 2002). To achieve a balance between the expression of these genes, the nucleus can regulate *PhAPG*s via so-called anterograde signals, while the plastid can modulate *PhANG*s via retrograde signals (RS). Multiple classes of transcription factors (TFs) form a network to tightly regulate *PhANG*s and *PhAPG*s in Arabidopsis. In the dark, PHYTOCHROME-INTERACTING FACTORs (PIFs) act as a major class of *PhANG* repressors (Huq et al., 2004; Monte et al., 2004; Stephenson et al., 2009). PIF1, PIF3, PIF4 and PIF5 repress etioplast development and Pchlide biosynthesis in concert with ETHYLENE-INSENSITIVE3 (EIN3) and ETHYLENE-INSENSITIVE3-LIKE1 (EIL1) (Liu et al., 2018; Zhong et al., 2009). The same PIFs also repress the expression of genes encoding sigma factors (*SIG*s) that act as anterograde signals responsible for activating *PhAPG*s transcription (Hwang et

al., 2022). In the light, PIFs, EIN3 and EIL1 are degraded by the 26S proteasome (An et al., 2010; Bauer et al., 2004; J. H. Lee et al., 2006; Park et al., 2004), thereby de-repressing *PhANG* transcription and promoting *PhAPG* transcription. Concurrently, positive regulators including ELONGATED HYPOCOTYL5 (HY5), GATA NITRATE-INDUCIBLE CARBON-METABOLISM-INVOLVED (GNC), CYTOKININ-RESPONSIVE GATA1 (CGA1), MYB-related transcription factors (MYBS) and GOLDEN2-LIKE (GLK) promote greening by activating *PhANG* transcription either alone or cooperatively (Chiang et al., 2012; Fitter et al., 2002; Frangedakis et al., 2024; Oyama et al., 1997; T. Zhang et al., 2024). Besides the direct activation of *PhANG*s by TFs, positive plastid-to-nucleus RS have been reported to be critical for the full induction of *PhANG*s (Dubreuil et al., 2018; Loudya et al., 2021; Woodson et al., 2011).

1.3 GLK transcription factors as master regulators of greening

GOLDEN2-LIKE 1 and 2 (GLK1 & 2) are a pair of greening regulators that have led to significant field applications, where ectopic expression of maize GLKs improved yield in rice by 30-70% (X. Li et al., 2020; Yeh et al., 2022). The *GOLDEN2* (*ZmG2*) gene was first discovered in a maize mutant line with impaired chloroplast development in bundle sheath cells (Jenkins, 1926; Langdale & Kidner, 1994), and maize G2 was later characterised together with maize GLK1 as transcriptional activators (Hall et al., 1998). GLK1 & 2 belong to the GARP (Golden2, ARR-B, Psr1) family of plant-specific TFs (Safi et al., 2017). Their N-terminal domains are responsible for transcriptional activation (Rossini et al., 2001; Tamai et al., 2002). The transactivation domain is followed by a nuclear localization signal, a DNA-binding domain, and a GLK/C-terminal box (GCT box) mediating dimerization (Rossini et al., 2001; D. Zhang et al., 2021). Dimerization is necessary for GLKs to physically bind their target DNA (N. Kim et al., 2023; Rossini et al., 2001), and previous studies have revealed that GLKs possess diverse binding motifs (Tu et al., 2022; Waters et al., 2009; Zubo et al., 2018).

GLKs exist in most plants as a paralogous pair (Fitter et al., 2002; Powell et al., 2012; Rossini et al., 2001; Tu et al., 2022), and they mainly act in the nuclei of mesophyll cells (Waters et al., 2008), where they promote chloroplast biogenesis and development by activating the transcription of the *PhANG*s encoding

thylakoid-associated protein components and chlorophyll biosynthetic enzymes (Tu et al., 2022; Waters et al., 2009). Arabidopsis *glk1 glk2* double knockout mutants show lower chlorophyll content, reduced chloroplast thylakoid stacking and lower seed yield, while overexpression of either *At*GLK1 or *At*GLK2 leads to higher chlorophyll level, more thylakoid stacking and a larger chloroplast area (Fitter et al., 2002; Zubo et al., 2018). These GLKs are also linked to chloroplast functions through both anterograde and retrograde signalling. On the anterograde side, GLKs activate the transcription of the *CHLOROPLAST-RELATED LONG NONCODING RNA* (*CHLORELLA*). *CHLORELLA* transcripts translocate into the chloroplasts to aid the accumulation of the plastid-encoded RNA polymerase complex, thereby maintaining RNA transcription in the chloroplast (Kang et al., 2025). On the retrograde side, functional chloroplasts sustain *GLK* expression via RS, and the expression of *GLK* in leaf vasculature is sufficient to prevent precocious flowering by controlling downstream gene activation (Susila et al., 2023).

1.4 GLKs are regulated at both the transcript and protein levels

The transcription of *GLK1* and *GLK2* is regulated by both light quality and light quantity. In dark-grown Arabidopsis seedlings, PIFs repress at least *GLK1* expression (G. Martin et al., 2016). When these seedlings are exposed to low or moderate light, most wavelengths induce *GLK* transcription, although to different degrees between *GLK1* and *GLK2* (Oh & Montgomery, 2014). When the etiolated seedlings are exposed to high light (more than 310 $\mu mol\ m^{-2}\ s^{-1}$), *GLK1* transcription is still induced, albeit to a lower level than in moderate light intensity. This slight repression by high light has been attributed to plastid-to-nucleus RS (G. Martin et al., 2016). Beyond light, *GLK* expression is regulated by the circadian clock (Fitter et al., 2002; Y. Song et al., 2018), phytohormones (Kobayashi et al., 2012; M. Wang et al., 2018; X. Yu et al., 2011) and various abiotic stresses (Hernández-Verdeja & Lundgren, 2024; Y. Li et al., 2022).

Diverse mechanisms exist to regulate GLKs on the protein level. D. Zhang et al. (2021) reported BRASSINOSTEROID INSENSITIVE 2 (BIN2) to be a kinase of GLKs, and that phosphorylation integrates brassinosteroid (BA) and light signalling to modulate GLK protein stability, binding affinity to target promoters, and transcription-activating capacity. Besides, when chloroplast development is arrested, GLKs are first polyubiquitinated, then degraded by the proteasome (Tokumaru et al., 2017). Similarly,

GLKs are degraded in response to long-term abscisic acid (ABA) treatment (J. Lee et al., 2021). GLKs also physically interact with a plethora of other nuclear proteins, and these interactions serve diverse functions *in planta* (reports on *At*GLKs are summarised in Table 1).

The necessity of fine-tuning GLK activity was demonstrated by M. Li et al. (2022), in which two TFs were reported to physically and antagonistically interact with GLKs, ultimately modulating cell death in response to external stress. Although *GLK* transcript levels are low in darkness (Fitter et al., 2002), and GLK protein is degraded in darkness (D. Zhang et al., 2021), GLKs still play a physiological role in seedling etiolation. Specifically, Arabidopsis *glk1 glk2* mutant seedlings accumulate less Pchlide and contain smaller etioplasts with smaller PLBs than the wild type (Waters et al., 2009). A recent study has shown that repressing *GLK1* expression in darkness is crucial for the repression of *PhANG*s in etiolated seedlings (Quevedo et al., 2025). Therefore, limiting the GLK protein activity to a moderate level during etiolation is likely also vital for seedling health.

We previously hypothesized that there are other unknown nuclear proteins that modulate GLK activity via direct protein-protein interactions. We tested this by screening an Arabidopsis TF library (Paz-Ares et al., 2002) using Arabidopsis GLK1 or GLK2 as baits in yeast two-hybrid, and we identified ABSCISIC ACID INSENSITIVE 4 (ABI4) as one of the GLK-interacting proteins (Yu, 2022, Master's Thesis).

Table 1. *At*GLKs physically interact with other nuclear proteins

GLK protein	Interactor	Interaction detection method	Interaction function
GLK1&2	G-BOX BINDING FACTORs (GBF1, 2, 3)	Y2H, pull-down (Tamai et al., 2002) Split-LUC, BiFC (T. Sun et al., 2025)	Photomorphogenesis
GLK2	ORESARA 1 (ORE1)	Y2H, BiFC, pull-down, co-IP (Rauf et al., 2013)	Leaf senescence
GLK1&2	*Turnip Yellow Mosaic Virus* virulence protein P69 (P69)	Y2H, BiFC, co-IP (Ni et al., 2017)	Pathogenesis
GLK1&2	SIGMA FACTOR-BINDING PROTEIN 1 (SIB1)	BiFC, co-IP (Lv et al., 2019)	Cell death
GLK1&2	LESION-SIMULATING DISEASE 1 (LSD1)	Co-IP-mass spec, BiFC, co-IP (M. Li et al., 2022)	Antagonistic to SIB1, stress response
GLK1&2	BRASSINOSTEROID INSENSITIVE 2 (BIN2)	Y2H, BiFC, pull-down, co-IP (D. Zhang et al., 2021)	BA signalling, photomorphogenesis
GLK1	CONSTITUTIVE PHOTOMORPHOGENIC 1 (COP1)	BiFC, co-IP (J. Lee et al., 2021)	ABA signalling, photomorphogenesis, salt stress tolerance
GLK1	TEOSINTE BRANCHED 1, CYCLOIDEA, and PROLIFERATING CELL FACTORS 15 (TCP15)	Y2H, BiFC (Alem et al., 2022)	Cotyledon opening and expansion
GLK1	PHOSPHATE STARVATION RESPONSE 1 (PHR1)	Y2H, BiFC, pull-down, co-IP (Y. Li et al., 2022)	Phosphate starvation response
GLK1&2	REPRESSOR OF PHOTOSYNTHETIC GENES (RPGE1-4)	Y2H, BiFC, pull-down, co-IP (Han et al., 2024; N. Kim et al., 2023; Tachibana et al., 2024, 2025)	Skotomorphogenesis, photomorphogenesis, BA signalling
GLK1&2	ELONGATED HYPOCOTYL 5 (HY5)	pull-down, split-LUC, co-IP (T. Zhang et al., 2024)	Photomorphogenesis

1.5 ABI4 as an interaction partner of GLKs

ABI4 belongs to the AP2/EREBP family of TFs (Okamuro et al., 1997), and it is well-conserved in land plants (Gregorio et al., 2014). ABI4 can act either as an activator (Bossi et al., 2009; Reeves et al., 2011) or a repressor (Giraud et al., 2009; B. Yu et al., 2016) of gene expression in the nucleus. Arabidopsis loss-of-function *abi4* mutants were first identified based on their insensitivity to ABA during seed germination (R. R. Finkelstein, 1994; R. R. Finkelstein et al., 1998) and their impaired sugar signalling (Huijser et al., 2000; Van Oosten et al., 1997). Since then, ABI4 has been reported to control multiple aspects of plant development and physiology, including seed dormancy (Shu et al., 2013), seed lipid mobilization (Penfield et al., 2006), hypocotyl elongation (P. Song et al., 2024; Xu et al., 2016), root emergence (Bai et al., 2020), flowering time (Shu et al., 2016), salt tolerance (P. C. Li et al., 2016; Shkolnik-Inbar et al., 2013) and drought tolerance (Khan et al., 2020).

Amongst the various functions of ABI4, the proposed role of ABI4 in regulating plastid-to-nucleus RS has generated controversy (Richter et al., 2023). The importance of RS is usually demonstrated by the observation that many *PhANG*s become transcriptionally repressed when seedlings are treated with inhibitors that specifically arrest chloroplast development (Susek et al., 1993). Although ABI4 was implicated in plastid-to-nucleus RS when several studies showed that *abi4* mutants are less sensitive to such inhibitor treatment (Koussevitzky et al., 2007; X. Sun et al., 2011; Z. W. Zhang et al., 2013), multiple later studies refuted these results (Kacprzak et al., 2019; Kerchev et al., 2011; G. Martin et al., 2016).

ABI4 activity falls under both transcriptional and post-translational controls. *ABI4* transcription is regulated by factors such as phytohormones (Huang et al., 2017; Shkolnik-Inbar & Bar-Zvi, 2010), exogenous sugars (Arroyo et al., 2003; Z. W. Zhang et al., 2013), osmotic and salinity stress (Arroyo et al., 2003; Luo et al., 2021) and nitrogen deprivation (Y. Yang et al., 2011). On the other hand, whether *ABI4* transcription is controlled by light is a seldom-reported topic. We could only find one study that investigated this question, and it reported that *ABI4* expression in etiolated Arabidopsis seedlings is elevated for 6-12 hours upon exposure to either low-intensity white, red, blue or far-red light (P. Song et al., 2024). Although this light-induced *ABI4* transcript accumulation correlates well with ABI4 protein abundance in wild-type seedlings, a role of post-translational regulation is still evident in the observation that

ABI4 shows light-induced protein accumulation when *ABI4* is ectopically overexpressed (P. Song et al., 2024). On the other hand, ABI4 is degraded by the 26S proteasome (R. Finkelstein et al., 2011; Gregorio et al., 2014), and this degradation was reported to occur in light (Xu et al., 2016). It is therefore unclear whether light promotes ABI4 stability or causes ABI4 degradation. Nonetheless, post-translational modifications such as phosphorylation and persulfidation are essential for ABI4 protein activity (Eisner et al., 2021; Maymon et al., 2022; Zhou et al., 2021). ABI4 also physically interacts with other nuclear proteins with pleiotropic functions *in planta* (reports on *At*ABI4 are summarised in Table 2).

Table 2. *At*ABI4 physically interacts with other nuclear proteins

Interactor	Interaction detection method	Interaction function
MITOGEN-ACTIVATED PROTEIN KINASE (MPK3&6)	Y2H, split-LUC, pull-down (Guo et al., 2016)	Regulate *LHCB1.2* (Guo et al., 2016) Adventitious root growth (Bai et al., 2020)
CONSTITUTIVE PHOTOMORPHOGENIC 1 (COP1)	pull-down, co-IP (Xu et al., 2016)	Photomorphogenesis
PROTEIN PHOSPHATASE 2C 12 (PP2C12)	Y2H, BiFC, pull-down, co-IP (Bai et al., 2020)	Adventitious root growth
POWERDRESS (PWS) & HISTONE DEACETYLASE9 (HDA9)	Y2H, co-IP (Khan et al., 2020)	Drought stress tolerance
DELLA proteins (RGA, RGL2&3)	Y2H, BiFC, pull-down, co-IP (Xian et al., 2024)	ABA & GA signalling
CRYPTOCHROME (CRY1&2)	Y2H, pull-down, co-IP (P. Song et al., 2024)	Hypocotyl elongation
PHYTOCHROME INTERACTING FACTOR 4 (PIF4)	Y2H, split-LUC, co-IP, BiFC (Luo et al., 2024; P. Song et al., 2024)	Hypocotyl elongation (P. Song et al., 2024) Germination (Luo et al., 2024)
LONG HYPOCOTYL IN FAR-RED (HFR1)	Y2H, split-LUC, pull-down, co-IP (Z. Wang et al., 2024)	Germination

1.6 Aims of this study

Since we identified ABI4 as a potential interacting protein of GLKs in Arabidopsis, we addressed the following two aims in this study:

1. To confirm the ABI4-GLK protein-protein interaction
2. To investigate the biological relevance of the ABI4-GLK interaction

2 Results

2.1 ABI4 physically interacts with GLK1 and GLK2

2.1.1 ABI4 interacts with GLKs in yeast two-hybrid

We first tested the ABI4-GLK interaction by using full-length ABI4 protein as the prey in yeast two-hybrid (Y2H). In order to use GLKs as bait, we first deleted the transactivation domain from the GLKs, then performed a Y2H assay using the GLK C-terminal domains as baits (Figure 2a). We observed an interaction between ABI4 and the C-terminal fragment of GLK2 (Figure 2b). Due to the sharing of conserved regions and functional redundancy between GLK1 and GLK2 (Rauf et al., 2013; Waters et al., 2009), we hypothesized that ABI4 interacts with GLK1 as well as GLK2. Although the GLK1 C-terminal domain did not interact with ABI4 (Figure 2b), we hypothesized that GLK1 N-terminal domains may be necessary for an interaction between GLK1 and ABI4. To test this, we deleted the transactivating glutamine-rich and proline-rich domains from ABI4 so that we could use ABI4 as the bait (Figure 2c). Indeed, ABI4$_{\Delta 188\text{-}289}$ interacted with full-length GLK1 and GLK2 in Y2H (Figure 2d).

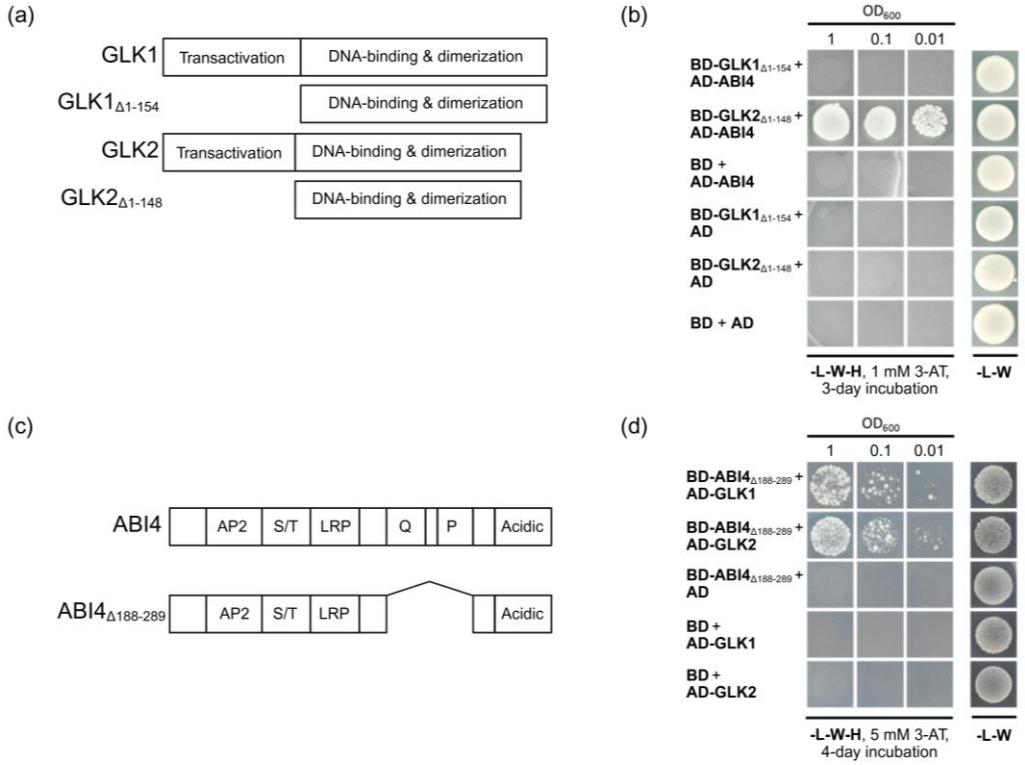

Figure 2. ABI4 physically interacts with GLK1 and GLK2 in yeast two-hybrid
(a) Scheme of GLK1 and GLK2 proteins and deletion-derivatives lacking the transactivation domain. The latter were used as baits in the yeast two-hybrid screen. **(b)** GLK2$_{\Delta 1\text{-}154}$ interacts with ABI4. **(c)** Scheme of ABI4 protein and a deletion-derivative lacking the transactivation domain, the latter was used as the bait in the following yeast two-hybrid assay. AP2 = APETALA2 domain; S/T = serine-/threonine-rich domain; LRP = LRP motif; Q and P = glutamine- and proline-rich domains, respectively. **(d)** ABI4$_{\Delta 188\text{-}289}$ interacts with full-length GLK1 and GLK2.

2.1.2 ABI4 interacts with GLKs *in planta*

We further confirmed the ABI4–GLK interaction *in planta*. First, we performed Förster resonance energy transfer by fluorescence lifetime imaging (FRET-FLIM) experiments after co-expressing YFP-tagged ABI4 and mCherry-tagged GLK proteins in leek epidermal cells by particle bombardment. As shown in Figure 3a and 3b, the lifetime of the donor fluorophore YFP was significantly reduced when YFP-ABI4 was co-expressed with either mCherry-GLK1 or mCherry-GLK2 compared to co-expression with mCherry, supporting an interaction between Arabidopsis ABI4 and GLK1 as well as GLK2. Next, we performed a luciferase complementation imaging assay after co-expressing nLUC- and cLUC-fused proteins in tobacco by *Agrobacterium* infiltration. We observed that both GLK1-nLUC and GLK2-nLUC generated luminescence when co-expressed with cLUC-ABI4 (Figure 3c and 3d), whereas the negative controls did not generate luminescence, supporting an interaction between Arabidopsis ABI4 and GLK in tobacco. Together, these assays corroborate the existence of an *in-planta* interaction between ABI4 and both GLKs.

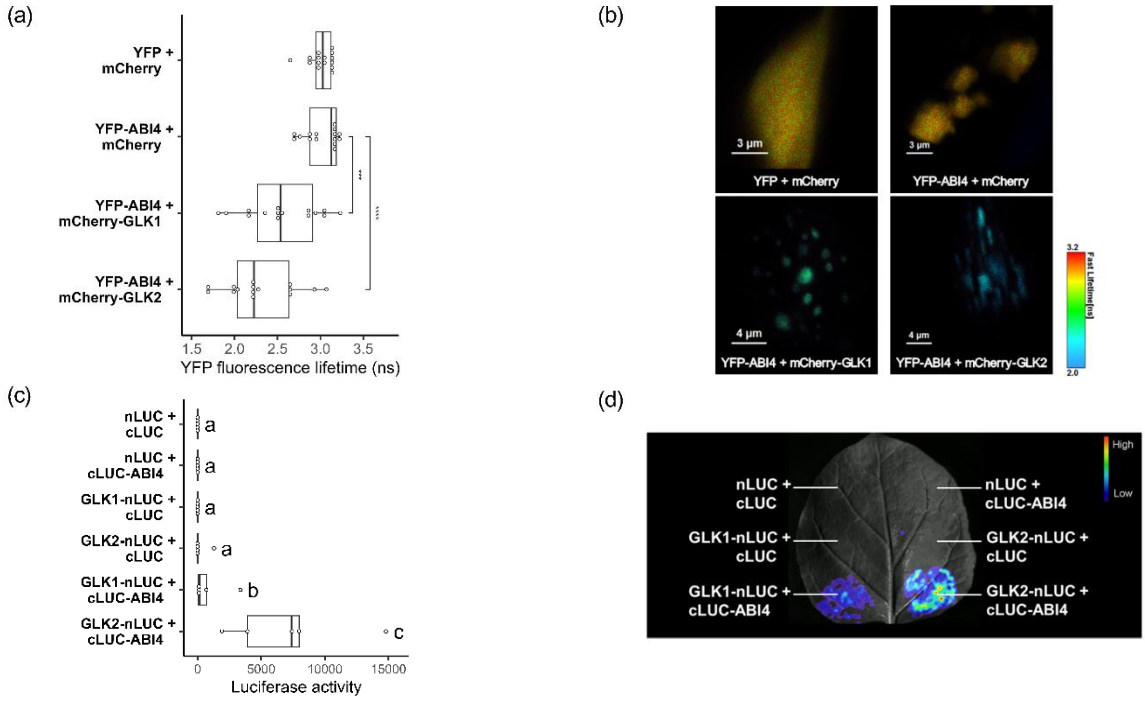

Figure 3. ABI4 physically interacts with GLK1 and GLK2 *in planta*
(a) Lifetime of donor fluorophore (YFP) measured by FRET-FLIM inside the nuclei of leek epidermal cells after particle bombardment, n=15 nuclei. Asterisks indicate a significant difference in lifetime between the indicated pair (Student's t-test, ***P < 0.001, ****P < 0.0001). **(b)** FLIM images of the representative nuclei from (a) showing changes in YFP lifetime. **(c)** Quantification of luminescence detected by a CCD camera from a luciferase complementation imaging assay in tobacco leaves, n=5 leaves. Combinations which are significantly different (P < 0.05) are labelled with different letters (Pairwise Wilcoxon test with multiple testing correction). **(d)** Representative leaf image from (c) showing the luminescence signal in sectors transfected with the indicated plasmid combinations.

2.1.3 ABI4 interacts with GLKs *in silico*

Next, in order to better understand the ABI4-GLK protein-protein interaction, we modelled the ABI4-GLK1 and ABI4-GLK2 protein complex structures with AlphaFold 3 (Abramson et al., 2024). As shown in Figure 4, both the ABI4-GLK1 and ABI4-GLK2 complex predictions produced low ipTM and pTM scores. The low ipTM scores indicate that the predicted subunit positions within the complexes are unlikely to be correct, and the low pTM scores suggest that the overall complex predictions are unlikely to be correct. These low scores were caused by the large stretches of disordered domains in both ABI4 and GLK proteins (Figure 4b), and these domains also produced very low pIDDT scores (Figure 4a), which show the confidence levels per residue. Nonetheless, AlphaFold 3 still demonstrated the in-silico interactions between ABI4 and GLKs, and it identified 19 residues in GLK1 and 22 residues in GLK2 within the high-confidence regions that may interact with ABI4. In GLK1, these residues are primarily located in the C-terminal DNA-binding and dimerization domains, while the ones in GLK2 are located in both the N- and C-terminal domains (Figure 4b). Here, despite the low confidence of the overall structural predictions, these data still suggest that ABI4 can interact with GLKs through possibly multivalent interactions.

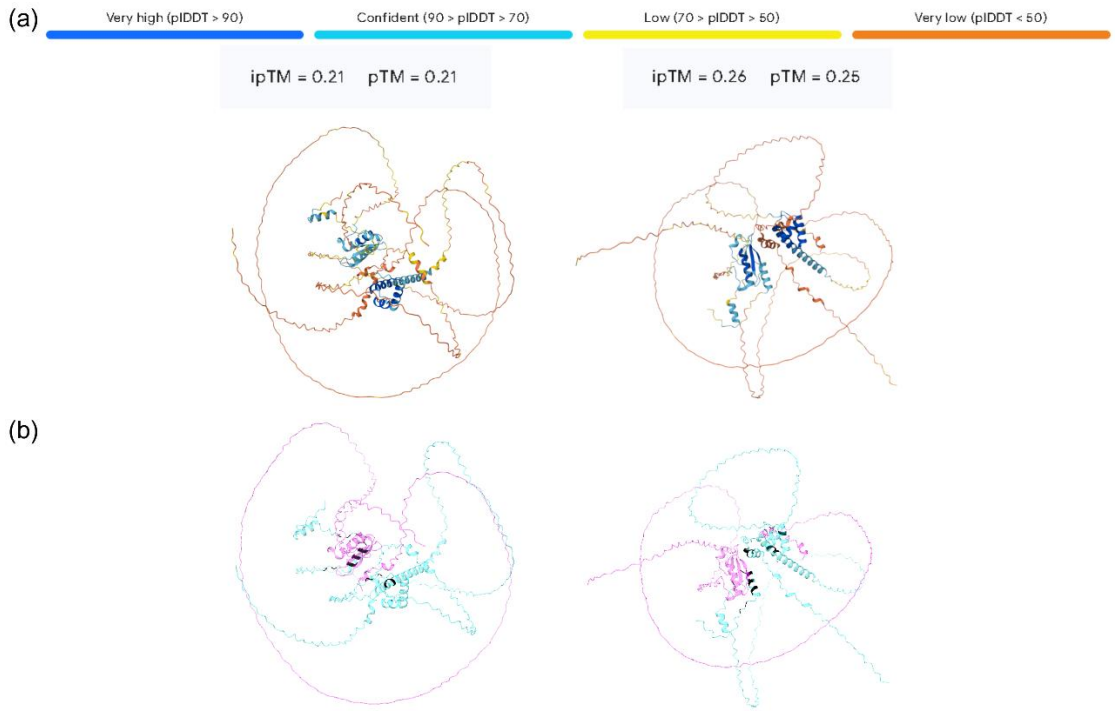

Figure 4. ABI4 interacts with GLKs *in silico*

(a) ABI4-GLK1 (left pane) and ABI4-GLK2 (right pane) protein complex structures predicted by AlphaFold 3, only the topmost structure for each complex is shown here. Protein residues are coloured according to their pIDDT scores. **(b)** The same structures as shown in (a), coloured by protein identity. ABI4 is coloured in magenta, whereas GLKs are coloured in blue. Residues in GLK proteins that are predicted to interact with ABI4 (atomic distance $\leqslant$ 3.5 Å) are coloured in black.

2.2 Greening-related phenotypes of etiolated *abi4* mutant seedlings are dependent on *GLK*s

2.2.1 Light-grown *abi4* mutant seedlings show wild-type chlorophyll levels

The ABI4-GLK interaction prompted us to investigate the biological relevance of this interaction. To this end, we compared the phenotypes of *abi4* and *glk1 glk2* loss-of-function mutants. First, because GLKs promote chlorophyll accumulation in light (Fitter et al., 2002), we quantified the chlorophyll content in seedlings grown on soil in a long-day photoperiod for 10 days. As described previously (Waters et al., 2008), the *glk1 glk2* double mutant accumulated significantly less chlorophyll than the *Col-0* wild type, while the *35Spro*::*GLK2-GFP* line accumulated slightly more chlorophyll than the wild type, though the difference was not statistically significant (Figure 5). We included two *abi4* knock-out mutant alleles: *abi4-1*, with a 1-bp deletion at *ABI4* codon 157 in the *Col-0* background (R. R. Finkelstein et al., 1998) and *abi4-103 gl1*, with a nonsense point mutation at *ABI4* codon 39 in the *gl1* background (Laby et al., 2000). Both *abi4* mutants accumulated similar levels of chlorophyll compared with their wild-type genotypes, indicating that the ABI4-GLK interaction does not play a role in chlorophyll homeostasis under these conditions.

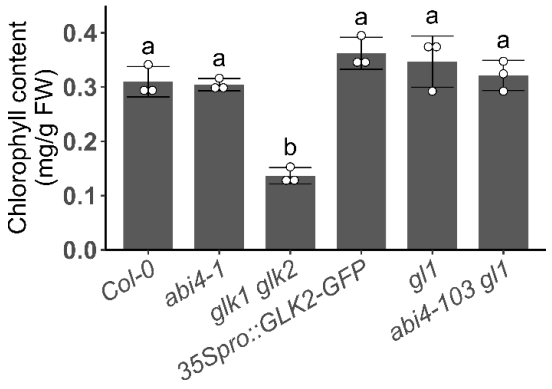

Figure 5. Chlorophyll accumulation is not altered in light-grown *abi4* mutants
Seedlings are grown for 10 days on soil in a long-day phytochamber with 100 µmol photons m^{-2} s^{-1} white light. Data were normalized to per gram fresh weight (/g FW). Genotypes which are significantly different are labelled with different letters (n=3 replicate extracts, ANOVA and Tukey's post hoc tests), error bars indicate SD.

2.2.2 Etiolated *abi4* mutant seedlings display *GLK*-dependent Pchlide overaccumulation and inefficient Pchlide photoreduction

Next, we hypothesized that the ABI4-GLK interaction plays a specific role in Pchlide accumulation during seedling skotomorphogenesis. In the following phenotypic assays, we included two *abi4* knock-out mutant alleles: the above-mentioned *abi4-1*, and *abi4-t* which contains a T-DNA insertion in *ABI4* (Alonso et al., 2003; Shu et al., 2013). To elucidate the genetic relationships between *ABI4* and *GLK*s, we generated the *glk1 glk2 abi4-1* triple mutant by crossing *glk1 glk2* with *abi4-1*. The *abi4-1* homozygosity in the *glk1 glk2 abi4-1* triple mutant was verified by genotyping using a derived Cleaved Amplified Polymorphic Sequences (dCAPS) marker (Figure S1) and observing a complete insensitivity to 1.5 µM ABA during seed germination (Figure 13). The *glk1 glk2* homozygosity in the *glk1 glk2 abi4-1* triple mutant was confirmed by the observation that the triple mutant has the same chlorophyll-deficient phenotype as the *glk1 glk2* double mutant (Figure 7c).

To determine Pchlide levels, we extracted and quantified the total Pchlide content in 5-day-old etiolated seedlings. We found that in comparison to the wild type, the *glk1 glk2* mutant accumulated significantly less Pchlide, while the *35Spro*::*GLK2-GFP* line accumulated more Pchlide (Figure 6a and 6b). Importantly, both *abi4* mutants had higher levels of Pchlide, thus resembling the *35Spro*::*GLK2-GFP* line, while the Pchlide content returned to a wild-type level in the *glk1 glk2 abi4-1* mutant (Figure 6a and 6b). This revealed that the total Pchlide overaccumulation in etiolated *abi4* mutants was completely dependent on *GLK*s.

According to previous studies, photoactive Pchlide is converted by PORs to Chlide within one millisecond of white light, while non-photoactive Pchlide is not efficiently photoreduced (Shibata, 1957; Xu et al., 2016). Therefore, we measured the non-photoactive Pchlide levels in 5-day-old etiolated seedlings exposed to 5 min of white light. We found that, similar to the *35Spro*::*GLK2-GFP* line, both *abi4* mutants did not efficiently convert all Pchlide to Chlide (Figure 6c), because they still contained more non-photoactive Pchlide than the wild type upon light exposure (Figure 6d). In contrast, all Pchlide was photoreduced in both the *glk1 glk2* mutant and the *glk1 glk2 abi4-1* mutant (Figure 6c), where the non-photoactive Pchlide content returned to a wild-type level (Figure 6d). We conclude that etiolated *abi4* mutant seedlings display inefficient Pchlide photoreduction and non-photoactive Pchlide overaccumulation, and that these phenotypes are completely dependent on *GLK*s.

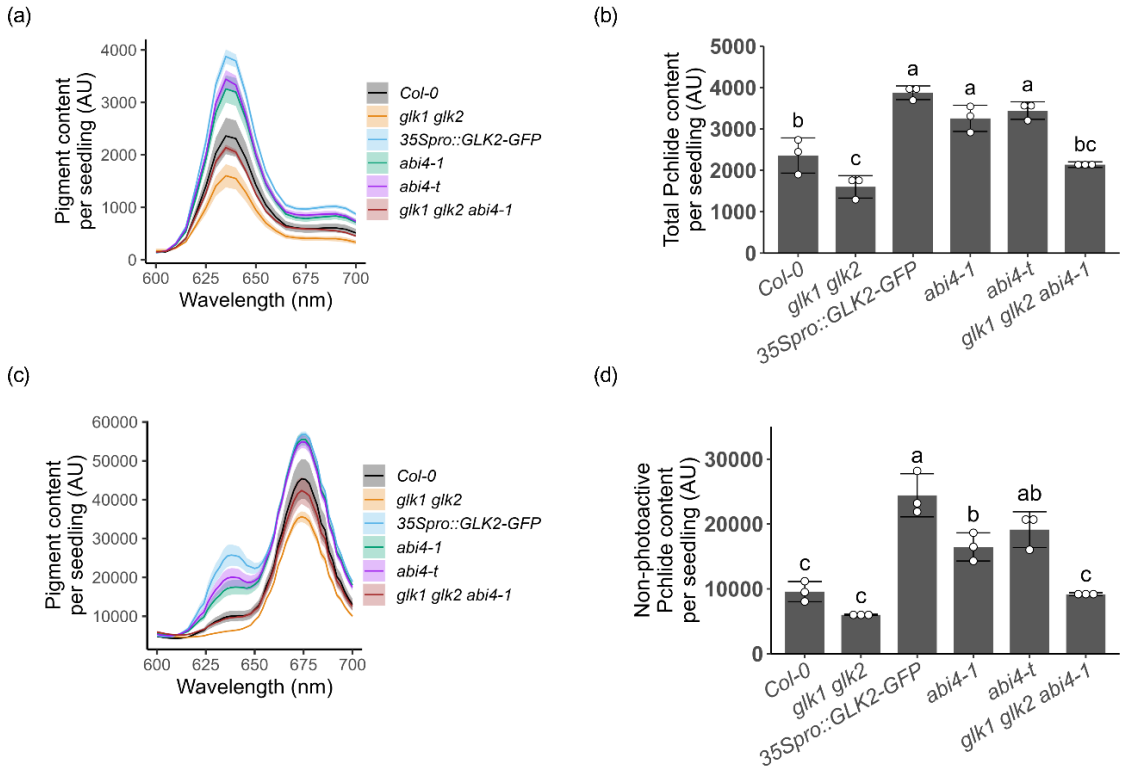

Figure 6. Etiolated *abi4* mutants overaccumulate Pchlide and cannot efficiently convert all Pchlide into Chlide, and these phenotypes are dependent on *GLK1* and *GLK2*

(a) Fluorescence of Pchlide at different emission wavelengths in 5-day-old etiolated seedlings, data are plotted as mean (solid lines) ± SD (shaded areas). **(b)** Comparison of total Pchlide content by the peak fluorescence at 634 nm from (a). Genotypes which are significantly different are labelled with different letters (n=3 replicate extracts, ANOVA and Tukey's post hoc tests), error bars indicate SD. **(c)** Fluorescence of Pchlide (634 nm) and Chlide (670 nm) in 5-day-old etiolated seedlings after transfer from darkness to 100 µmol m^{-2} s^{-1} white light for 5 min. **(d)** Comparison of non-photoactive Pchlide content using the peak fluorescence at 634 nm from (c). Genotypes which are significantly different are labelled with different letters (n=3 replicate extracts, ANOVA and Tukey's post hoc tests), error bars indicate SD.

2.2.3 Etiolated *abi4* mutant seedlings exhibit a *GLK*-dependent reduced greening rate when exposed to light

Non-photoactive Pchlide is a photosensitizer that can cause pigment photobleaching and inhibition of greening (Erdei et al., 2005; Meskauskiene et al., 2001). Since etiolated *abi4* mutant seedlings contained more non-photoactive Pchlide than the wild type, we performed cotyledon greening assays using seedlings that were first etiolated for 1 to 5 days and then exposed to 3 days of white light. A visual examination revealed that 2-day-old etiolated seedlings of all investigated genotypes developed green cotyledons after transfer to white light (Figure 7a, first row). However, when seedlings were etiolated for 5 days before the transfer to white light (Figure 7a, second row), a small portion of the *Col-0* wild-type seedlings failed to develop green cotyledons. In

comparison, most seedlings of the *35Spro*::*GLK2-GFP* line and the two *abi4* mutants had cotyledons that failed to green, and this low greening rate was rescued in the *glk1 glk2 abi4-1* triple mutant. After prolonging the light exposure to 10 days (Figure 7a, third row), we observed that higher cotyledon greening rates corresponded to higher seedling establishment and survival rates, while seedlings that failed to green showed arrested development. We therefore designate the fail-to-green cotyledon phenotype as a photobleaching phenotype. Since sucrose is known to suppress cotyledon photobleaching by stimulating Pchlide photoreduction (Barnes et al., 1996; Mu et al., 2022), we assessed the effect of adding 2% sucrose exogenously to the culture medium. As shown in Figure 7a (fourth row), sucrose indeed partially rescued cotyledon photobleaching, especially in the *35Spro*::*GLK2-GFP* line and the two *abi4* mutants, suggesting that the photobleaching phenotype in these lines could be due to inefficient Pchlide photoreduction.

We quantified the proportion of greened seedlings by visually categorizing seedlings as green or bleached. As seen in Figure 7b, the *35Spro*::*GLK2-GFP* line and the two *abi4* mutants displayed consistently lower greening rates than *Col-0* and *glk1 glk2* when etiolation lasted longer than 3 days. Importantly, the *glk1 glk2* mutations in the *abi4-1* background rescued the failure of *abi4-1* to green. To further quantify the degree of photobleaching, we measured the chlorophyll levels in seedlings grown either without etiolation or with 4 days of etiolation prior to exposure to white light for 5 days. As shown in Figure 7c, in seedlings grown without prior etiolation, *Col-0*, *35Spro*::*GLK2-GFP* and the two *abi4* mutants contained similar levels of chlorophyll, whereas the chlorophyll levels of *glk1 glk2* and *glk1 glk2 abi4-1* mutants were similar to each other, but significantly lower than that of the wild type. The 4 days of prior etiolation did not significantly change the light-induced chlorophyll accumulation level in *Col-0* nor *glk1 glk2* mutant seedlings, but it significantly decreased the seedling chlorophyll levels in *35Spro*::*GLK2-GFP* and the two *abi4* mutants. Strikingly, the *glk1 glk2* mutations rescued the inhibited chlorophyll accumulation caused by the 4 days of prior etiolation in the *abi4-1* mutant background, demonstrating again that the *GLK*s are necessary for the photobleaching of light-exposed etiolated seedlings. To summarize, etiolated *abi4* mutants and *35Spro*::*GLK2-GFP* seedlings have lower greening rates compared to the wild type when exposed to light, and this photobleaching phenotype is dependent on *GLK*s.

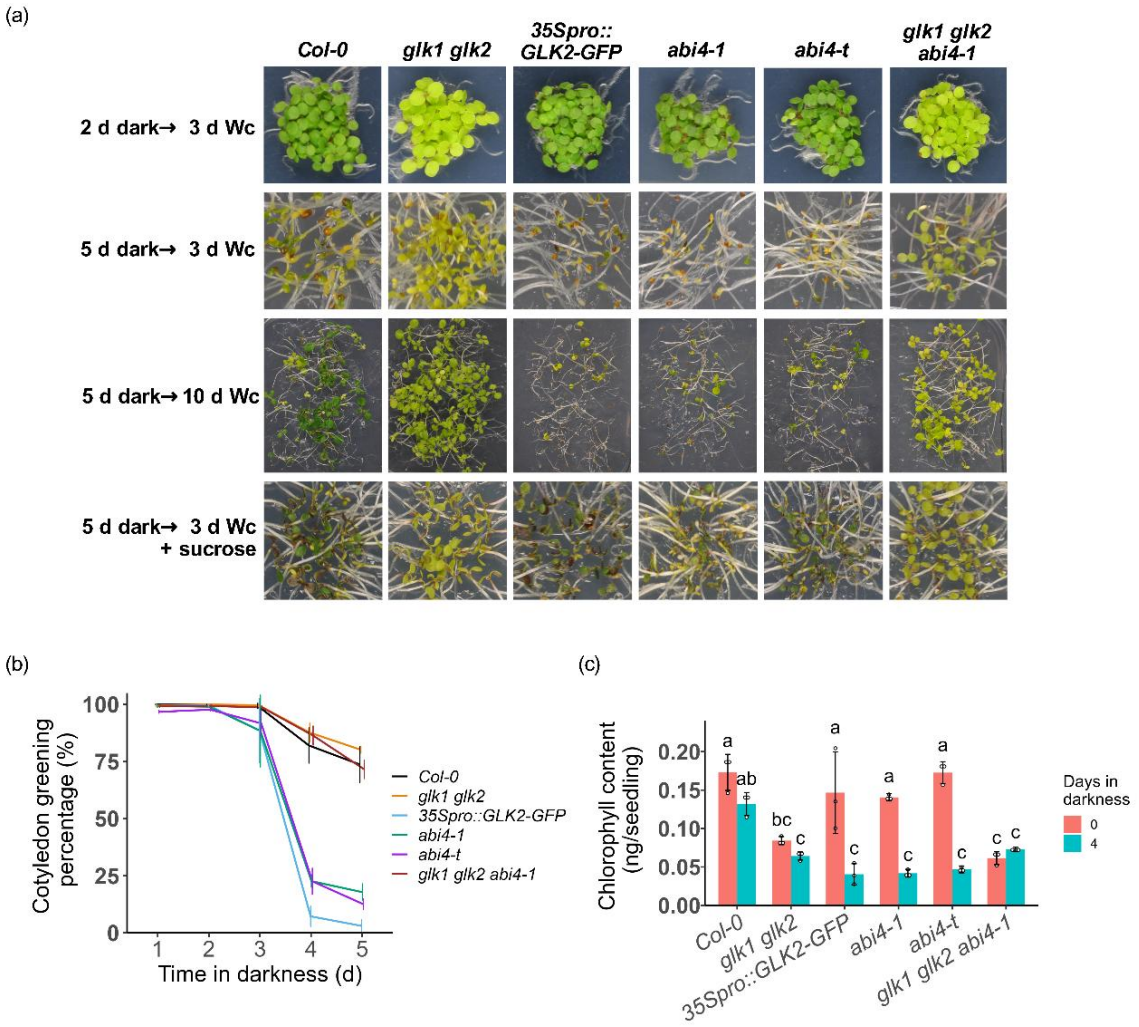

Figure 7. A *35Spro*::*GLK2-GFP* line and two *abi4* mutants fail to green when seedlings etiolated for more than 4 days are exposed to light

(a) Photographs of seedlings that were etiolated for the indicated number of days, followed by transfer to constant white light (Wc) for the indicated time. Seedlings shown in the last row were grown on 2% sucrose. **(b)** Quantification of cotyledon greening percentage of etiolated seedlings exposed to Wc for 3 days, n=3 replicate plates, error bars indicate SD. **(c)** Quantification of chlorophyll content of seedlings grown either without prior etiolation or with 4 days of etiolation, then exposed to Wc for 5 days. Genotypes which are significantly different are labelled with different letters (n=3 replicate extracts, ANOVA and Tukey's post hoc tests), error bars indicate SD.

2.2.4 Photobleaching of etiolated seedlings corresponds to singlet oxygen accumulation in the cotyledons

Although multiple species of ROS exist in Arabidopsis, the cause of Pchlide-induced photobleaching has been attributed to the generation of singlet oxygen ($^1O_2$) during photosensitization (Meskauskiene et al., 2001; Triantaphylidès et al., 2008). Hence, we quantified the $^1O_2$ generated in 5-day-old etiolated seedlings before and after exposure to light. To detect $^1O_2$ *in planta*, we stained seedlings with the fluorescent

probe Singlet Oxygen Green (SOSG) (Flors et al., 2006) and then detected both SOSG fluorescence and chlorophyll autofluorescence in the cotyledons using a confocal microscope. Before exposure to white light (0 d Wc), all genotypes contained a low level of $^1O_2$ and displayed limited chlorophyll autofluorescence (Figure 8a, b). After 3 days of light exposure (3 d Wc), the *35Spro::GLK2-GFP* line and both *abi4* mutants failed to accumulate chlorophyll, and this phenotype correlated with high $^1O_2$ accumulation levels. In contrast, light-exposed wild-type seedlings and—to a lesser extent—*glk1 glk2* and *glk1 glk2 abi4-1* mutant seedlings exhibited chlorophyll autofluorescence and low levels of $^1O_2$. Together, these $^1O_2$ levels are consistent with the Pchlide and photobleaching phenotypes reported above: when compared to the wild type, etiolated *abi4* mutant and *35Spro::GLK2-GFP* seedlings contained higher levels of non-photoactive Pchlide, displayed low greening rates and high $^1O_2$ content when exposed to light. Again, the lower $^1O_2$ level generated by photosensitization in the *glk1 glk2 abi4-1* mutant seedlings compared to that in the *abi4-1* mutant seedlings supports the conclusion that the photobleaching observed in etiolated *abi4* mutant seedlings is dependent on *GLK*s, and that GLK activity plays a central role in singlet oxygen accumulation when etiolated seedlings are exposed to light.

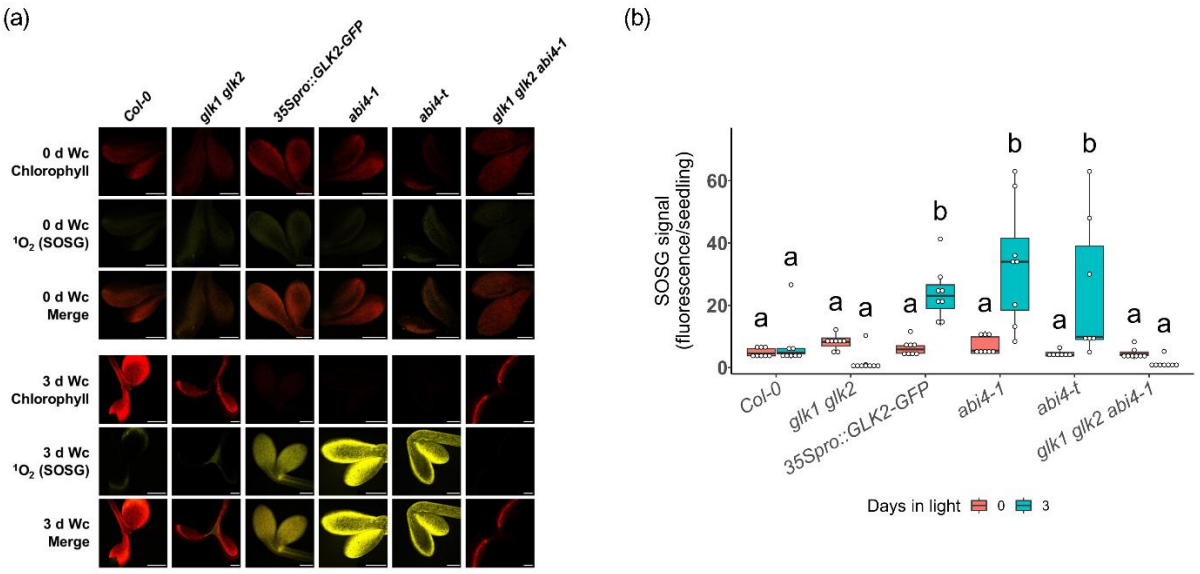

Figure 8. Photobleaching of etiolated, then light-exposed *abi4* mutant and *35Spro*::*GLK2-GFP* seedlings correlates with high singlet oxygen ($^1O_2$) accumulation
(a) Representative fluorescence microscopy images of chlorophyll autofluorescence and Singlet Oxygen Sensor Green fluorescence (SOSG, detecting $^1O_2$) in 5-day-old etiolated seedlings before (0 d Wc) and after exposure to 100 µmol m^{-2} s^{-1} constant white light for 3 days (3 d Wc). Scale bars = 200 µm. **(b)** Quantification of SOSG fluorescence per seedling in cotyledons of seedlings grown as in (a). Groups which are significantly different are labelled with different letters (n=8 seedlings, ANOVA and Tukey's post hoc tests).

2.2.5 Eight *PhANG*s exhibit GLK-dependent upregulation in etiolated *abi4* mutant seedlings

To investigate the cause of Pchlide overaccumulation in etiolated *abi4* mutants, we quantified the transcript levels of three main GLK target genes that are involved in Pchlide biosynthesis. As seen in Figure 9a, both *HEMA1* and *CHLH* transcripts accumulated to slightly higher levels in the *35Spro*::*GLK2-GFP* line and the two *abi4* mutants compared to the wild type, although ANOVA and Tukey's post hoc tests did not indicate clear statistically significant differences. *GUN4* transcript level was significantly upregulated in the *35Spro*::*GLK2-GFP* line, and its transcript levels in the two *abi4* mutants were slightly elevated from the wild-type level, albeit not significantly. In comparison, the transcript levels of all three genes were lowest in *glk1 glk2* and *glk1 glk2 abi4*. Together, the data demonstrate that GLKs can at least partially promote the accumulation of *HEMA1*, *CHLH* and *GUN4* transcripts in darkness, and the transcript accumulation patterns of these three genes may partially explain the Pchlide overaccumulation in etiolated *abi4* mutant seedlings.

Next, we hypothesized that low *POR* transcript accumulation also contributed to the inefficient Pchlide photoreduction in the *abi4* mutant seedlings. Since sucrose rescued the photobleaching phenotype (Figure 7a) and sucrose indirectly promotes *POR* gene expression (Mu et al., 2022), we quantified the transcript levels of *PORA* and *PORB* in etiolated seedlings grown with or without 2% sucrose supplementation. As demonstrated in Figure 9b, the transcript levels of *PORA* and *PORB* in the two *abi4* mutants were similar to those in the wild type, irrespective of the presence or absence of sucrose. Therefore, we conclude that the photobleaching observed in etiolated *abi4* mutant seedlings is not a result of low *POR* transcript levels.

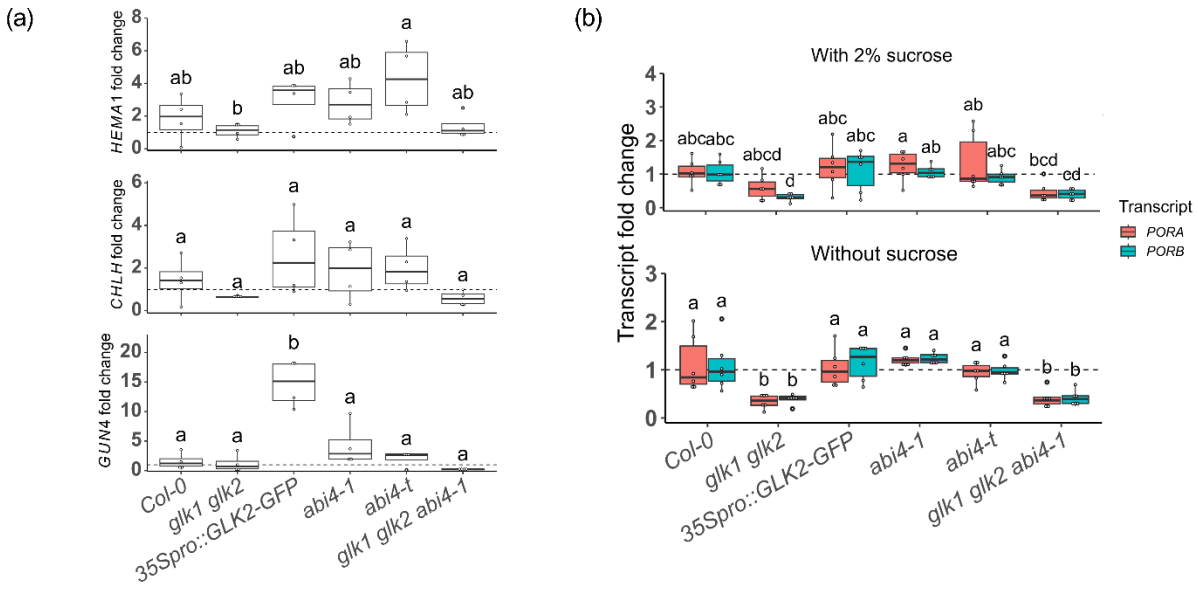

Figure 9. Transcript levels of *HEMA1*, *CHLH* and *GUN4*, but not the transcript levels of *PORA* or *PORB*, may explain the Pchlide overaccumulation and inefficient photoreduction in etiolated *abi4* mutant seedlings

Seedlings were grown on MS agar plates without sucrose (unless indicated otherwise) for 5 days, and the transcript levels were quantified using RT-qPCR. Mean transcript level in *Col-0* was set to 1 (indicated by the dashed line), and data were compared with ANOVA and Tukey's post hoc tests. Transcript levels which are significantly different are labelled with different letters. **(a)** Three main chlorophyll biosynthesis genes are targeted by GLKs (n=4). **(b)** Transcript levels of *PORA* and *PORB* are not lower in *abi4* mutants with (top panel) or without 2% sucrose (bottom panel), n=6.

An overexpression of *LHCB*—encoding the Light Harvesting Complex proteins surrounding photosystem II—has been reported to exacerbate cotyledon photobleaching without changing the total Pchlide content (Liu et al., 2018). Since *LHC*s are also a main class of GLK targets (Waters et al., 2009), we quantified their transcript levels in 5-day-old etiolated seedlings. Amongst the *LHC*s we examined, five had a higher transcript level in the *35Spro*::*GLK2-GFP* line than in the wild type: *LHCB2.1*, *LHCB2.2*, *LHCB2.3*, *LHCB3* and *LHCB6* (Figure 10). Their transcript levels were also either significantly or slightly elevated in the two *abi4* mutants. Importantly, the accumulation levels of these transcripts were again lowest in *glk1 glk2* and *glk1 glk2 abi4* mutants, showing that the high *LHC* induction in etiolated *abi4*-1 mutant seedlings was completely dependent on *GLK*s. The levels of these *LHCB* transcripts may contribute to the photobleaching, independently of Pchlide homeostasis, in light-exposed etiolated *abi4* mutant seedlings.

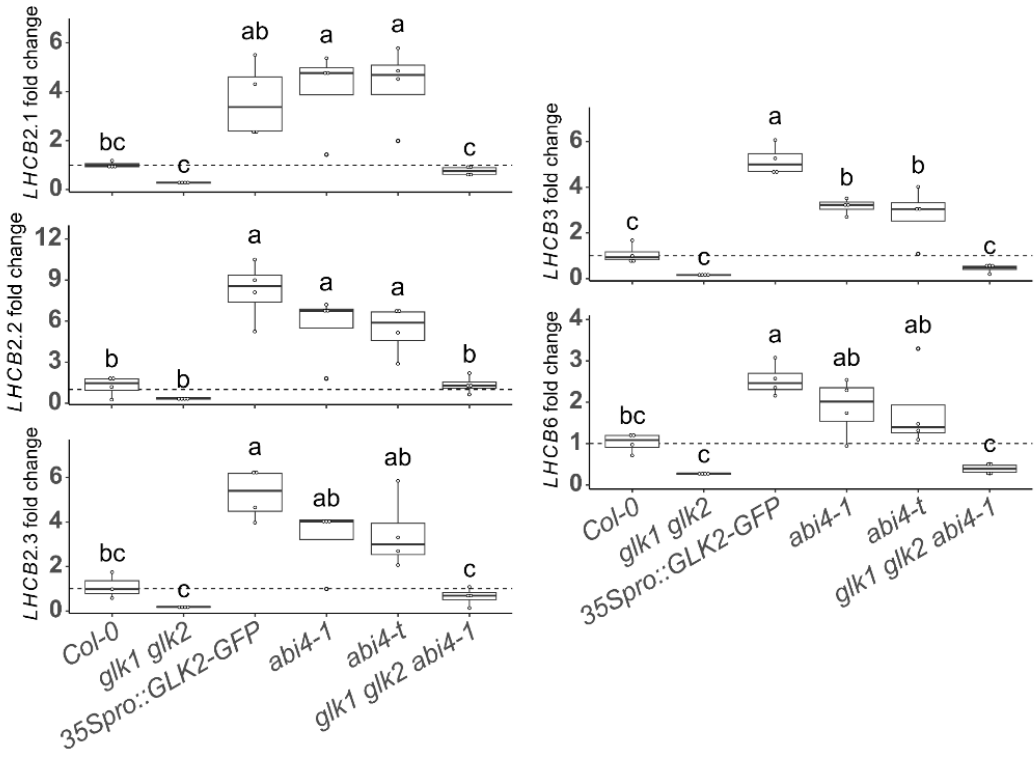

Figure 10. Transcript levels of *LHCB*s may contribute to the photobleaching in light-exposed etiolated *abi4* mutant seedlings

Seedlings were grown on MS agar plates without sucrose for 5 days, and the transcript levels were quantified using RT-qPCR. Mean transcript level in *Col-0* was set to 1 (indicated by the dashed line), and data were compared with ANOVA and Tukey's post hoc tests. Transcript levels which are significantly different are labelled with different letters (n=4).

The overexpression of *LHCB* impairs cotyledon greening in the light by promoting precocious prothylakoid (PT) proliferation in darkness (Liu et al., 2018). Hence, we examined the etioplast ultrastructure in these 5-day-old etiolated seedlings using transmission electron microscopy (TEM). As shown in Figure 11a, we observed that the membrane structures within some etioplasts showed an "inverted staining", where both the PLB and the PTs appeared as white instead of black against the dark stroma. The occurrence of such inverted staining did not strictly correlate to certain genotypes, since seedlings of the *Col-0* and *abi4-t* genotypes contained both etioplasts that were stained normally and etioplasts with inverted staining. Nevertheless, the staining status *per se* did not affect the etioplast ultrastructure. When compared with the wild type, the *abi4* mutants and the *35Spro::GLK2-GFP* seedlings did not have significantly different etioplast sizes (Figure 11b). However, the *abi4-t* mutant etioplasts showed significantly longer PT than the wild type, and this result remained the same when the PT length was adjusted to the total etioplast area (Figure 11b). Together, our data indicate that the accumulation patterns of *LHCB* transcripts in darkness may also

partially explain the greening-related phenotypes of etiolated *abi4* mutant seedlings, and hint at the possibility that these mutant seedlings have a higher activity of GLKs.

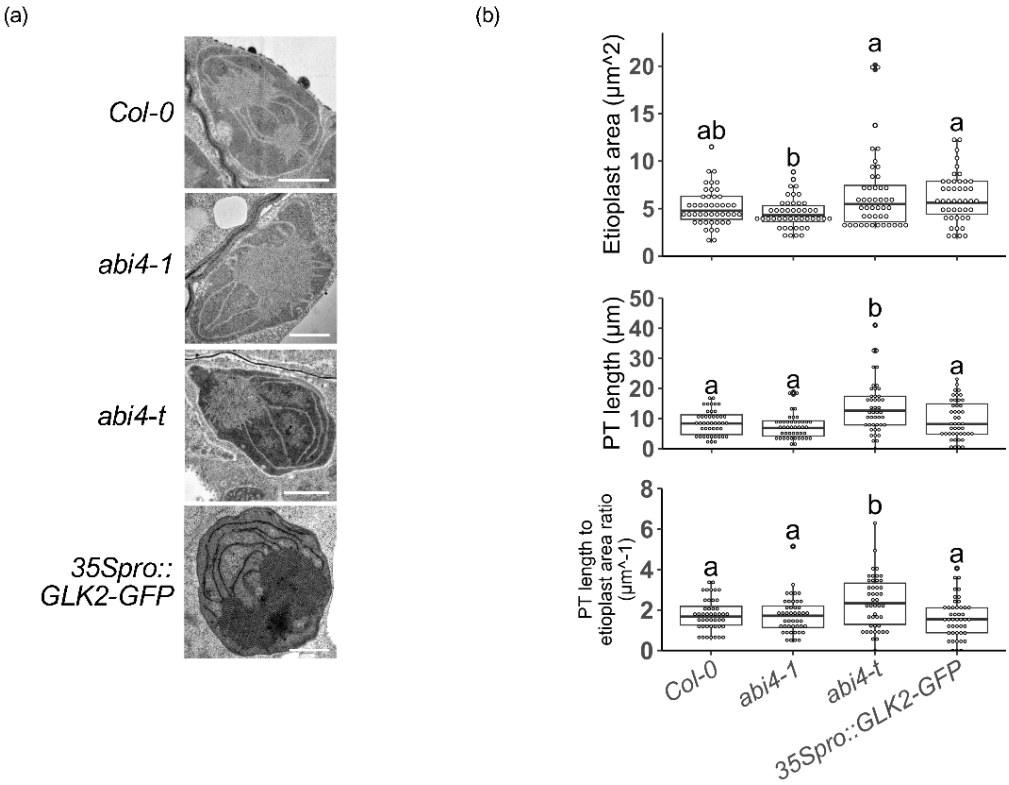

Figure 11. Ultrastructure of etioplasts in 5-day-old etiolated cotyledons under transmission electron microscope
(a) Representative photos of the etioplasts, scale bars = 1 µm. **(b)** Quantification of etioplast area (upper panel), prothylakoid (PT) length (middle panel) and the PT length to etioplast area ratio (lower panel). Genotypes which are significantly different are labelled with different letters (n=45 etioplasts, ANOVA and Tukey's post hoc tests).

2.2.6 Plastid-to-nucleus retrograde signalling in light does not require ABI4

Since we showed that *abi4* mutant seedlings accumulate more *LHCB* transcripts than wild-type seedlings during etiolation (Figure 10), and previous studies connected ABI4 to plastid-to-nucleus RS by quantifying *LHCB* transcript level in *abi4* mutants (Koussevitzky et al., 2007; X. Sun et al., 2011; Z. W. Zhang et al., 2013), we also examined whether the RS response is altered in *abi4* mutants. Specifically, we grew seedlings on MS agar plates with or without 0.5 mM of the plastid inhibitor lincomycin for 5 d in light and quantified the transcript levels of *LHCB2.2*—the *LHCB* expressed to the highest level in Figure 9. As shown in Figure 12, lincomycin equally inhibited the *LHCB2.2* transcript accumulation in the two *abi4* mutants compared with the wild type. We therefore conclude that chloroplast-to-nucleus RS does not require ABI4 under these conditions.

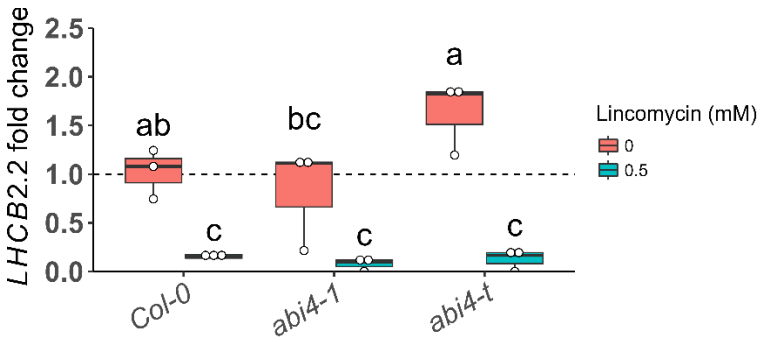

Figure 12. Transcript accumulation of *LHCB2.2* is not insensitive to the plastid inhibitor lincomycin in light-grown *abi4* mutant seedlings
Seedlings were grown on MS agar plates without sucrose under 100 µmol m^{-2} s^{-1} constant white light for 5 days, and the transcript levels were quantified using RT-qPCR. Mean transcript level in *Col-0* without lincomycin was set to 1 (indicated by the dashed line), and data were compared with ANOVA and Tukey's post hoc tests. Transcript levels which are significantly different are labelled with different letters (n=3).

2.2.7 ABA-insensitive germination of *abi4* mutants is not dependent on *GLK*s

We further hypothesized that the ABI4-GLK physical interaction may affect the ABA sensitivity during seed germination. To test this, we quantified the germination rate either without or with 1.5 µM exogenous ABA treatment. As shown in Figure 13, the germination rates were similar in all genotypes when grown without ABA treatment. Wild-type germination was significantly inhibited by the exogenous ABA. In comparison, germination of the *glk1 glk2* mutant was also inhibited by ABA, but the sensitivity to ABA appeared lower than that seen in the wild type. The two *abi4* mutants showed ABA-insensitive germination rates. Importantly, the *glk1 glk2 abi4-1* triple mutant showed the same ABA insensitivity as the *abi4* mutants. These data revealed that *abi4* mutants are not dependent on *GLK*s to show ABA-insensitive germination.

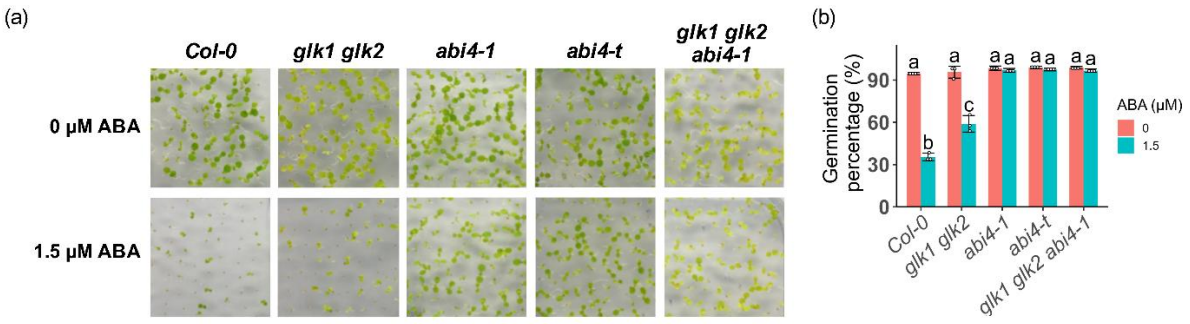

Figure 13. ABA-insensitive germination of *abi4* mutants is not dependent on *GLK*s
(a) Photographs of seed germination on MS agar plates ± 1.5 µM ABA. **(b)** Quantification of germination rate from (a). Genotypes which are significantly different are labelled with different letters (n=3 replicate plates, ANOVA and Tukey's post hoc tests), error bars indicate SD.

2.3 ABI4 possibly regulates GLKs post-transcriptionally in etiolated seedlings

2.3.1 *GLK* expression is not altered in *abi4* mutants

We established above that the photobleaching of etiolated *abi4* mutant seedlings is likely due to de-repressed transcript accumulation of *PhANG*s. Because GLKs are transcriptional activators of *PhANG*s (Waters et al., 2009), we first hypothesized that *GLK* transcript levels may be altered in the *abi4* mutants. To test this, we quantified the transcript levels of *GLK1* and *GLK2* by performing RT-qPCR using RNA isolated from 5-day-old etiolated seedlings. However, as shown in Figure 14, both *abi4* mutants showed similar *GLK1* and *GLK2* transcript levels to those in the wild type, indicating that *ABI4* did not affect *GLK1* or *GLK2* transcript levels under these conditions. There were also no significant changes observed for *GLK1* nor *GLK2* transcript levels in the *glk1 glk2 abi4-1* mutant compared to the *glk1 glk2* mutant, indicating that *ABI4* did not affect *GLK1* nor *GLK2* transcript levels in this genetic background either. Thus, the enhanced photobleaching observed in *abi4* mutants is not caused by a change in *GLK1* or *GLK2* transcript levels.

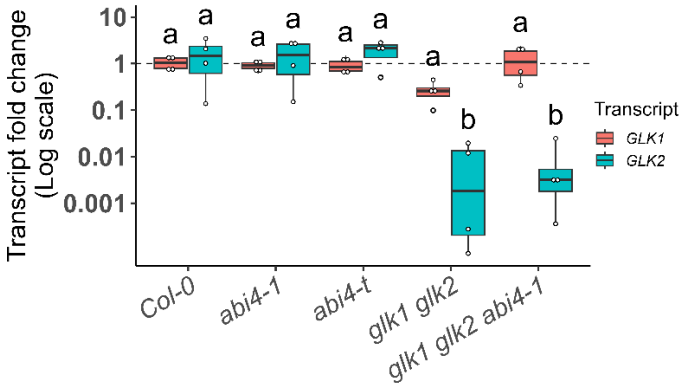

Figure 14. *GLK1* and *GLK2* transcript levels are not changed by *abi4* mutations in 5-day-old etiolated seedlings
Seedlings were grown on MS agar plates without sucrose, and the transcript levels were quantified using RT-qPCR. Mean transcript level in *Col-0* was set to 1 (indicated by the dashed line), and data were compared with ANOVA and Tukey's post hoc tests. Transcript levels which are significantly different are labelled with different letters (n=4 replicate extracts).

2.3.2 ABI4 does not significantly reduce the activation of the *LHCB2.2* promoter by GLK1 in transfected tobacco

We showed that etiolated *abi4* mutant seedlings may have a higher activity of GLKs, and this is not caused by higher *GLK* transcript accumulation. Therefore, we suspected that ABI4 inhibits GLK protein activity via direct protein-protein interaction.

We first tested whether such inhibition can be seen in a dual-luciferase reporter assay in transfected tobacco leaves. In this assay, we co-expressed GLK1 either with GFP as a negative control or ABI4, and we quantified and compared the activation of the *LHCB2.2* promoter by these effector combinations (Figure 15a). Renilla LUC (REN) was co-expressed to assess the transfection efficiency. As shown in Figure 15b, although we observed in some leaves an increased LUC/REN signal in the area where GFP was co-expressed with GLK1 compared with where only GFP was expressed, this increase was not statistically significant, meaning that GLK1 did not significantly activate the *LHCB2.2* promoter. When we repeated the experiment twice with 10 leaves as biological replicates (Figure 15c), we only observed once a statistically significant, but weak activation of *LHCB2.2pro* by GLK1 (left pane). Moreover, in both Figure 15b and 15c, we did not observe any clear change in the LUC/REN signal in the area where GLK1 was co-expressed with ABI4 compared with where GFP and GLK1 were co-expressed. Therefore, we conclude that ABI4 does not significantly reduce the activation of the *LHCB2.2* promoter by GLK1 in transfected tobacco.

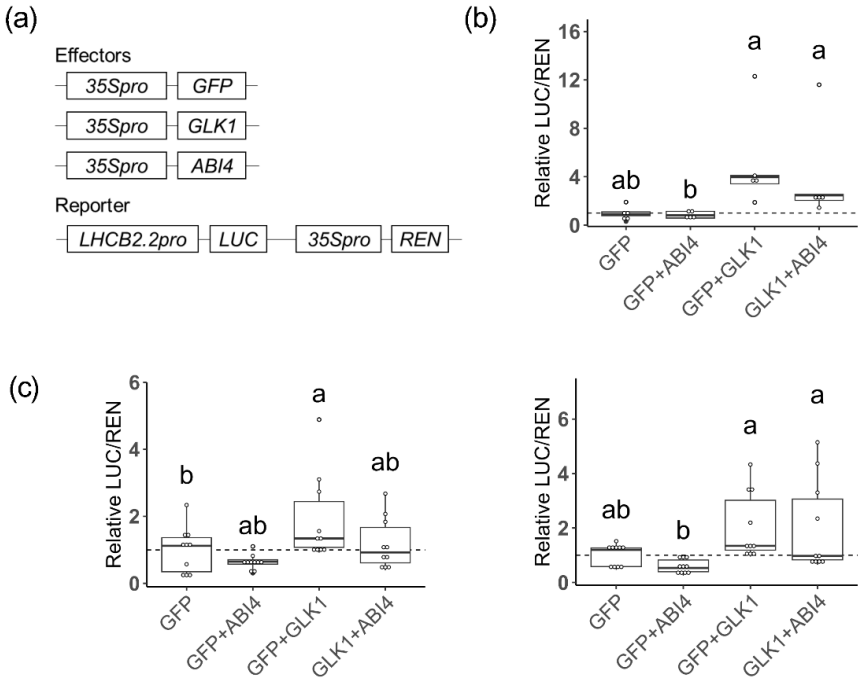

Figure 15. ABI4 does not significantly reduce the activation of the *LHCB2.2* promoter by GLK1 in transfected tobacco

(a) Schematic drawings of various constructs used in the transient dual-luciferase reporter assay. **(b)** Combinations of the control (GFP), GLK1 and ABI4 effectors were co-expressed with the reporter. Mean LUC/REN ratio in the control was set to 1 (indicated by the dashed line), data with the other combinations were normalized to the control on the same leaf, and the relative LUC/REN ratios were compared with ANOVA and Tukey's post hoc tests. Groups that are significantly different are labelled with different letters (n=5 leaves). **(c)** Two independent repeats of the experiment in (b), n=10 leaves.

2.3.3 ABI4 affects the transcriptional activation capacity of GLK1 in transformed yeast but not in transfected tobacco

Although we did not observe any effect of ABI4 on GLK1 target gene activation in transfected tobacco leaves (Figure 15), we still considered it worthwhile to perform other experiments to investigate the mechanism by which ABI4 affects GLK1 activity. We hypothesized that ABI4 inhibits the transcriptional activation capacity of GLK1. We first tested this by performing a yeast trans-activation assay. In this assay (shown in Figure 16a), we co-expressed BD-GLK1 either with YFP as a negative control or ABI4, and we quantified and compared the activation of the *LacZ* reporter by these effector combinations. BD-GLK1 is designed here to activate the *LacZ* reporter through the binding of BD to the *UAS* (Figure 16a), and ABI4, being a plant-specific protein, is unlikely to affect the interaction between BD and *UAS*. We thus reasoned that if ABI4 affects the activation of the *LacZ* reporter by BD-GLK1, it may reflect the effect of ABI4 on the transcriptional activation capacity of GLK1. As shown in Figure 16b, BD-GLK1 significantly activated the *LacZ* reporter. When ABI4 was co-expressed with BD-GLK1, the *LacZ* reporter activity significantly decreased compared with when YFP was co-expressed with BD-GLK1. These data indicate that ABI4 may inhibit the transcriptional activation capacity of GLK1 in transformed yeast.

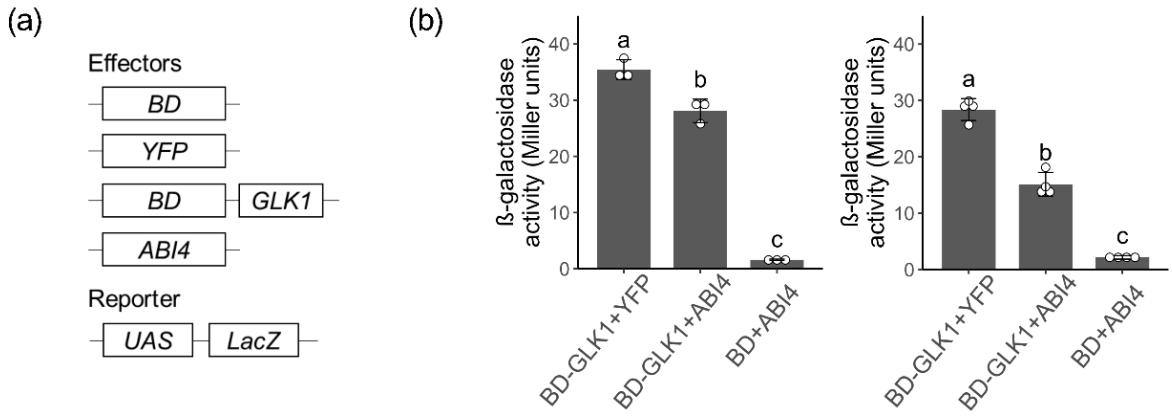

Figure 16. ABI4 significantly reduces the activation of the *UAS* promoter by BD-GLK1 in a yeast trans-activation assay

(a) Schematic drawings of various constructs used in the yeast trans-activation assay. BD stands for the GAL4 DNA-binding domain that binds to the upstream activating sequence (*UAS*). The effectors are transiently expressed in yeast, whereas the reporter is stably integrated into the yeast genome. **(b)** Combinations of the controls (BD and YFP), BD-GLK1 and ABI4 effectors were co-expressed. The ß-galactosidase activities were measured by an ONPG assay and compared with ANOVA and Tukey's post hoc tests. Groups that are significantly different are labelled with different letters (n=3, left pane). The experiment was independently repeated with n=4 (right pane).

Next, we tested the same hypothesis by performing a dual-luciferase reporter assay in transfected tobacco. In this assay (shown in Figure 17), we co-expressed GLK1-BD either with YFP as a control or ABI4, and we quantified and compared the activation of the yeast *UAS* promoter by these combinations. As shown in Figure 17b, GLK1-BD significantly activated the *UAS* promoter in two independent repeats of the experiment. However, the co-expression of ABI4 did not significantly reduce the activation of the *UAS* promoter by GLK1-BD when compared to the co-expression of YFP. Therefore, we conclude that ABI4 does not significantly inhibit the transcriptional activation capacity of GLK1 in transfected tobacco.

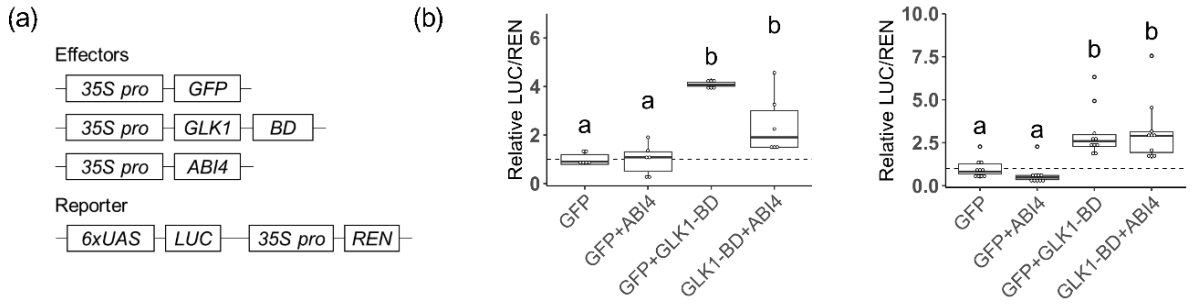

Figure 17. ABI4 does not significantly reduce the activation of the *UAS* promoter by BD-GLK1 in transfected tobacco
(a) Schematic drawings of various constructs used in the transient dual-luciferase reporter assay. BD stands for the GAL4 DNA-binding domain that binds to the upstream activating sequence (UAS). **(b)** Combinations of the control (GFP), GLK1-BD and ABI4 effectors were co-expressed with the reporter. Mean LUC/REN ratio in the control was set to 1 (indicated by the dashed line), data with the other combinations were normalized to the control on the same leaf, and the relative LUC/REN ratios were compared with ANOVA and Tukey's post hoc tests. Two independent repeats of the experiment are presented, and groups that are significantly different are labelled with different letters (left pane: n=6 leaves, right pane: n=10 leaves).

3 Discussion

3.1 Physiological relevance of the ABI4-GLK interaction

In the present work, we identified ABI4 as a GLK-interacting protein in yeast two-hybrid (Figure 2), *in planta* (Figure 3) and *in silico* (Figure 4). We found that etiolated, dark-grown seedlings of two *abi4* mutants are phenotypically similar to seedlings overexpressing GLK2 (*35Spro*::*GLK2-GFP*): etiolated *abi4* mutant and *35Spro*::*GLK2-GFP* seedlings contain more Pchlide (Figure 6), fail to green when exposed to light (Figure 7), generate more $^1O_2$ after the dark-to-light transition (Figure 8) and accumulate higher transcript levels of *PhANG*s in darkness (Figure 9 & 10) than the wild type. This suggests that GLKs and ABI4 have antagonistic functions during etiolation. Indeed, etiolated *glk1 glk2* mutant seedlings have opposite phenotypes to those of *abi4* mutants: etiolated *glk1 glk2* mutant seedlings contain less Pchlide (Figure 6), green normally when exposed to light (Figure 7), generate low $^1O_2$ upon light exposure (Figure 8) and accumulate slightly lower transcript levels of *PhANG*s in darkness (Figure 9 & 10) than the wild type.

The *abi4* mutants and *35Spro*::*GLK2-GFP* seedlings are not phenotypically similar to each other in terms of chlorophyll accumulation in light (Figure 5), nor in terms of ABA sensitivity during seed germination (Figure 13). This means that the ABI4-GLK antagonism may be specific to etiolated seedlings. The direct protein-protein interaction between GLKs and ABI4 indicates that the antagonistic activities of GLKs and ABI4 are a result of the GLK-ABI4 interaction. Our finding that the *abi4* mutant phenotype during etiolation fully depends on *GLK1* and *GLK2* supports this idea and suggests that ABI4 acts upstream of GLK1 and GLK2 by inhibiting the activities of the GLK1 and GLK2 proteins. The alternative possibility that ABI4 represses the expression of *GLK1* and *GLK2* can be excluded since *GLK1* and *GLK2* transcript levels were unaltered in *abi4* mutants (Figure 14).

3.1.1 GLK and ABI4 antagonistically impact cotyledon greening due to their effects on Pchlide and singlet oxygen accumulation

In our greening assays, etiolated *abi4-1* and *abi4-t* mutant seedlings exhibited reduced greening rates compared to the wild type after the seedlings were exposed to light (Figure 7). This is not due to any major defect in chlorophyll biosynthesis, because *abi4* mutant seedlings green normally when grown without prior etiolation (Figures 5 & 7c) or even after 2 days of etiolation (Figure 7a). This is confirmed by Shu et al. (2013), where both *abi4-1* and *abi4-t* mutant seedlings achieved similar greening percentages compared to *Col-0* when grown with 1% sucrose and without prior etiolation. Since Pchlide is a photosensitizer that can inhibit seedling greening in light (Meskauskiene et al., 2001), we hypothesized that the photobleaching of etiolated *abi4* mutant seedlings is due to an overaccumulation of Pchlide in these seedlings. We found that etiolated *abi4* mutant seedlings, as well as etiolated *35Spro*::*GLK2-GFP* seedlings, accumulated more Pchlide than wild-type seedlings (Figure 6), which correlated with lower greening rates after seedlings were exposed to light (Figure 7). In contrast, the *glk1 glk2* mutant accumulated less total Pchlide than the wild type as etiolated seedlings (Figures 6a & 6b), and it showed high greening rates in the cotyledon greening assay (Figure 7). Importantly, the *glk1 glk2* mutations returned both the Pchlide accumulation (Figure 6) and the cotyledon greening rate (Figure 7) of *abi4-1* mutant seedlings to a wild-type level. We therefore conclude that the Pchlide overaccumulation in etiolated *abi4* mutant seedlings causes the photobleaching of these seedlings after the dark-to-light transition, and this Pchlide overaccumulation may be due to de-repressed GLK activity. Nonetheless, it cannot be excluded that signalling pathways of other phytochemicals, such as ethylene (Zhong et al., 2014) and brassinosteroid (L. Wang, Tian, et al., 2020), may contribute to the photobleaching of etiolated *abi4* mutant seedlings during dark-to-light transition.

Next, we hypothesized that the photobleaching of etiolated *abi4* mutant seedlings in light is caused by singlet oxygen generated by Pchlide photosensitization. Singlet oxygen in plants is primarily generated in the plastids, either by chlorophyll molecules during photosynthesis or by chlorophyll precursors during dark-to-light transitions (Wang et al., 2020). $^1O_2$ is toxic to the cell (Apel & Hirt, 2004), and its accumulation with other ROS species can lead to programmed cell death (C. Kim et al., 2012; Wagner et al., 2004). Because of the direct role of GLKs in promoting Pchlide

biosynthesis, it was not surprising to find that etiolated *glk1 glk2* seedlings contained less $^1O_2$ and showed a high greening rate, while etiolated *35Spro*::*GLK2-GFP* seedlings contained more $^1O_2$ and showed a low greening rate upon light exposure compared to the wild type (Figures 7 & 8). A recent publication also supports the conclusion that limiting GLK activity in dark-grown seedlings acts to promote cotyledon greening during de-etiolation (Tachibana et al., 2025). Additionally, we observed high $^1O_2$ levels and low greening rates in both *abi4* mutants after their etiolated seedlings were transferred to light (Figures 7 & 8). This seems to contrast with a previous study in which two *abi4* loss-of-function mutations both rescued the lethal phenotype of the *flu* mutant under dark/light cycles (Z. W. Zhang et al., 2023). The *flu* mutant seedlings accumulate at least four times as much Pchlide as the wild type during etiolation, leading to rapid cotyledon bleaching and death after the dark-to-light transition (Meskauskiene et al., 2001; Z. W. Zhang et al., 2023). Intriguingly, the *abi4* mutations did not alter the Pchlide accumulation in etiolated *flu* mutant seedlings, nor the $^1O_2$ accumulation upon light exposure, but they lowered the transcript levels of $^1O_2$-responsive genes in light (Z. W. Zhang et al., 2023). Because chloroplast $^1O_2$ stress responses are controlled by multiple pathways (Tano et al., 2023), we suggest the pathways mediating the photobleaching of etiolated *flu* and *abi4* mutant seedlings in light may be different.

We further hypothesized that etiolated *abi4* mutant seedlings accumulate high levels of Pchlide due to an upregulated Pchlide biosynthetic pathway. We showed that the *HEMA1*, *CHLH* and *GUN4* transcript levels in the etiolated seedlings of the *35Spro*::*GLK2-GFP* line and the two *abi4* mutants were at least slightly elevated compared to the wild type (Figure 9a), and this likely upregulated the Pchlide biosynthesis in these seedlings. The similarity between etiolated *35Spro*::*GLK2-GFP* and *abi4* mutant seedlings suggests again that GLK protein activity may be de-repressed in etiolated *abi4* mutant seedlings. *HEMA1*, *CHLH* and *GUN4* are activated by GLKs in light-grown plants (Waters et al., 2009), and we demonstrated here that their transcript accumulation in etiolated seedlings in the *abi4-1* mutant background is dependent on *GLK1* and *GLK2* (Figure 9a). As expected, these *GLK*-dependent transcript levels correlated with the *GLK*-dependent Pchlide accumulation during etiolation (Figures 6a & 6b) and greening patterns after the dark-to-light transition (Figure 7). Since the transcript levels presented here came from

end-point analyses, future studies can generate transgenic Arabidopsis lines each expressing a luciferase driven by promoters of *HEMA1*, *CHLH* or *GUN4*, whereby the transcriptional dynamics of these promoters can be monitored in real-time by luciferase luminescence during etiolation and compared among different genotypes.

We also investigated whether the *POR* transcript level is altered in etiolated *abi4* mutant seedlings, due to the direct role of PORs in Pchlide photoreduction. Knocking out either *PORA* or *PORB* produces seedlings with smaller PLBs, unstructured PTs and a delayed-greening phenotype (S. Masuda et al., 2009; T. Masuda et al., 2003). *PORA* and *PORB* are both transcriptionally activated by GLKs in seedlings grown under long-day photoperiod (Waters et al., 2009). In comparison, we observed only a slight transcript overaccumulation of either *POR*s in etiolated *35Spro*::*GLK2-GFP* seedlings compared to the wild type (Figure 9b). Moreover, we observed no significant change in *PORA* and *PORB* transcript levels in both *abi4* mutants compared to the wild-type etiolated seedlings (Figure 9b). This differs from the report of Xu et al. (2016), where etiolated *abi4-1* mutant seedlings were shown to contain a lower *PORA* transcript level compared to that in the wild type. Our observation remained the same, either without supplementary sucrose in the growth medium, or with 2% supplementary sucrose, as that used by Xu et al. (2016). We therefore conclude that the *POR* transcript level is unlikely to have significantly affected our results.

3.1.2 Impact of GLKs and ABI4 on the expression of *PhANG*s and on the etioplast structure

Beyond the PLB, the ultrastructure of the PTs also affects the greening process (B. Li et al., 2024; Liu et al., 2018). Two chloroplastic proteins, which are commonly associated with photosynthesis, have been reported to cause structural changes in the PTs. A recent study showed that an overaccumulation of PsbE—a cytochrome b_{559} apoprotein—created condensed PLBs and over-proliferated PTs within tobacco transgenic etioplasts (B. Li et al., 2024). These transgenic tobacco plants were pale, stunted, and developed partial leaf necrosis. However, the fact that *PsbE* is encoded in the chloroplast genome and not targeted by GLKs (Waters et al., 2009) led to the conclusion that PsbE is unlikely to have created confounding effects in our assays. In contrast, LHCBs are encoded in the nuclear genome, and *LHCB*s are known targets

of GLKs (Waters et al., 2009). Overexpressing either *LHCB1.1* or *LHCB2.1* produces seedlings with low greening rates when the seedlings are exposed to light after prolonged etiolation (Liu et al., 2018). These transgenic seedlings contain a wild-type level of total Pchlide, but they develop etioplasts with no PLBs and only over-proliferated PTs. This agrees with our findings that the *35Spro*::*GLK2-GFP* line and the two *abi4* mutants, which accumulated more *LHCB* transcripts than the wild type as etiolated seedlings (Figure 10), showed lower greening rates in the cotyledon greening assay (Figure 7). In seedlings of these genotypes, only the *abi4-t* mutant exhibited over-proliferated PTs compared to the wild type (Figure 11). This could be due to the fact that TEM sections only represent the three-dimensional etioplast ultrastructure at a two-dimensional level, and that different etioplasts show high structural variation.

We propose that the photobleaching of the *LHCB*-overexpressing etiolated seedlings used by Liu et al. (2018) can occur via two mechanisms. First, instead of an altered total Pchlide level, the lack of PLBs in these seedlings suggests a reduced photoactive-to-nonphotoactive Pchlide ratio, and this elevates the $^1O_2$ generation through Pchlide photosensitization. Second, the over-proliferated PTs have a large surface area. If the LHCB proteins are inserted into the PTs, yet the intact photosystems and the downstream electron transport chain have not been assembled, this may cause excessive light harvesting during illumination and $^1O_2$ generation (Macpherson et al., 1993). Amongst the different LHC isoforms, at least LHCB2 accumulates during seedling etiolation to a level detectable by western blotting (Armarego-Marriott et al., 2019), therefore, future studies can investigate whether the *35Spro*::*GLK2-GFP* line and the two *abi4* mutants accumulate more LHCB proteins than the wild type in etiolated seedlings. Additionally, we observed that some etioplasts showed an “inverted staining” (Figure 11a). Although such inverted staining has occurred in other etioplast studies before (Liang et al., 2022; Vinti et al., 2005), we presently cannot explain why in our experiment even seedlings of the same genotype were found to contain both normally stained and invertedly stained etioplasts.

3.1.3 Model on the antagonistic activities of GLKs and ABI4

In this study, we propose that the ABI4-GLK protein-protein interaction regulates the greening of etiolated seedlings in light, and we have included a model of this regulation

in Figure 18. Findings from this thesis and other reports underline the role of protein-protein interactions between nuclear proteins in regulating Pchlide biosynthesis and etioplast development (D. Chen et al., 2013; Liu et al., 2018; T. Sun et al., 2019). Although the yeast trans-activation assay suggests that ABI4 may inhibit the transcriptional activation capacity of GLK1 (Figure 16), our assays using transfected tobacco did not reveal any significant effect of ABI4 on the intrinsic transactivation capacity of GLK1 (Figure 17), nor on the binding and activation of the *LHCB2.2* promoter by GLK1 (Figure 15). These assays have the drawback that the protein abundance of ABI4 and GLK1 is not easily quantifiable. There is also the possibility that ABI4 is necessary, but not sufficient, to inhibit GLK1 in Arabidopsis. Therefore, future studies should perform transactivation assays by expressing tagged ABI4 and GLK1 proteins as effectors in Arabidopsis protoplasts. Transgenic Arabidopsis lines that overexpress ABI4 can also be used to examine whether ABI4 overexpression leads to inhibited Pchlide biosynthesis in etiolated seedlings.

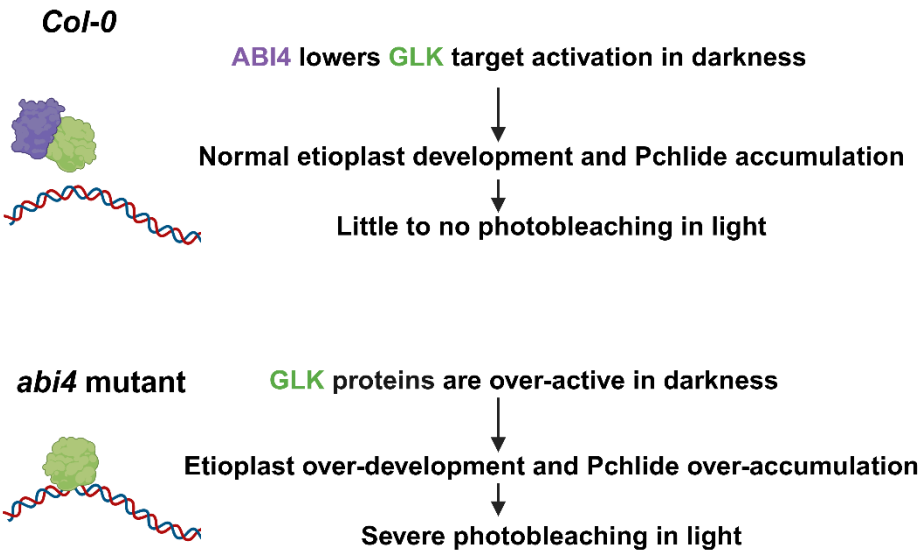

Figure 18. Model on the ABI4-GLK protein-protein interaction regulating greening of etiolated seedlings in light

ABI4 (in purple) is proposed as an inhibitor of GLK (in green) protein functions. Only one possible mechanism (ABI4 inhibits the DNA-binding of GLK) is displayed here. Figure was generated with BioRender.

Through the direct protein-protein interaction, ABI4 may reduce GLK protein stability, inhibit GLK dimerization, limit GLK binding to its target promoters and/or repress the transcriptional activation capacity of GLK. D. Zhang et al. (2021) reported that GLK1 and GLK2 are protected from proteasomal degradation after being phosphorylated by

BRASSINOSTEROID INSENSITIVE 2 (BIN2), and since BIN2 is inactivated by darkness, GLK proteins are less stable in darkness. N. Kim et al. (2023) revealed that REPRESSOR OF PHOTOSYNTHETIC GENES 1 (RPGE1) represses GLK1 homodimerization and DNA-binding, thereby limiting *PhANG*s activation in shade. Intriguingly, it was shown by M. Li et al. (2022) that treating plants with salicylic acid alters the GLK interactome, reduces the binding of GLK to *PhANG*s promoters, and enhances the stress response. These reports illustrate the various mechanisms whereby GLK protein activity can be modulated.

Since ABI4 physically interacts with GLK, a direct binding of ABI4 to GLK target promoters is not necessary for ABI4 to inhibit GLK target gene expression. Nevertheless, ABI4 has been shown to bind *LHCB* promoters in Y1H, *in vitro* and *in planta* (Guo et al., 2016; Koussevitzky et al., 2007; Z. W. Zhang et al., 2023). We therefore cannot exclude the possibility that ABI4 can regulate the expression of certain *PhANG*s independently of GLKs. Moreover, the antagonistic GLK-ABI4 interaction that we propose here may integrate another layer of complexity to a transcriptional factor network based on direct protein-protein interactions, including those between GLKs and HY5 (T. Zhang et al., 2024) and those between ABI4 and PIF4 (Luo et al., 2024; P. Song et al., 2024). The co-action of these transcriptional factors would serve to fine-tune the pigment biosynthesis and plastid development according to the needs of the developing seedling.

3.2 ABI4 and GLKs in chloroplast-to-nucleus retrograde signalling

ABI4 was first identified as a regulator of chloroplast-to-nucleus RS in a screen for *gun* (GENOMES UNCOUPLED) mutants (Koussevitzky et al., 2007). The authors showed that *abi4* seedlings accumulate more *LHCB1* mRNA than the wild type when grown on plates containing 220µg/ml (~540µM) lincomycin. However, the authors did not report the *LHCB1.2* mRNA level without lincomycin treatment. In contrast, Kacprzak et al. (2019) quantified *LHCB1.2* and *LHCB2.1* expression without lincomycin, and they found no difference between *abi4* mutants and the wild type. ABI4 and GLKs have been reported to regulate *LHCB1* mRNA level in opposite directions by Kakizaki et al. (2009), however, the authors defined ABI4 and GLKs as parallel pathways controlling *LHCB* expression.

In the present study, light-grown *abi4* mutant seedlings accumulated similar levels of *LHCB2.2* transcript as the wildtype, and the *abi4* mutant seedlings were as sensitive as the wildtype to 0.5 mM lincomycin (Figure 12), indicating that *abi4* mutants are not defective in chloroplast RS under these conditions. This agrees with previous reports in which the authors did not observe a *gun* phenotype in *abi4* mutants (Cottage & Gray, 2011; Kacprzak et al., 2019; Kerchev et al., 2011; G. Martin et al., 2016), whereby they concluded that ABI4 probably plays no role in chloroplast-to-nucleus RS. Interestingly, Leister & Kleine (2016) reported GLK overexpressors as *gun* mutants using *LHCB1.2* transcript level as the selection criterion, and this result has been supported by a recent study (Quevedo et al., 2025). It is therefore possible that *abi4* mutants may resemble the GLK overexpressors in certain assay conditions, leading to *LHCB* overexpression. Our findings suggest that the *gun* phenotype initially observed in *abi4* mutants was possibly caused by a specific *LHCB* overexpression in the *abi4* mutants without lincomycin. According to our model proposed here, ABI4 represses *LHCB* expression by inhibiting the function of GLKs, which may explain why both *abi4* mutant and GLK overexpressors were identified as *gun* mutants. Since *GLK1* expression is inhibited by lincomycin (G. Martin et al., 2016), while *ABI4* expression is induced by lincomycin (Kacprzak et al., 2019; X. Sun et al., 2011), future research in chloroplast-to-nucleus RS should investigate the nature of the retrograde signal(s) that regulate *GLK1* and *ABI4* expression.

3.3 Summary and outlook

This study confirmed the importance of limiting Pchlide biosynthesis and preventing precocious etioplast-to-chloroplast differentiation in etiolated Arabidopsis seedlings. When these processes are de-repressed, the dark-grown seedlings suffer from photobleaching and show a high mortality rate upon exposure to light. The key findings of the thesis are: 1. the identification of Arabidopsis ABI4 as a protein-protein interaction partner of GLK1 and GLK2; 2. GLK1 and GLK2 promote *PhANG*s transcription and Pchlide biosynthesis during seedling etiolation, while ABI4 plays an opposite role in these processes; 3. High GLK protein activity and low ABI4 protein activity in etiolated seedlings both result in high accumulation of singlet oxygen, high photobleaching rate and high mortality rate when these seedlings are exposed to light;

4. These opposite functions of ABI4 and GLK may result from the direct physical interaction between these proteins, meaning that ABI4 may act as a direct repressor of GLK proteins.

It remains unknown which domains or residues are involved in the ABI4-GLK interaction. Although our attempts to predict the ABI4-GLK protein complex structures were complicated by the presence of disordered domains (Figure 4), the quality of these structural predictions may improve in the future with the advancement of bioinformatic methods such as AlphaFold-Metainference (Brotzakis et al., 2025). Y2H and luciferase complementation assays can be utilized to investigate whether certain GLK domains are necessary for the ABI4-GLK interaction, the results of which may provide a clue as to the mechanism by which ABI4 inhibits GLK. As an ideal way to reveal the biological relevance of the ABI4-GLK interaction, ABI4 and GLK proteins should be mutated in a way that only disrupts the ABI4-GLK interaction without affecting their main function as TFs. However, this would be a very challenging task, since there may be residues in these proteins that are critical for both the intermolecular interaction and the TF functions, and the nature of the ABI4-GLK interaction may be multivalent (suggested by Figure 4), similar to other interactions between TFs (Trojanowski et al., 2022).

At the moment, the mechanism(s) by which ABI4 represses GLK activity is also not clear. Whether ABI4 reduces GLK protein stability can be assessed by comparing GLK protein abundance amongst a *35Spro*::*GLK-GFP* transgenic Arabidopsis line, a *35Spro*::*GLK-GFP 35Spro*::*ABI4-HA* line and a *35Spro*::*GLK-GFP abi4* line. These lines can also be used in CHIP-qPCR experiments with GFP antibodies to investigate whether ABI4 reduces GLK binding to its target promoters. Tagged ABI4 and GLK proteins can be produced recombinantly in *E. coli* to test whether ABI4 reduces GLK dimerization, and these recombinant proteins can be used in electrophoretic mobility shift assays (EMSAs) with GLK target DNA fragments to test the effect of ABI4 on the DNA-binding capacity of GLK. Transient expression systems in Arabidopsis protoplasts would also be suitable for testing these hypotheses in the native environment of these proteins.

The present study revealed that ABI4 and GLKs regulate the chlorophyll biosynthetic pathway antagonistically, and this regulation occurs specifically in the etiolated

seedlings (Figure 7) and not in light-grown seedlings (Figure 5). Nonetheless, it cannot be excluded that ABI4 may repress GLK activity for other purposes, such as promoting leaf senescence (Kang et al., 2025) and generating shade avoidance responses (N. Kim et al., 2023), wherein limiting chloroplast activities becomes necessary. Moreover, orthologues of ABI4 and GLK exist in both angiosperms and gymnosperms (Gregorio et al., 2014; Hernández-Verdeja & Lundgren, 2024). If the ABI4-GLK interaction also occurs in gymnosperms, it will be interesting to study the biological function of such an interaction, because the photooxidative damage caused by Pchlide photosensitization upon light exposure is unlikely to be a major problem for gymnosperm seedlings due to the action of their light-independent POR proteins. Therefore, future research can further investigate the biological relevance of the ABI4-GLK interaction in Arabidopsis and other taxa.

4 Materials and Methods

4.1 Materials

4.1.1 Chemicals and media

Chemicals and media used in this thesis are listed in Table 3, solvents are Milli-Q water unless stated otherwise.

Table 3. Chemicals and media used in this thesis

For Phusion PCR	
10x Phusion reaction buffer	200 mM Tris, adjusted to pH 8.8 with HCl 100 mM $(NH_4)2SO4$ 100 mM KCl 1 % (v/v) Triton X-100 1 mg/ml BSA 20 mM $MgSO_4$
For agarose gel electrophoresis	
50x TAE buffer	242 g/l Tris 57,1 ml/l acetic acid (anhydrous) 100 ml/l 0,5 M EDTA (pH 8,0)
For crude DNA extraction from plant	
DNA Extraction buffer	200 mM Tris/HCl pH 7.5 250 mM NaCl 25 mM EDTA 0.5 % SDS
For Y2H His growth assay	
SD medium	6.7 g/l nitrogen base without amino acids 40 mg/l adenine hemisulfate 0.7 g/l drop-out supplement 24 g/l agar (Difco) Adjust to pH 5.8 with KOH 20 g/l sterilized glucose solution added after autoclaving
3-AT stock solution	84.08 g/l 3-amino-1,2,4-triazole in H_2O (1M)
For growing *E. coli* during cloning	
LB medium	10 g/l tryptone 5 g/l yeast extract 24 g/l agar (Difco) – for agar plates 10 g/l NaCl
For tobacco infiltration	
MES washing buffer	100 mM 2-(N-morpholino) ethanesulfonic acid (MES) in water adjusted to pH 5.6 (filter sterlized) 100mM MgCl2 in water (autoclaved) freshly prepared 3 mg/ml acetosyringone in 70% EtOH

For luciferase complementation assay in tobacco	
Luciferin solution	15.92 mg D-Luciferin 2.5 µL Triton X-100 Water to 10 ml
For growing Arabidopsis on plates	
MS agar	4.4 g/l MS salt with modified vitamins (Duchefa) 10 g/l agar (Serva) Adjust pH to 5.8 with KOH
For TEM experiment	
0.2 M Phosphate buffer	100 mM Na_2HPO_4 100 mM NaH_2PO_4 Adjust pH to 7.4
Fixation buffer	2.5% glutaraldehyde 4% paraformaldehyde (PFA) in 0.1 M phosphate buffer
Osmium solution	1% OsO_4 2 mM $CaCl_2$ 0.8% potassium ferricyanide In 0.1 M phosphate buffer
For ONPG assay in yeast	
Z-buffer	10.7 g/l Na_2HPO_4 x 2 H_2O 5.5 g/l NaH_2PO_4 x H_2O 0.75 g/l KCl 0.246 g/l $MgSO_4$ x 7 H_2O

4.1.2 Kits and enzymes

Kits and enzymes used in this thesis are listed in Table 4.

Table 4. Kits and Enzymes used in this thesis

Name	Manufacturer
NucleoSpin® Gel and PCR Clean-up Kit	Macherey-Nagel, Düren, Germany
NucleoSpin® Plasmid Purification Kit	Macherey-Nagel, Düren, Germany
Zymoprep Yeast Plasmid Miniprep II	Zymo Research, Germany
Frozen EZ-yeast transformation kit	Zymo Research, Germany
NucleoSpin RNA Plant Mini Kit	Macherey-Nagel, Düren, Germany
GoTaq® qPCR Master Mix	Promega
Dual-Luciferase® Reporter Assay System	Promega
Gateway™ LR Clonase™ II Enzyme mix	Invitrogen, Karlsruhe, Germany
Gateway™ BP Clonase™ II Enzyme mix	Invitrogen, Karlsruhe, Germany

ClonExpress II One Step Cloning Kit	Vazyme
In-Fusion Snap Assembly Master Mix	Takara Bio
Phusion DNA Polymerase	Produced in-house
PrimeSTAR GXL DNA Polymerase	Takara Bio
5X PrimeSTAR GXL buffer	Takara Bio
RevertAid H Minus Reverse Transcriptase	Thermo Fisher Scientific, Schwerte, Germany
FastDigest restriction enzymes	Thermo Fisher Scientific, Schwerte, Germany
T4 DNA ligase	Thermo Fisher Scientific, Schwerte, Germany
T4 DNA ligase buffer	Thermo Fisher Scientific, Schwerte, Germany

4.1.3 Oligonucleotides

Oligonucleotides were purchased from Sigma Aldrich (Munich, Germany). They are listed in Table 5.

Table 5. Oligonucleotides used in this thesis

For dCAPS	
abi4-1-AluI-F	CTCAACTTAACCCCTTCGTCTCCTTC
abi4-1-AluI-R	GGGATACCGTACGGACCAAAGTTAG
For cloning Y2H constructs	
pENTR3C-GLK1$_{\Delta 1\text{-}154}$-F	ACTGGATCCGGTACCGAATTcAAAGTGGATTGGACACCAGAGC
pENTR3C-GLK1$_{\Delta 1\text{-}154}$-R	CTCGAGTGCGGCCGCGAATTTCAGGCACAAGACGCGGTCG
pENTR3C-GLK2$_{\Delta 1\text{-}148}$-F	ACTGGATCCGGTACCGAATTCAAGGTGGATTGGACGCCGGA
pENTR3C-GLK2$_{\Delta 1\text{-}148}$-R	CTCGAGTGCGGCCGCGAATTTCAAGGAAGAGGAGGAACATTAGAAA
pENTR3C-ABI4$_{\Delta 188\text{-}289}$-F	ACTGGATCCGGTACCGAATTcATGGACCCTTTAGCTTCCCA
pENTR3C-ABI4$_{\Delta 188\text{-}289}$-R	CTCGAGTGCGGCCGCGAATTATAGAATTCCCCCAAGATGGGA
For cloning luciferase complementation assay constructs	
pCAMBIA1300-GLK1-nLUC-F	gacgagctcggtaccATGTTAGCTCTGTCTCCGGCG
pCAMBIA1300-GLK1-nLUC-R	gtacgagatctggtcgacGGCACAAGACGCGGTCG
pCAMBIA1300-GLK2-nLUC-F	ggggacgagctcggtaccATGTTAACTGTTTCTCCGGCTCCA

pCAMBIA1300-GLK2-nLUC-R	gcgtacgagatctggtcgacAGGAAGAGGAGGAACATTAGAAACTCC
pCambia1300-cLUC-ABI4-F	tacgcgtcccggggcggtaccATGGACCCTTTAGCTTCCCA
pCambia1300-cLUC-ABI4-R	acgaaagctctgcaggtcgacTTAATAGAATTCCCCCAAGATGG
For cloning tobacco dual-luciferase assay constructs	
pGreenII0800-LHCB2.2pro-F	GGCGAATTGGGTACCGGGCCcttgtaatttttaatttatttgatgaacca
pGreenII0800-LHCB2.2pro-R	AGTGGATCCCCCGGGCTGCAgtgattcgttgaaagagtttagtt
pENTR3C-GLK1-GAL4BD-F1	ACTGGATCCGGTACCGAATTcATGTTAGCTCTGTCTCCGGCGACA
pENTR3C-GLK1-GAL4BD-R1	atagaagacagtagcttcatGGCACCCGCCCCTGCTCCag
pENTR3C-GLK1-GAL4BD-F2	ctGGAGCAGGGGCGGGTGCCatgaagctactgtcttctatcg
pENTR3C-GLK1-GAL4BD-R2	CTCGAGTGCGGCCGCGAATTtcacgatacagtcaactgtctttg
pGreenII0800-6xUAS-F	GGCGAATTGGGTACCGGGCCgaaacgacaatctgatctctagcccat
pGreenII0800-6xUAS-R	AGTGGATCCCCCGGGCTGCAtgtcctctccaaatgaaatgaacttccttatataga
For cloning yeast transactivation assay constructs	
pGADT7-ABI4-w/oAD-F	agaaaggtcgaattgggtaccATGGACCCTTTAGCTTCCCA
pGADT7-ABI4-w/oAD-R	acgattcatctgcagctcgagTTAATAGAATTCCCCCAAGATGG
For qPCR	
ACT2-F	CAAGGCCGAGTATGATGAGG
ACT2-R	GAAACGCAGACGTAAGTAAAAAC
TUB2-F	GAGCCTTACAACGCTACTCTGTCTGTC
TUB2-R	CACCAGACATAGTAGCAGAAATCAAG
GLK1-F	CCGTATTTACCGACCGTAGCTACGAGA
GLK1-R	TACATCGTGTGATGCGGCGGCAGAG
GLK2-F	TGTGTGTAAGCAAGAGGGTGG
GLK2-R	CTACCCCTAATTGCTCCACCG
PORA-F	CCCTCTTCCCTCCTTTCCAG
PORA-R	GCTCCAATACACTCCCGACTTC
PORB-F	ACTTGCTCAGGTGGTGAGTG
PORB-R	CCACACTTTACGAGCCTTCT
HEMA1-F	GCTTCTTCTGATTCTGCGTC
HEMA1-R	GCTGTGTGAATACTAAGTCCAATC

CHLH-F	CATTGCTGACACTACAACTGC
CHLH-R	CTTCTCTATCTCACGAACTCCTTC
GUN4-F	CAATCTCACTTCGGACCAAC
GUN4-R	TTGAAACGGCAGATACGG
LHCB2.1-F	ACCCGGAGACATTCGCTAAGAAC
LHCB2.1-R	TGGATCAAGTTAGGGTTTCCGAGG
LHCB2.2-F	AGCAGATGGGCTATGTTGGGT
LHCB2.2-R	CTCAGCCAAGTTCAATGGGTCG
LHCB2.3-F	CGTCAAGTCTACTCCTCAGAGCATC
LHCB2.3-R	TAATATGCTTTGCGCGTGGATCAAG
LHCB3-F	GCCGGTTCACAAATCTTCTCCG
LHCB3-R	AGTAACTGGATCATCAGCGAGACC
LHCB6-F	TGGCTCGCTACCAGGAGATTTC
LHCB6-R	CAATTGGGTTCCAAGAAGCGACC

4.1.4 Plasmids

Plasmids used in this thesis are listed in Table 6.

Table 6. Plasmids used in this thesis

Name	Description	Reference/Source
For Y2H		
pENTR3C	Gateway entry vector	Invitrogen
pDEST32	Destination vector containing GAL4 DNA-binding domain (BD)	Invitrogen
pDEST22	Destination vector containing GAL4 activation domain (AD)	Invitrogen
pENTR3C_GLK1$_{\Delta 1\text{-}154}$	Entry vector with GLK1$_{\Delta 1\text{-}154}$	This study
pENTR3C_GLK2$_{\Delta 1\text{-}148}$	Entry vector with GLK2$_{\Delta 1\text{-}148}$	This study
pDEST32_GLK1$_{\Delta 1\text{-}154}$	Destination vector with BD-GLK1$_{\Delta 1\text{-}154}$	This study
pDEST32_GLK2$_{\Delta 1\text{-}148}$	Destination vector with BD-GLK2$_{\Delta 1\text{-}148}$	This study
pDEST22_ABI4	Destination vector with AD-ABI4	(Paz-Ares et al., 2002)
pAS	Destination vector containing GAL4 DNA-binding domain (BD)	Clontech
pACT	Destination vector containing GAL4 activation domain (AD)	Clontech
pENTR3C_ABI4$_{\Delta 188\text{-}289}$	Entry vector with ABI4$_{\Delta 188\text{-}289}$	This study
pENTR3C_GLK1	Entry vector with GLK1 CDS	(Hansen, 2020, Master's Thesis)
pENTR3C_GLK2	Entry vector with GLK2 CDS	(Hansen, 2020, Master's Thesis)

pAS_ ABI4$_{\Delta 188\text{-}289}$	Destination vector with BD-ABI4$_{\Delta 188\text{-}289}$	This study
pACT_GLK1	Destination vector with AD-GLK1	(Hansen, 2020, Master's Thesis)
pACT_GLK2	Destination vector with AD-GLK2	(Hansen, 2020, Master's Thesis)
For FRET-FLIM assay		
pENSG-YFP	Destination vector for expressing YFP fusion protein under 35Spro	(Laubinger et al., 2006)
pAmarena	Destination vector for expressing mCherry fusion protein under 35Spro	(Steffens et al., 2014)
pDONR221_ABI4	Entry vector with ABI4	This study
pENSG-YFP_ABI4	Destination vector with YFP-ABI4	This study
pAmarena_GLK1	Destination vector with mCherry-GLK1	(Hansen, 2020, Master's Thesis)
pAmarena_GLK2	Destination vector with mCherry-GLK2	(Hansen, 2020, Master's Thesis)
For luciferase complementation assay		
pCAMBIA1300-nLUC	Destination vector with nLUC	(H. Chen et al., 2008)
pCAMBIA1300-cLUC	Destination vector with cLUC	(H. Chen et al., 2008)
pCAMBIA1300-GLK1-nLUC	Destination vector with GLK1-nLUC	This study
pCAMBIA1300-GLK2-nLUC	Destination vector with GLK2-nLUC	This study
pCambia1300-cLUC-ABI4	Destination vector with cLUC-ABI4	This study
For tobacco dual-luciferase assay		
pFAST-R02	Destination vector for expressing protein under 35Spro	(Shimada et al., 2010)
pFAST-R06	Destination vector for expressing GFP fusion protein under 35Spro	(Shimada et al., 2010)
pFAST-R02-GLK1	Destination vector with GLK1	This study
pFAST-R02-ABI4	Destination vector with ABI4	This study
pFAST-R02-GLK1-BD	Destination vector with GLK1-BD	This study
pGreenII0800-LUC	Reporter with Fluc and the normalizing Rluc	(R. P. Hellens et al., 2005)
UBQ10pro::GVG	Template with 6xUAS+mini35Spro	(Doumane et al., 2021)
pGreenII0800-LHCB2.2pro	Reporter with LHCB2.2pro driving Fluc	This study
pGreenII0800-6xUAS	Reporter with 6xUAS+mini35Spro driving Fluc	This study

For yeast transactivation assay		
pGBT9	Destination vector containing GAL4 DNA-binding domain (BD)	Takara Bio
pGADT7	Destination vector containing GAL4 activation domain (AD)	Takara Bio
pGBT9-GLK1	Destination vector with BD-GLK1	This study
pGADT7-YFP-w/oAD	Destination vector with YFP without AD	(Hansen, 2024, Doctoral Thesis)
pGADT7-ABI4-w/oAD	Destination vector with ABI4 without AD	This study

4.1.5 Bacteria and yeast strains

Bacteria and yeast strains used in this thesis are listed in Table 7. Empty Gateway vectors were propagated using *E. coli* strain DB3.1, while the Mach1 strain was used for cloning and propagating other vectors. For *Agrobacterium*-mediated expression pGreen-based vectors were transformed into Agro strain GV3101-pSOUP (R. Hellens et al., 2000), while other vectors were transformed into GV3101. The RK19 Agro was added for tobacco infiltration. For Y2H growth assays the yeast strain AH109 was used, while for transactivation assay the strain Y190 was used.

Table 7. Bacteria and yeast strains used in this thesis

Organism	Strain	Genotype and source
E. coli	DB3.1	F-gyrA462 endA Δ(sr1-recA) mcrB mrr hsdS20 (rB-,-mB-) supE44 ara-14 galK2lacY1 proA2 rpsL20 (SmR) xyl5 λ-leu mtl1 (Life Technologies, Karlsruhe, Germany)
E. coli	Mach1	F–Φ80lacZΔM15 ΔlacX74 hsdR(rK–,mK+) ΔrecA1398 endA1 tonA (Thermo Fisher Scientific, Schwerte, Germany)
A. tumefaciens	GV3101 -pSOUP	C58 (rifR) Ti pMP90 (pTiC58DT-DNA) (gentR) pSOUP Nopaline
A. tumefaciens	GV3101	C58 (rif R) Ti pMP90 (pTiC58DT-DNA) (gentR) Nopaline
A. tumefaciens	RK19	expressing anti-silencing 19K protein (Voinnet et al., 1999)
S. cerevisiae	AH109	MATa, trp1-901, leu2-3, 112, ura3-52, his3-200, gal4Δ, gal80Δ, LYS2::GAL1-HIS3, GAL2-ADE2, URA3::MEL1-lacZ (James et al., 1996)
S. cerevisiae	Y190	MATa ura3-52 his3-200 lys2-801 ade2-101 trp1-901 leu2-3, 112 gal4Δ gal80Δ LYS2::GAL1UAS-HIS3TATA-HIS3, URA3::GAL1UAS-GAL1TATA-lacz (Wade Harper et al., 1993)

4.1.6 Accession numbers

Arabidopsis gene sequences were retrieved from The Arabidopsis Information Resource (TAIR, https://www.arabidopsis.org/). Gene identifiers are listed in Table 8.

Table 8. Gene sequences involved in this thesis

Gene name	Identifier
ABI4	AT2G40220
GLK1	AT2G20570
GLK2	AT5G44190
PORA	AT5G54190
PORB	AT4G27440
HEMA1	AT1G58290
CHLH	AT5G13630
GUN4	AT3G59400
LHCB2.1	AT2G05100
LHCB2.2	AT2G05070
LHCB2.3	AT3G27690
LHCB3	AT5G54270
LHCB6	AT1G15820
ACT2	AT3G18780
TUB2	AT5G62690

4.1.7 Arabidopsis genotypes

All Arabidopsis lines used in this study were in the Columbia ecotype, and they are listed in Table 9.

Table 9. Arabidopsis lines used in this thesis

Line name	NASC ID	Reference	Selection
glk1 glk2	N9807	(Fitter et al., 2002)	Basta^{R}, Pale phenotype
35Spro::*GLK2-GFP*	N2107721	(Waters et al., 2008)	Kan^{R}, PCR
abi4-1	N8104	(R. R. Finkelstein et al., 1998) Gift from Dr. Kim Boutilier	dCAPS
abi4-t	N580095	(Shu et al., 2013)	PCR
abi4-103 gl1	N3838	(Laby et al., 2000)	-
gl1	N1688	(Oppenheimer et al., 1991)	-
glk1 glk2 abi4-1	-	This study	Pale phenotype dCAPS

4.2 Methods

4.2.1 Polymerase chain reaction (PCR)

All Phusion PCRs' reagents are listed in Table 10. The PCR program is listed in Table 11. Elongation time (X) was adjusted to the amplicon length (0.5 min/kb).

Table 10. Phusion PCR reagents

Component	Volume (µL)
H2O	37
Phusion polymerase	1
10X Phusion buffer	5
Primer fwd (10 µM)	2.5
Primer rv (10 µM)	2.5
Template	1
dNTPs (10 mM)	1

Table 11. Cycling conditions for Phusion PCRs

Temp. [˚C]	Time [min]	
95	3:00	
95	0:30	35-40x
55	0:30	
72	X	
72	2:00	
15	unlimited	

Reagents for PrimeSTAR PCRs are listed in Table 12. The PCR program is listed in Table 13. Elongation time (X) was adjusted to the amplicon length (1 min/kb).

Table 12. PrimeSTAR PCR reagents

Component	Volume (µL)
H2O	29.5
PrimeSTAR GXL polymerase	0.5
5X PrimeSTAR GXL Buffer	10
Primer fwd (10 µM)	2
Primer rv (10 µM)	2
gDNA Template	2
dNTPs (2.5 mM)	4

Table 13. Cycling conditions for PrimeSTAR PCRs

Temp. [˚C]	Time [min]	
98	3:00	
98	0:10	40X
55	0:15	
68	X	
68	2:00	
15	unlimited	

4.2.2 Molecular cloning

For Y2H, we generated the entry clones for BD-GLK1$_{\Delta 1\text{-}154}$, BD-GLK2$_{\Delta 1\text{-}148}$, BD-ABI4$_{\Delta 188\text{-}289}$ by first PCR-amplifying the coding sequences from Arabidopsis cDNA, then cloning into pENTR3C using the ClonExpress II kit. The entry clone for AD-ABI4 was obtained by isolating the pDEST22-ABI4 vector from the yeast REGIA library using the Zymoprep kit and mixing pDEST22-ABI4 with pDONR221 in a BP Gateway reaction. Then the destination plasmids were each cloned by mixing the respective entry clone with a destination vector in an LR Gateway reaction.

For FRET-FLIM, the destination plasmids were cloned via LR reactions. For luciferase complementation assay, all nLUC- and cLUC-expression vectors were generated by conventional digestion-ligation cloning using FastDigest enzymes and T4 DNA ligase. GLK1 and GLK2 were cloned into the pCambia1300-nLUC vector, and ABI4 was cloned into pCambia1300-cLUC, in all cases using the KpnI and SalI restriction sites.

For dual-luciferase assays in tobacco, the entry clone for GLK1-BD was made first by PCR-amplifying GLK1 and GAL4BD respectively, then these fragments were fused using overlap extension PCR. The GLK1-BD fragment was cloned into pENTR3C using the ClonExpress II kit. All pFAST effectors were cloned using LR reactions. For the reporters, LHCB2.2pro was amplified from Arabidopsis gDNA, whereas 6xUAS was amplified from a published UBQ10pro:GVG construct (Doumane et al., 2021), both using PrimeStar Polymerase. These two promoter fragments were each cloned into pGreenII0800 via the PstI and ApaI restriction sites using In-Fusion assembly.

For yeast transactivation assay, GLK1 was cloned into pGBT9 using a LR reaction. pGADT7 was digested with KpnI and Xho to remove the AD sequence, then ABI4 was cloned in using the ClonExpress II kit.

All PCRs were performed using Phusion polymerase, unless otherwise indicated. After the PCRs and restriction digests, DNA fragments were examined by agarose gel electrophoresis in 1xTAE buffer, and the correct fragments were purified using the NucleoSpin clean-up kit. Primers used for cloning are listed in Table 5.

4.2.3 *E. coli* transformation

After thawing chemically competent *E. coli* cells on ice, the plasmid(s) was added and the cells were subjected to: 1. incubation on ice for 15 min; 2. heat shock at 42 °C for 90 s; 3. incubation on ice for 1 min; 4. addition of 450 µL LB medium; 5. incubation for 30 min at 37 °C, shaking at 200 rpm; 6. plating on LB agar plates containing the corresponding antibiotics.

4.2.4 T4 Ligation cloning

Both backbone vectors and inserts were digested to produce compatible sticky ends, and the purified fragments were mixed in a 20 µl reaction with 2 µl 10x T4 buffer, 1 µl T4 ligase, 50 ng backbone and insert at a volume according to the backbone-to-insert size ratio. The reactions were either incubated at 4°C overnight or room temperature for 10 min, then transformed into *E. coli*.

4.2.5 Cloning with kits

Cloning with LR Clonase, BP Clonase, ClonExpress II and In-Fusion were performed according to the instructions by the manufacturers. A quarter of the recommended reaction volume was used.

4.2.6 Yeast two-hybrid assays

Gal4-based yeast two-hybrid assays, specifically the histidine growth selection assay, were performed. The BD- and AD-plasmids were transformed into the yeast strain AH109 using the Frozen-EZ Yeast Transformation II Kit. Transformants were then selected on Synthetic Drop-out auxotrophic plates (SD -L -W) containing 2% glucose. 10 co-transformed yeast colonies were suspended in sterile water and plated on both SD -L -W and SD -L -W -H plates containing 2% glucose. The yeast was grown at 30 °C, and 3 aminotriazole (3-AT) was used in the SD -L -W -H plates to prevent autoactivation.

4.2.7 FRET-FLIM assays

For the FRET-FLIM assays, leek epidermal cells were transiently transformed with different FRET constructs by particle bombardment as described by Ponnu et al. (2019). The FLIM experiments were also performed according to (Ponnu et al., 2019), with the difference that the curve-fitting processes were done in the software SymPhoTime 64 (PicoQuant).

4.2.8 *Agrobacterium tumefaciens* transformation

Electrocompetent *A. tumefaciens* cells were transformed by electroporation. 100 ng of plasmid DNA were added to 50 µl of competent cells, the cells were electroporated using a MicropulserTM electroporator (Bio-Rad Laboratories, Munich, Germany) set to the program “EC2” according to the manufacturer’s instructions. Subsequently, 600 µl LB medium was added to the cells and incubated at 28 °C, 200 rpm for 40 min. Finally, a brief centrifugation was performed to collect the cells, which were plated onto LB plates containing the appropriate antibiotics for selection. The plates were incubated at 28°C for 3-4 days.

4.2.9 Luciferase complementation imaging assays

Constructs expressing GLK1, GLK2 or ABI4 proteins fused to the C-terminal or N-terminal half of firefly luciferase were transformed into the *A. tumefaciens* strain *GV3101*, and different combinations of transformed *Agrobacterium* were infiltrated into *N. benthamiana* leaves. The infiltration procedure and luminescence imaging were performed as described in (Kreiss et al., 2023). The luminescence intensity was quantified, and the bright-field and luminescence images were overlapped using Fiji (Schindelin et al., 2012). Data were plotted without normalization.

4.2.10 ABI4-GLK complex structure prediction using AlphaFold 3

The structures of the protein complexes ABI4-GLK1 and ABI4-GLK2 were respectively predicted using the AlphaFold webserver (https://alphafoldserver.com/). Protein sequences were retrieved from TAIR and uploaded to the server without post-translational modifications. The modelled structures were downloaded, and the complexes were coloured according to subunit identities and predicted interacting residues using ChimeraX (Meng et al., 2023).

4.2.11 Plant growth conditions

For plate experiments, Arabidopsis seeds of roughly the same ages were surface-sterilized, stratified for 3 days in darkness at 4°C, then sown on Murashige and Skoog (MS) media containing 10 g/L Agar (SERVA) (without sucrose unless indicated otherwise). The sown seeds were exposed to white light (100 µmol m^{-2} s^{-1}) for 4 hours to induce germination, then left in a growth chamber either under the same white light or in darkness at 21°C. For analysis of chlorophyll content, plants were grown on soil in a climate-controlled walk-in growth chamber under long-day photoperiod (16 h of 100 µmol m^{-2} s^{-1} white light/8 h darkness) at 21 °C. The white light was generated by Lumilux L36W/840 cool white fluorescent tubes (Osram, Munich, Germany).

4.2.12 Generation and verification of the *glk1 glk2 abi4-1* mutant

The *glk1 glk2 abi4-1* triple mutant was generated by crossing *glk1 glk2* with *abi4-1*. From the F2 population, those homozygous for *glk1* and *glk2* were identified by their pale-green cotyledons. Genomic DNA was isolated individually from these plants and subjected to a dCAPS analysis for *abi4-1* homozygosity. A sequence encompassing the *abi4-1* locus was PCR-amplified using Phusion, and the PCR products were digested by AluI. Primers used for dCAPS analysis are listed in Table 5.

4.2.13 Chlorophyll, Pchlide and Chlide quantification

For chlorophyll quantification of plants grown in long-day photoperiod, 50-100 mg of leaf tissue per replicate was harvested and weighed, frozen in liquid nitrogen and ground to fine powder with a TissueLyser (Qiagen). 1.5 ml 80% acetone was added and samples were vortexed for 5 min then centrifuged at 13.200 rpm for 5 min. Finally, 100 µl of the supernatant was aliquoted into a transparent 96-well plate, and the absorbance was measured at 645 and 663 nm (Tecan Infinite 200 PRO). Total chlorophyll in mg per g fresh weight is calculated using the following formula: $((A_{663}*0.00802)+(A_{645}*0.0202))\times1.5$/fresh weight (Arnon, 1949). For chlorophyll quantification in the cotyledon greening assay, the procedure was kept the same, with the difference that 25 representative seedlings per replicate were harvested, frozen, ground, then added to 150 µl 80% acetone. Total chlorophyll in ng per seedling is calculated using the following formula: $((A_{663}*8.02)+(A_{645}*20.2))\times0.15/25$.

For Pchlide and Chlide quantification, 15 etiolated seedlings per replicate were harvested from MS agar plates in darkness. The samples were lysed and homogenized in 300 µl ice-cold 80% acetone, then centrifuged at 5,000 g for 2 min. 100 µl of the supernatant was aliquoted into a white 96-well plate. The fluorescence emission spectra of the sample were scanned from 600 to 700 nm using a spectrophotometer with an excitation wavelength of 440 nm (Tecan Infinite 200 PRO).

4.2.14 Cotyledon greening assays

Around 100 seeds sown on each replicate MS agar plate were stratified, grown for varied numbers of days in the dark, followed by 3 d in white light (100 µmol m^{-2} s^{-1}), all at 21°C. After 3 days, the germinated seedlings were classified into green/bleached by manually examining the phenotype of individual seedlings.

4.2.15 Fluorescence imaging of SOSG staining

Seedlings were incubated with 100 µM SOSG (Lumiprobe) in the dark for 20 min. The excess SOSG solution was then removed, and the seedlings were washed with sterile water. The SOSG signal was captured by laser excitation at 488 nm and emission at 525 nm. Chlorophyll autofluorescence was visualized by excitation at 610 nm and emission at 630 nm. The laser and detector settings were kept the same for all measurements. The imaging was performed using the Leica TCS SP8 (Leica microsystems). Image analyses were performed in Fiji (Schindelin et al., 2012).

4.2.16 Reverse transcription-quantitative PCR (RT-qPCR)

Total RNA was extracted from Arabidopsis seedlings (around 40 seedlings per replicate), using the NucleoSpin RNA Plant Mini Kit according to the manufacturer's instructions. For cDNA synthesis, 1 µg RNA, 2 µl 10 µM Oligo-dT primer and RNase-free water were added to a total volume of 27 µl. The reaction was incubated at 65°C for 5 min, then cooled on ice for 2 min. Subsequently, 8 µl 5 x RevertAid buffer, 4 µl 10 mM dNTPs and 1 µl RevertAid H Minus Reverse Transcriptase were added to the reaction, and the mix was incubated at 37°C for 5 min, at 42°C for 1 h for cDNA synthesis, then at 70°C for 5 min for heat-inactivation.

For qPCR analysis, 0.5 µl of cDNA was mixed with 0.5 µl 10 µM forward and reverse primers and 5 µl GoTaq qPCR Master Mix in a 10 µl reaction. The qPCR was

performed on a QuantStudio 5 Real-Time PCR System (Thermo Fisher) with the cycling conditions listed in Table 14. The relative transcript levels were calculated using the $2^{-\Delta\Delta Ct}$ method (Livak & Schmittgen, 2001), and *ACT2* was used for normalization in all qPCRs, except in the lincomycin experiment where *TUB2* was used. Primers used for qPCR are listed in Table 5.

Table 14. Cycling conditions for qPCRs

Temp. [˚C]	Time [min]	
50	2:00	
95	10:00	
95	0:15	40x dectection
60	1:00	
95	0:15	
60	1:00	

4.2.17 Transmission electron microscopy (TEM) of etiolated cotyledons

TEM was performed at the Center for Advanced Imaging (CAi) at Heinrich Heine University Düsseldorf with the help of Miriam Bäumers. Seeds sown on MS agar plates were first stratified, then kept in darkness at 21 °C for 5 days. On Day 1, whole seedlings (~30 per genotype) were fixed in the fixation buffer by vacuum infiltration for 1 h under a fume hood and stored overnight at 4 °C. On Day 2, samples were washed twice quickly and then three times for 5 min each with 0.1M phosphate buffer at room temperature. Post-fixation was carried out in osmium solution for 1 h in the dark on ice. Next, samples were washed seven times with 0.1 M phosphate buffer at RT. Seedlings were then dehydrated in 50% ethanol (1 h on ice), and subsequently in 70% ethanol (overnight at 4°C). On Day 3, en bloc staining was performed by incubating samples in 1% uranyl acetate in 70% ethanol for 1h in the dark at RT, then seedlings were washed twice quickly and then five times 5 min each in 70% ethanol on ice. Dehydration was carried out by graded ethanol series (80%, 90%, 96%, and 100%) for 30 min at each step (100% twice) on ice. Afterwards, the samples were washed with 100% acetone (2x30 min), followed by overnight rotation in an Epon™:acetone (1:3) mixture (Merck, Epoxy Embedding Medium kit, cat. no. 45359-1EA-F) at RT.

On Day 4, Epon™ infiltration was continued by rotating samples in progressively higher concentrations of Epon™:acetone (1:2 for 30 min, 1:1 for 1 h, 2:1 for 1 h, and 3:1 for 2 × 1 h), followed by incubation in pure Epon™ for 2 h. Fresh Epon™ was then

added for the overnight rotation at RT. On Day 5, seedlings were incubated in fresh EponTM for 2 h at RT, then the cotyledons were excised and embedded in moulds filled with EponTM, which were polymerized at 65°C for 72h. Ultrathin sections (70 nm) were prepared using an ultramicrotome (UC Enuity, Leica Microsystems). Sections were stained with 2% aqueous uranyl acetate for 5 min, rinsed with distilled water, and subsequently stained with Reynolds' lead citrate (Reynolds, 1963) for 4 min under CO_2-free conditions, followed by a final rinse with distilled water. The sections were examined with a transmission electron microscope (Zeiss EM 902) operated at 80 keV, and images were captured using a slow-scan CCD camera (Type 7899). Three seedlings per genotype were examined.

4.2.18 Retrograde signalling experiment

Seeds were sown on MS agar plates with or without 0.5 mM filter-sterilized Lincomycin. The plates were put directly in white light (100 µmol m^{-2} s^{-1}) for 5 d, after which total RNA was extracted from the seedlings.

4.2.19 Germination experiment

Seeds were sown on MS agar plates with or without 1.5 µM ABA. The plates were put directly in the growth chamber under the long-day photoperiod. After 7 days, the seeds were assessed for germination based on radicle protrusion.

4.2.20 Dual-luciferase transactivation assays in tobacco

Effector plasmids were transformed into the *A. tumefaciens* strain *GV3101*, and reporter plasmids were transformed into the strain *GV3101-pSOUP*. Overnight *A. tumefaciens* cultures were harvested by centrifugation at 5000 g for 15 min, resuspended in MES washing buffer to achieve an OD600 of 0.8. Equal parts of Agro expressing each effector and RK19 were mixed, and Agro expressing the reporter was added at 1/10 of the volume. This mixture was incubated at room temperature for 20 min to 2 h before infiltration into *N. benthamiana* leaves using a needleless syringe. The infiltrated tobacco plants were grown for 2–3 days under standard long-day conditions. Tissue samples were taken from the infiltrated area with an 8 mm biopsy skin punch (Mediware), immersed in 100 µl 1x lysis buffer (Dual-Luciferase Assay kit, Promega), and lysed in a 96-well plate using the flat side of a plastic pestle (Merck).

The LUC and REN luminescence were generated as per kit instructions (Dual-Luciferase Assay kit, Promega) and detected using a spectrophotometer (Tecan Infinite 200 PRO).

4.2.21 Yeast transactivation assay

Activator and effector plasmids were co-transformed into the yeast strain Y190 using the Frozen-EZ Yeast Transformation II Kit following the manufacturer's instructions. 1 µg of each plasmid was added and co-transformed into 10 µl of chemically competent Y190 cells. The cells were plated on SD -L W plates and incubated at 30°C for 3-4 days to select for transformed cells. For each replicate in the ONPG assay, 10 yeast colonies on the transformant plate were harvested and resuspended in 1 mL of H_2O. After vortexing, two spots of 15 µl suspension were dropped onto SD -L W plates. The plates were incubated at 30 °C for two days, then the cells were harvested and resuspended in 1 mL of Z-buffer. The OD_{600} was measured and adjusted to 1 in a total volume of 300 µl with Z-buffer. The samples were frozen in liquid nitrogen and disrupted by four freeze/thaw cycles, then each sample was split into two technical replicates of 150 µl each. Subsequently, 700 µl of Z-buffer containing 0.27 % (v/v) β-Mercaptoethanol was added, followed by 150 µl Z-buffer containing 4 g/l ONPG. The samples were incubated at 30 °C until a yellow color was visible (for 3-3.5 h). To stop the reaction, 400 µl 1 M Na_2CO_3 was added, and the incubation time was recorded. After a centrifugation at 13,000 rpm for 10 min, 150 µl supernatant was transferred into a transparent 96-well microplate. The OD_{420} was measured by a TECAN Infinite 200 microplate reader, and the β-galactosidase activity was calculated in Miller units using the following formula: $(1000*OD_{420})/(\text{incubation time in min}*\text{measured volume in µl}*OD_{600})$.

4.2.22 Statistical analyses

All statistical analyses were performed in the R environment (R Core Team, 2019), and the data were visualized using the ggplot2 package (Wickham, 2009). Each individual replicate is plotted as a dot, and summary statistics are plotted as indicated in each figure. For boxplots, the hinges on each box indicate the lower and upper quantiles, and the whiskers show the data range. The median is represented by a horizontal line within the box. No data were excluded from the analyses.

5. References

Abramson, J., Adler, J., Dunger, J., Evans, R., Green, T., Pritzel, A., Ronneberger, O., Willmore, L., Ballard, A. J., Bambrick, J., Bodenstein, S. W., Evans, D. A., Hung, C. C., O'Neill, M., Reiman, D., Tunyasuvunakool, K., Wu, Z., Žemgulytė, A., Arvaniti, E., … Jumper, J. M. (2024). Accurate structure prediction of biomolecular interactions with AlphaFold 3. *Nature*, *630*(8016), 493–500. https://doi.org/10.1038/S41586-024-07487-W

Alem, A. L., Ariel, F. D., Cho, Y., Hong, J. C., Gonzalez, D. H., & Viola, I. L. (2022). TCP15 interacts with GOLDEN2-LIKE 1 to control cotyledon opening in Arabidopsis. *Plant Journal*, *110*(3), 748–763. https://doi.org/10.1111/tpj.15701

Alonso, J. M., Stepanova, A. N., Leisse, T. J., Kim, C. J., Chen, H., Shinn, P., Stevenson, D. K., Zimmerman, J., Barajas, P., Cheuk, R., Gadrinab, C., Heller, C., Jeske, A., Koesema, E., Meyers, C. C., Parker, H., Prednis, L., Ansari, Y., Choy, N., … Ecker, J. R. (2003). Genome-wide insertional mutagenesis of *Arabidopsis thaliana*. *Science*, *301*(5633), 653–657. https://doi.org/10.1126/science.1086391

An, F., Zhao, Q., Ji, Y., Li, W., Jiang, Z., Yu, X., Zhang, C., Han, Y., He, W., Liu, Y., Zhang, S., Ecker, J. R., & Guo, H. (2010). Ethylene-induced stabilization of ETHYLENE INSENSITIVE3 and EIN3-LIKE1 is mediated by proteasomal degradation of EIN3 binding F-box 1 and 2 that requires EIN2 in Arabidopsis. *Plant Cell*, *22*(7), 2384–2401. https://doi.org/10.1105/tpc.110.076588

Apel, K., & Hirt, H. (2004). Reactive oxygen species: metabolism, oxidative stress, and signal transduction. *Annual Review of Plant Biology*, *55*, 373–399. https://doi.org/10.1146/ANNUREV.ARPLANT.55.031903.141701

Apel, K., Santel, H. -J, Redlinger, T. E., & Falk, H. (1980). The protochlorophyllide holochrome of barley (*Hordeum vulgare* L.): Isolation and characterization of the NADPH:protochlorophyllide oxidoreductase. *European Journal of Biochemistry*, *111*(1), 251–258. https://doi.org/10.1111/J.1432-1033.1980.TB06100.X,

Armarego-Marriott, T., Kowalewska, Ł., Burgos, A., Fischer, A., Thiele, W., Erban, A., Strand, D., Kahlau, S., Hertle, A., Kopka, J., Walther, D., Reich, Z., Schöttler, M.

A., & Bock, R. (2019). Highly resolved systems biology to dissect the etioplast-to-chloroplast transition in tobacco leaves. *Plant Physiology*, *180*(1), 654–681. https://doi.org/10.1104/PP.18.01432

Armstrong, G. A., Runge, S., Frick, G., Sperling, U., & Apel, K. (1995). Identification of NADPH:protochlorophyllide oxidoreductases A and B: a branched pathway for light-dependent chlorophyll biosynthesis in *Arabidopsis thaliana*. *Plant Physiology*, *108*(4), 1505–1517. https://doi.org/10.1104/PP.108.4.1505

Arnon, D. I. (1949). Copper enzymes in isolated chloroplasts. Polyphenoloxidase in Beta vulgaris. *Plant Physiology*, *24*(1), 1–15. https://doi.org/10.1104/PP.24.1.1

Arroyo, A., Bossi, F., Finkelstein, R. R., & León, P. (2003). Three genes that affect sugar sensing (abscisic acid insensitive 4, abscisic acid insensitive 5, and constitutive triple response 1) are differentially regulated by glucose in Arabidopsis. *Plant Physiology*, *133*(1), 231–242. https://doi.org/10.1104/PP.103.021089

Bai, Z., Zhang, J., Ning, X., Guo, H., Xu, X., Huang, X., Wang, Y., Hu, Z., Lu, C., Zhang, L., & Chi, W. (2020). A kinase–phosphatase–transcription factor module regulates adventitious root emergence in Arabidopsis root–hypocotyl junctions. *Molecular Plant*, *13*(8), 1162–1177. https://doi.org/10.1016/J.MOLP.2020.06.002

Barnes, S. A., Nishizawa, N. K., Quaggio, R. B., Whitelam, G. C., & Chua, N. H. (1996). Far-red light blocks greening of Arabidopsis seedlings via a phytochrome A-mediated change in plastid development. *Plant Cell*, *8*(4), 601–615. https://doi.org/10.1105/TPC.8.4.601,

Bar-On, Y. M., Phillips, R., & Milo, R. (2018). The biomass distribution on Earth. *Proceedings of the National Academy of Sciences of the United States of America*, *115*(25). https://doi.org/10.1073/pnas.1711842115

Bauer, D., Viczián, A., Kircher, S., Nobis, T., Nitschke, R., Kunkel, T., Panigrahi, K. C. S., Ádám, É., Fejes, E., Schäfer, E., & Nagy, F. (2004). Constitutive photomorphogenesis 1 and multiple photoreceptors control degradation of phytochrome interacting factor 3, a transcription factor required for light signaling in Arabidopsis. *Plant Cell*, *16*(6), 1433–1445. https://doi.org/10.1105/tpc.021568

Bossi, F., Cordoba, E., Dupré, P., Mendoza, M. S., Román, C. S., & León, P. (2009). The Arabidopsis ABA-INSENSITIVE (ABI) 4 factor acts as a central transcription activator of the expression of its own gene, and for the induction of ABI5 and SBE2.2 genes during sugar signaling. *Plant Journal*, *59*(3), 359–374. https://doi.org/10.1111/J.1365-313X.2009.03877.X

Brotzakis, Z. F., Zhang, S., Murtada, M. H., & Vendruscolo, M. (2025). AlphaFold prediction of structural ensembles of disordered proteins. *Nature Communications 2025 16:1*, *16*(1), 1–9. https://doi.org/10.1038/s41467-025-56572-9

Cackett, L., Luginbuehl, L. H., Schreier, T. B., Lopez-Juez, E., & Hibberd, J. M. (2022). Chloroplast development in green plant tissues: the interplay between light, hormone, and transcriptional regulation. *New Phytologist*, *233*(5), 2000–2016. https://doi.org/10.1111/nph.17839

Cao, M. J., Wang, Z., Wirtz, M., Hell, R., Oliver, D. J., & Xiang, C. Bin. (2013). SULTR3;1 is a chloroplast-localized sulfate transporter in *Arabidopsis thaliana*. *Plant Journal*, *73*(4), 593–604. https://doi.org/10.1111/tpj.12059

Chen, D., Xu, G., Tang, W., Jing, Y., Ji, Q., Fei, Z., & Lin, R. (2013). Antagonistic basic helix-loop-helix/bZIP transcription factors form transcriptional modules that integrate light and reactive oxygen species signaling in Arabidopsis. *Plant Cell*, *25*(5), 1657–1673. https://doi.org/10.1105/TPC.112.104869

Chen, H., Zou, Y., Shang, Y., Lin, H., Wang, Y., Cai, R., Tang, X., & Zhou, J. M. (2008). Firefly luciferase complementation imaging assay for protein-protein interactions in plants. *Plant Physiology*, *146*(2), 323–324. https://doi.org/10.1104/PP.107.111740

Chiang, Y. H., Zubo, Y. O., Tapken, W., Kim, H. J., Lavanway, A. M., Howard, L., Pilon, M., Kieber, J. J., & Eric Schaller, G. (2012). Functional characterization of the GATA transcription factors GNC and CGA1 reveals their key role in chloroplast development, growth, and division in Arabidopsis. *Plant Physiology*, *160*(1), 332–348. https://doi.org/10.1104/PP.112.198705

Cottage, A., & Gray, J. C. (2011). Timing the switch to phototrophic growth: a possible role of GUN1. *Plant Signaling & Behavior*, *6*(4), 578–582. https://doi.org/10.4161/PSB.6.4.14900

Demko, V., Pavlovič, A., Valková, D., Slováková, L., Grimm, B., & Hudák, J. (2009). A novel insight into the regulation of light-independent chlorophyll biosynthesis in *Larix decidua* and *Picea abies* seedlings. *Planta*, *230*(1), 165–176. https://doi.org/10.1007/S00425-009-0933-3

Doumane, M., Lebecq, A., Colin, L., Fangain, A., Stevens, F. D., Bareille, J., Hamant, O., Belkhadir, Y., Munnik, T., Jaillais, Y., & Caillaud, M. C. (2021). Inducible depletion of PI(4,5)P2 by the synthetic iDePP system in Arabidopsis. *Nature Plants*, *7*(5), 587–597. https://doi.org/10.1038/s41477-021-00907-z

Dubreuil, C., Jin, X., Barajas-López, J. de D., Hewitt, T. C., Tanz, S. K., Dobrenel, T., Schröder, W. P., Hanson, J., Pesquet, E., Grönlund, A., Small, I., & Strand, Å. (2018). Establishment of photosynthesis through chloroplast development is controlled by two distinct regulatory phases. *Plant Physiology*, *176*(2), 1199–1214. https://doi.org/10.1104/pp.17.00435

Eisner, N., Maymon, T., Sanchez, E. C., Bar-Zvi, D., Brodsky, S., Finkelstein, R., & Bar-Zvi, D. (2021). Phosphorylation of Serine 114 of the transcription factor ABSCISIC ACID INSENSITIVE 4 is essential for activity. *Plant Science*, *305*, 110847. https://doi.org/10.1016/J.PLANTSCI.2021.110847

Erdei, N., Barta, C., Hideg, É., & Böddi, B. (2005). Light-induced wilting and its molecular mechanism in epicotyls of dark-germinated pea (*Pisum sativum* L.) seedlings. *Plant and Cell Physiology*, *46*(1), 185–191. https://doi.org/10.1093/PCP/PCI012,

Finkelstein, R., Lynch, T., Reeves, W., Petitfils, M., & Mostachetti, M. (2011). Accumulation of the transcription factor ABA-insensitive (ABI)4 is tightly regulated post-transcriptionally. *Journal of Experimental Botany*, *62*(11), 3971–3979. https://doi.org/10.1093/jxb/err093

Finkelstein, R. R. (1994). Mutations at two new Arabidopsis ABA response loci are similar to the abi3 mutations. *Plant Journal*, *5*(6), 765–771. https://doi.org/10.1046/j.1365-313X.1994.5060765.x

Finkelstein, R. R., Wang, M. L., Lynch, T. J., Rao, S., & Goodman, H. M. (1998). The Arabidopsis abscisic acid response locus ABI4 encodes an APETALA 2 domain protein. *Plant Cell*, *10*(6), 1043–1054. https://doi.org/10.1105/tpc.10.6.1043

Fitter, D. W., Martin, D. J., Copley, M. J., Scotland, R. W., & Langdale, J. A. (2002). GLK gene pairs regulate chloroplast development in diverse plant species. *Plant Journal*, *31*(6), 713–727. https://doi.org/10.1046/j.1365-313X.2002.01390.x

Flors, C., Fryer, M. J., Waring, J., Reeder, B., Bechtold, U., Mullineaux, P. M., Nonell, S., Wilson, M. T., & Baker, N. R. (2006). Imaging the production of singlet oxygen in vivo using a new fluorescent sensor, Singlet Oxygen Sensor Green®. *Journal of Experimental Botany*, *57*(8), 1725–1734. https://doi.org/10.1093/JXB/ERJ181,

Frangedakis, E., Yelina, N. E., Billakurthi, K., Hua, L., Schreier, T., Dickinson, P. J., Tomaselli, M., Haseloff, J., & Hibberd, J. M. (2024). MYB-related transcription factors control chloroplast biogenesis. *Cell*, *187*(18), 4859-4876.e22. https://doi.org/https://doi.org/10.1016/J.CELL.2024.06.039

Giraud, E., van Aken, O., Ho, L. H. M., & Whelan, J. (2009). The transcription factor ABI4 is a regulator of mitochondrial retrograde expression of ALTERNATIVE OXIDASE1a. *Plant Physiology*, *150*(3), 1286–1296. https://doi.org/10.1104/PP.109.139782

Gregorio, J., Hernández-Bernal, A. F., Cordoba, E., & León, P. (2014). Characterization of evolutionarily conserved motifs involved in activity and regulation of the ABA-INSENSITIVE (ABI) 4 transcription factor. *Molecular Plant*, *7*(2), 422–436. https://doi.org/10.1093/mp/sst132

Guo, H., Feng, P., Chi, W., Sun, X., Xu, X., Li, Y., Ren, D., Lu, C., David Rochaix, J., Leister, D., & Zhang, L. (2016). Plastid-nucleus communication involves calcium-modulated MAPK signalling. *Nature Communications 2016 7:1*, *7*(1), 1–15. https://doi.org/10.1038/ncomms12173

Hall, L. N., Rossini, L., Cribb, L., & Langdale, J. A. (1998). GOLDEN 2: a novel transcriptional regulator of cellular differentiation in the maize leaf. *Plant Cell*, *10*(6), 925–936. https://academic.oup.com/plcell/article/10/6/925/5999425

Han, Y., Li, F., Wu, Y., Wang, D., Luo, G., Wang, X., Wang, X., Kuang, H., & Larkin, R. M. (2024). PSEUDO-ETIOLATION IN LIGHT proteins reduce greening by binding GLK transcription factors. *Plant Physiology*, *194*(3), 1722–1744. https://doi.org/10.1093/PLPHYS/KIAD641

Hellens, R., Mullineaux, P., & Klee, H. (2000). Technical Focus: A guide to Agrobacterium binary Ti vectors. *Trends in Plant Science*, *5*(10), 446–451. https://doi.org/10.1016/S1360-1385(00)01740-4

Hellens, R. P., Allan, A. C., Friel, E. N., Bolitho, K., Grafton, K., Templeton, M. D., Karunairetnam, S., Gleave, A. P., & Laing, W. A. (2005). Transient expression vectors for functional genomics, quantification of promoter activity and RNA silencing in plants. *Plant Methods*, *1*(13). https://doi.org/10.1186/1746-4811-1-13

Hernández-Verdeja, T., & Lundgren, M. R. (2024). GOLDEN2-LIKE transcription factors: A golden ticket to improve crops? *Plants People Planet*, *6*(1), 79–93. https://doi.org/10.1002/ppp3.10412

Huang, X., Zhang, X., Gong, Z., Yang, S., & Shi, Y. (2017). ABI4 represses the expression of type-A ARRs to inhibit seed germination in Arabidopsis. *Plant Journal*, *89*(2), 354–365. https://doi.org/10.1111/tpj.13389

Huijser, C., Kortstee, A., Pego, J., Weisbeek, P., Wisman, E., & Smeekens, S. (2000). The Arabidopsis *SUCROSE UNCOUPLED-6* gene is identical to *ABSCISIC ACID INSENSITIVE-4*: Involvement of abscisic acid in sugar responses. *Plant Journal*, *23*(5), 577–585. https://doi.org/10.1046/j.1365-313X.2000.00822.x

Huq, E., Al-Sady, B., Hudson, M., Kim, C., Apel, K., & Quail, P. H. (2004). Phytochrome-interacting factor 1 is a critical bHLH: Regulator of chlorophyll biosynthesis. *Science*, *305*(5692), 1937–1941. https://doi.org/10.1126/SCIENCE.1099728

Hwang, Y., Han, S., Yoo, C. Y., Hong, L., You, C., Le, B. H., Shi, H., Zhong, S., Hoecker, U., Chen, X., & Chen, M. (2022). Anterograde signaling controls plastid

transcription via sigma factors separately from nuclear photosynthesis genes. *Nature Communications*, *13*(1), 1–16. https://doi.org/10.1038/s41467-022-35080-0

James, P., Halladay, J., & Craig, E. A. (1996). Genomic libraries and a host strain designed for highly efficient two-hybrid selection in yeast. *Genetics*, *144*(4), 1425–1436. https://doi.org/10.1093/GENETICS/144.4.1425

Jenkins, M. T. (1926). A second gene producing golden plant color in maize. *The American Naturalist*, *60*(670), 484–488. http://www.jstor.org/stable/2456413

Kachroo, P., Burch-Smith, T. M., & Grant, M. (2021). An emerging role for chloroplasts in disease and defense. *Annual Review of Phytopathology*, *59*, 423–445. https://doi.org/10.1146/annurev-phyto-020620-115813

Kacprzak, S. M., Mochizuki, N., Naranjo, B., Xu, D., Leister, D., Kleine, T., Okamoto, H., & Terry, M. J. (2019). Plastid-to-nucleus retrograde signalling during chloroplast biogenesis does not require ABI4. *Plant Physiology*, *179*(1), 18–23. https://doi.org/10.1104/pp.18.01047

Kakizaki, T., Matsumura, H., Nakayama, K., Che, F. S., Terauchi, R., & Inaba, T. (2009). Coordination of plastid protein import and nuclear gene expression by plastid-to-nucleus retrograde signaling. *Plant Physiology*, *151*(3), 1339–1353. https://doi.org/10.1104/pp.109.145987

Kang, M. H., Lee, J., Kim, J., Mohammad, H. B., Park, J., Jung, H. J., Kim, S., Lee, H., Yang, S. W., Kwak, J. M., Kim, M. S., Lee, J. C., & Lim, P. O. (2025). The chloroplast-targeted long noncoding RNA CHLORELLA mediates chloroplast functional transition across leaf ageing via anterograde signalling. *Nature Plants*. https://doi.org/10.1038/S41477-025-02129-Z

Kawamoto, N., & Morita, M. T. (2022). Gravity sensing and responses in the coordination of the shoot gravitropic setpoint angle. *New Phytologist*, *236*(5), 1637–1654. https://doi.org/10.1111/NPH.18474

Kerchev, P. I., Pellny, T. K., Vivancos, P. D., Kiddle, G., Hedden, P., Driscoll, S., Vanacker, H., Verrier, P., Hancock, R. D., & Foyer, C. H. (2011). The transcription factor ABi4 is required for the ascorbic acid-dependent regulation of growth and

regulation of jasmonate-dependent defense signaling pathways in Arabidopsis. *Plant Cell*, *23*(9), 3319–3334. https://doi.org/10.1105/tpc.111.090100

Khan, I. U., Ali, A., Khan, H. A., Baek, D., Park, J., Lim, C. J., Zareen, S., Jan, M., Lee, S. Y., Pardo, J. M., Kim, W. Y., & Yun, D. J. (2020). PWR/HDA9/ABI4 complex epigenetically regulates ABA dependent drought stress tolerance in Arabidopsis. *Frontiers in Plant Science*, *11*. https://doi.org/10.3389/fpls.2020.00623

Kim, C., Meskauskiene, R., Zhang, S., Lee, K. P., Ashok, M. L., Blajecka, K., Herrfurth, C., Feussner, I., & Apela, K. (2012). Chloroplasts of Arabidopsis are the source and a primary target of a plant-specific programmed cell death signaling pathway. *Plant Cell*, *24*(7), 3026–3039. https://doi.org/10.1105/TPC.112.100479/DC1

Kim, K., Shin, J., Lee, S. H., Kweon, H. S., Maloof, J. N., & Choi, G. (2011). Phytochromes inhibit hypocotyl negative gravitropism by regulating the development of endodermal amyloplasts through phytochrome-interacting factors. *Proceedings of the National Academy of Sciences of the United States of America*, *108*(4), 1729–1734. https://doi.org/10.1073/PNAS.1011066108

Kim, N., Jeong, J., Kim, J., Oh, J., & Choi, G. (2023). Shade represses photosynthetic genes by disrupting the DNA binding of GOLDEN2-LIKE1. *Plant Physiology*, *191*(4), 2334–2352. https://doi.org/10.1093/PLPHYS/KIAD029

Klein, S., & Schiff, J. A. (1972). The correlated appearance of prolamellar bodies, protochlorophyll(ide) species, and the Shibata Shift during development of bean etioplasts in the dark. *Plant Physiology*, *49*(4), 619–626. https://doi.org/10.1104/pp.49.4.619

Kobayashi, K., Baba, S., Obayashi, T., Sato, M., Toyooka, K., Keränen, M., Aro, E. M., Fukaki, H., Ohta, H., Sugimoto, K., & Masuda, T. (2012). Regulation of root greening by light and auxin/cytokinin signaling in Arabidopsis. *Plant Cell*, *24*(3), 1081–1095. https://doi.org/10.1105/tpc.111.092254

Koussevitzky, S., Nott, A., Mockler, T. C., Hong, F., Sachetto-Martins, G., Surpin, M., Lim, J., Mittler, R., & Chory, J. (2007). Signals from chloroplasts converge to regulate nuclear gene expression. *Science*, *316*(5825), 715–719. https://doi.org/10.1126/science.1140516

Kreiss, M., Haas, F. B., Hansen, M., Rensing, S. A., & Hoecker, U. (2023). Co-action of COP1, SPA and cryptochrome in light signal transduction and photomorphogenesis of the moss *Physcomitrium patens*. *Plant Journal*, *114*(1), 159–175. https://doi.org/10.1111/TPJ.16128

Laby, R. J., Kincaid, M. S., Kim, D., & Gibson, S. I. (2000). The Arabidopsis sugar-insensitive mutants *sis4* and *sis5* are defective in abscisic acid synthesis and response. *Plant Journal*, *23*(5), 587–596. https://doi.org/10.1046/J.1365-313X.2000.00833.X

Langdale, J. A., & Kidner, C. A. (1994). *Bundle sheath defective*, a mutation that disrupts cellular differentiation in maize leaves. *Development*, *120*(3). https://doi.org/10.1242/dev.120.3.673

Laubinger, S., Marchal, V., Gentillhomme, J., Wenkel, S., Adrian, J., Jang, S., Kulajta, C., Braun, H., Coupland, G., & Hoecker, U. (2006). Arabidopsis SPA proteins regulate photoperiodic flowering and interact with the floral inducer CONSTANS to regulate its stability. *Development*, *133*(16), 3213–3222. https://doi.org/10.1242/DEV.02481

Lebedev, N., & Timko, M. P. (1999). Protochlorophyllide oxidoreductase B-catalyzed protochlorophyllide photoreduction in vitro: Insight into the mechanism of chlorophyll formation in light-adapted plants. *Proceedings of the National Academy of Sciences of the United States of America*, *96*(17), 9954–9959. https://doi.org/10.1073/PNAS.96.17.9954

Lee, J., Choi, B., Yun, A., Son, N., Ahn, G., Cha, J. Y., Kim, W. Y., & Hwang, I. (2021). Long-term abscisic acid promotes golden2-like1 degradation through constitutive photomorphogenic 1 in a light intensity-dependent manner to suppress chloroplast development. *Plant Cell and Environment*, *44*(9), 3034–3048. https://doi.org/10.1111/pce.14130

Lee, J. H., Deng, X. W., & Kim, W. T. (2006). Possible role of light in the maintenance of EIN3/EIL1 stability in Arabidopsis seedlings. *Biochemical and Biophysical Research Communications*, *350*(2), 484–491. https://doi.org/10.1016/j.bbrc.2006.09.074

Leister, D., & Kleine, T. (2016). Definition of a core module for the nuclear retrograde response to altered organellar gene expression identifies GLK overexpressors as *gun* mutants. *Physiologia Plantarum*, *157*(3), 297–309. https://doi.org/10.1111/PPL.12431

Li, B., Armarego-Marriott, T., Kowalewska, Ł., Thiele, W., Erban, A., Ruf, S., Kopka, J., Schöttler, M. A., & Bock, R. (2024). Membrane protein provision controls prothylakoid biogenesis in tobacco etioplasts. *The Plant Cell*, *36*(12), 4862–4880. https://doi.org/10.1093/PLCELL/KOAE259

Li, M., Lee, K. P., Liu, T., Dogra, V., Duan, J., Li, M., Xing, W., & Kim, C. (2022). Antagonistic modules regulate photosynthesis-associated nuclear genes via GOLDEN2-LIKE transcription factors. *Plant Physiology*, *188*(4), 2308–2324. https://doi.org/10.1093/plphys/kiab600

Li, P. C., Huang, J. G., Yu, S. W., Li, Y. Y., Sun, P., Wu, C. A., & Zheng, C. C. (2016). Arabidopsis YL1/BPG2 is involved in seedling shoot response to salt stress through ABI4. *Scientific Reports*, *6*. https://doi.org/10.1038/SREP30163

Li, X., Wang, P., Li, J., Wei, S., Yan, Y., Yang, J., Zhao, M., Langdale, J. A., & Zhou, W. (2020). Maize GOLDEN2-LIKE genes enhance biomass and grain yields in rice by improving photosynthesis and reducing photoinhibition. *Communications Biology*, *3*(1). https://doi.org/10.1038/s42003-020-0887-3

Li, Y., Cao, T., Guo, Y., Grimm, B., Li, X., Duanmu, D., & Lin, R. (2025). Regulatory and retrograde signaling networks in the chlorophyll biosynthetic pathway. *Journal of Integrative Plant Biology*, *67*(4), 887–911. https://doi.org/10.1111/JIPB.13837

Li, Y., Li, Y., Yao, X., Wen, Y., Zhou, Z., Lei, W., Zhang, D., & Lin, H. (2022). Nitrogen-inducible GLK1 modulates phosphate starvation response via the PHR1-dependent pathway. *New Phytologist*, *236*(5), 1871–1887. https://doi.org/10.1111/nph.18499

Liang, Z., Yeung, W. T., Ma, J., Mai, K. K. K., Liu, Z., Chong, Y. L. F., Cai, X., & Kang, B. H. (2022). Electron tomography of prolamellar bodies and their transformation

into grana thylakoids in cryofixed Arabidopsis cotyledons. *Plant Cell*, *34*(10), 3830–3843. https://doi.org/10.1093/PLCELL/KOAC205

Liu, X., Liu, R., Li, Y., Shen, X., Zhong, S., & Shi, H. (2018). EIN3 and PIF3 form an interdependent module that represses chloroplast development in buried seedlings. *Plant Cell*, *29*(12), 3051–3067. https://doi.org/10.1105/TPC.17.00508

Livak, K. J., & Schmittgen, T. D. (2001). Analysis of relative gene expression data using real-time quantitative PCR and the 2-ΔΔCT method. *Methods*, *25*(4), 402–408. https://doi.org/10.1006/meth.2001.1262

Loudya, N., Mishra, P., Takahagi, K., Uehara-Yamaguchi, Y., Inoue, K., Bogre, L., Mochida, K., & López-Juez, E. (2021). Cellular and transcriptomic analyses reveal two-staged chloroplast biogenesis underpinning photosynthesis build-up in the wheat leaf. *Genome Biology*, *22*(1). https://doi.org/10.1186/s13059-021-02366-3

Luo, X., Dai, Y., Xian, B., Xu, J., Zhang, R., Rehmani, M. S., Zheng, C., Zhao, X., Mao, K., Ren, X., Wei, S., Wang, L., He, J., Tan, W., Du, J., Liu, W., Yuan, S., & Shu, K. (2024). PIF4 interacts with ABI4 to serve as a transcriptional activator complex to promote seed dormancy by enhancing ABA biosynthesis and signaling. *Journal of Integrative Plant Biology*, *66*(5), 909–927. https://doi.org/10.1111/JIPB.13615/SUPPINFO

Luo, X., Dai, Y., Zheng, C., Yang, Y., Chen, W., Wang, Q., Chandrasekaran, U., Du, J., Liu, W., & Shu, K. (2021). The ABI4-RbohD/VTC2 regulatory module promotes reactive oxygen species (ROS) accumulation to decrease seed germination under salinity stress. *New Phytologist*, *229*(2), 950–962. https://doi.org/10.1111/nph.16921

Lv, R., Li, Z., Li, M., Dogra, V., Lv, S., Liu, R., Lee, K. P., & Kim, C. (2019). Uncoupled expression of nuclear and plastid photosynthesis-associated genes contributes to cell death in a lesion mimic mutant. *Plant Cell*, *31*(1), 210–230. https://doi.org/10.1105/tpc.18.00813

Macpherson, A. N., Telfer, A., Barber, J., & Truscott, T. G. (1993). Direct detection of singlet oxygen from isolated Photosystem II reaction centres. *Biochimica et*

Biophysica Acta (BBA) - Bioenergetics, *1143*(3), 301–309. https://doi.org/10.1016/0005-2728(93)90201-P

Maike Hansen. (2020). Master's Thesis: Functional and molecular analysis of the COP1/SPA complex in the moss *Physcomitrella patens*. University of Cologne.

Maike Hansen. (2024). Doctoral Thesis: Evolution of light signaling: Conservation of the COP1/SPA complex in *P. patens* and *M. endlicherianum*. University of Cologne.

Martin, G., Leivar, P., Ludevid, D., Tepperman, J. M., Quail, P. H., & Monte, E. (2016). Phytochrome and retrograde signalling pathways converge to antagonistically regulate a light-induced transcriptional network. *Nature Communications*, *7*. https://doi.org/10.1038/ncomms11431

Martin, W., Rujan, T., Richly, E., Hansen, A., Cornelsen, S., Lins, T., Leister, D., Stoebe, B., Hasegawa, M., & Penny, D. (2002). Evolutionary analysis of Arabidopsis, cyanobacterial, and chloroplast genomes reveals plastid phylogeny and thousands of cyanobacterial genes in the nucleus. *Proceedings of the National Academy of Sciences of the United States of America*, *99*(19), 12246–12251. https://doi.org/10.1073/PNAS.182432999

Masuda, S., Ikeda, R., Masuda, T., Hashimoto, H., Tsuchiya, T., Kojima, H., Nomata, J., Fujita, Y., Mimuro, M., Ohta, H., & Takamiya, K. I. (2009). Prolamellar bodies formed by cyanobacterial protochlorophyllide oxidoreductase in Arabidopsis. *Plant Journal*, *58*(6), 952–960. https://doi.org/10.1111/J.1365-313X.2009.03833.X

Masuda, T., Fusada, N., Oosawa, N., Takamatsu, K., Yamamoto, Y. Y., Ohto, M., Nakamura, K., Goto, K., Shibata, D., Shirano, Y., Hayashi, H., Kato, T., Tabata, S., Shimada, H., Ohta, H., & Takamiya, K. I. (2003). Functional analysis of isoforms of NADPH:Protochlorophyllide Oxidoreductase (POR), PORB and PORC, in *Arabidopsis thaliana*. *Plant and Cell Physiology*, *44*(10), 963–974. https://doi.org/10.1093/pcp/pcg128

Maymon, T., Eisner, N., & Bar-Zvi, D. (2022). The ABCISIC ACID INSENSITIVE (ABI) 4 transcription factor is stabilized by stress, ABA and phosphorylation. *Plants*, *11*(16). https://doi.org/10.3390/plants11162179

Mayta, M. L., Hajirezaei, M. R., Carrillo, N., & Lodeyro, A. F. (2019). Leaf senescence: the chloroplast connection comes of age. *Plants*, *8*(11). https://doi.org/10.3390/plants8110495

Meng, E. C., Goddard, T. D., Pettersen, E. F., Couch, G. S., Pearson, Z. J., Morris, J. H., & Ferrin, T. E. (2023). UCSF ChimeraX: Tools for structure building and analysis. *Protein Science*, *32*(11). https://doi.org/10.1002/pro.4792

Meskauskiene, R., Nater, M., Goslings, D., Kessler, F., Op den Camp, R., & Apel, K. (2001). FLU: A negative regulator of chlorophyll biosynthesis in *Arabidopsis thaliana*. *Proceedings of the National Academy of Sciences of the United States of America*, *98*(22), 12826–12831. https://doi.org/10.1073/PNAS.221252798

Monte, E., Tepperman, J. M., Al-Sady, B., Kaczorowski, K. A., Alonso, J. M., Ecker, J. R., Li, X., Zhang, Y., & Quail, P. H. (2004). The phytochrome-interacting transcription factor, PIF3, acts early, selectively, and positively in light-induced chloroplast development. *Proceedings of the National Academy of Sciences of the United States of America*, *101*(46), 16091–16098. https://doi.org/10.1073/PNAS.0407107101

Mu, X. R., Tong, C., Fang, X. T., Bao, Q. X., Xue, L. N., Meng, W. Y., Liu, C. Y., Loake, G. J., Cao, X. Y., Jiang, J. H., & Meng, L. S. (2022). Feedback loop promotes sucrose accumulation in cotyledons to facilitate sugar-ethylene signaling-mediated, etiolated-seedling greening. *Cell Reports*, *38*(11). https://doi.org/10.1016/j.celrep.2022.110529

Ni, F., Wu, L., Wang, Q., Hong, J., Qi, Y., & Zhou, X. (2017). Turnip Yellow Mosaic Virus P69 interacts with and suppresses GLK transcription factors to cause pale-green symptoms in Arabidopsis. *Molecular Plant*, *10*(5), 764–766. https://doi.org/10.1016/j.molp.2016.12.003

Oh, S., & Montgomery, B. L. (2014). Phytochrome-dependent coordinate control of distinct aspects of nuclear and plastid gene expression during anterograde

signaling and photomorphogenesis. *Frontiers in Plant Science*, *5*. https://doi.org/10.3389/fpls.2014.00171

Okamuro, J. K., Caster, B., Villarroel, R., Van Montagu, M., & Jofuku, K. D. (1997). The AP2 domain of APETALA2 defines a large new family of DNA binding proteins in Arabidopsis. *Proceedings of the National Academy of Sciences of the United States of America*, *94*(13), 7076–7081. https://doi.org/10.1073/pnas.94.13.7076

Oppenheimer, D. G., Herman, P. L., Sivakumaran, S., Esch, J., & Marks, M. D. (1991). A myb gene required for leaf trichome differentiation in Arabidopsis is expressed in stipules. *Cell*, *67*(3), 483–493. https://doi.org/10.1016/0092-8674(91)90523-2

Oyama, T., Shimura, Y., & Okada, K. (1997). The Arabidopsis *HY5* gene encodes a bZIP protein that regulates stimulus-induced development of root and hypocotyl. *Genes & Development*, *11*(22), 2983–2995. https://doi.org/10.1101/GAD.11.22.2983

Park, E., Kim, J., Lee, Y., Shin, J., Oh, E., Chung, W. Il, Jang, R. L., & Choi, G. (2004). Degradation of phytochrome interacting factor 3 in phytochrome-mediated light signaling. *Plant and Cell Physiology*, *45*(8), 968–975. https://doi.org/10.1093/pcp/pch125

Paz-Ares, J., Valencia, A., Costantino, P., Vittorioso, P., Davies, B., Gilmartin, P., Giraudat, J., Parcy, F., Reindl, A., Sablowski, R., Coupland, G., Martin, C., Angenent, G. C., Baumlein, H., Mock, H. P., Carbonero, P., Colombo, L., Tonelli, C., Engström, P., … Traas, J. (2002). REGIA, an EU project on functional genomics of transcription factors from *Arabidopsis thaliana*. *Comparative and Functional Genomics*, *3*(2), 102–108. https://doi.org/10.1002/cfg.146

Penfield, S., Li, Y., Gilday, A. D., Graham, S., & Graham, I. A. (2006). Arabidopsis ABA INSENSITIVE4 Regulates Lipid Mobilization in the Embryo and Reveals Repression of Seed Germination by the Endosperm. *Plant Cell*, *18*(8), 1887–1899. https://doi.org/10.1105/TPC.106.041277

Pengxin Yu. (2022). Master's Thesis: Identifying novel interaction partners of Arabidopsis GOLDEN2-LIKE (GLK) transcription factors. University of Cologne.

Pipitone, R., Eicke, S., Pfister, B., Glauser, G., Falconet, D., Uwizeye, C., Pralon, T., Zeeman, S. C., Kessler, F., & Demarsy, E. (2021). A multifaceted analysis reveals two distinct phases of chloroplast biogenesis during de-etiolation in Arabidopsis. *ELife*, *10*, 1–32. https://doi.org/10.7554/eLife.62709

Ponnu, J., Riedel, T., Penner, E., Schrader, A., & Hoecker, U. (2019). Cryptochrome 2 competes with COP1 substrates to repress COP1 ubiquitin ligase activity during Arabidopsis photomorphogenesis. *Proceedings of the National Academy of Sciences of the United States of America*, *116*(52), 27133–27141. https://doi.org/10.1073/PNAS.1909181116

Powell, A. L. T., Nguyen, C. V., Hill, T., Cheng, K. L. L., Figueroa-Balderas, R., Aktas, H., Ashrafi, H., Pons, C., Fernández-Muñoz, R., Vicente, A., Lopez-Baltazar, J., Barry, C. S., Liu, Y., Chetelat, R., Granell, A., Van Deynze, A., Giovannoni, J. J., & Bennett, A. B. (2012). Uniform ripening encodes a Golden 2-like transcription factor regulating tomato fruit chloroplast development. *Science*, *336*(6089), 1711–1715. https://doi.org/10.1126/science.1222218

Quevedo, M., Kubalová, I., Brun, A., Cervela-Cardona, L., Monte, E., & Strand, Å. (2025). Retrograde signals control dynamic changes to the chromatin state at photosynthesis-associated loci. *Nature Communications*, *16*(1). https://doi.org/10.1038/S41467-025-61831-W

R Core Team. (2019). R: A language and environment for statistical computing. In *R Foundation for Statistical Computing*.

Rauf, M., Arif, M., Dortay, H., Matallana-Ramírez, L. P., Waters, M. T., Gil Nam, H., Lim, P. O., Mueller-Roeber, B., & Balazadeh, S. (2013). ORE1 balances leaf senescence against maintenance by antagonizing G2-like-mediated transcription. *EMBO Reports*, *14*(4), 382–388. https://doi.org/10.1038/embor.2013.24

Reeves, W. M., Lynch, T. J., Mobin, R., & Finkelstein, R. R. (2011). Direct targets of the transcription factors ABA-Insensitive (ABI)4 and ABI5 reveal synergistic action by ABI4 and several bZIP ABA response factors. *Plant Molecular Biology*, *75*(4–5), 347–363. https://doi.org/10.1007/s11103-011-9733-9

Reynolds, E. S. (1963). The use of lead citrate at high pH as an electron-opaque stain in electron microscopy. *The Journal of Cell Biology*, *17*(1), 208–212. https://doi.org/10.1083/jcb.17.1.208

Richter, A. S., Nägele, T., Grimm, B., Kaufmann, K., Schroda, M., Leister, D., & Kleine, T. (2023). Retrograde signaling in plants: A critical review focusing on the GUN pathway and beyond. *Plant Communications*, *4*(1). https://doi.org/10.1016/j.xplc.2022.100511

Rolland, N., Curien, G., Finazzi, G., Kuntz, M., Maréchal, E., Matringe, M., Ravanel, S., & Seigneurin-Berny, D. (2012). The biosynthetic capacities of the plastids and integration between cytoplasmic and chloroplast processes. *Annual Review of Genetics*, *46*, 233–264. https://doi.org/10.1146/annurev-genet-110410-132544

Rossini, L., Cribb, L., Martin, D. J., & Langdale, J. A. (2001). The maize *Golden2* gene defines a novel class of transcriptional regulators in plants. *Plant Cell*, *13*, 1231–1244. https://doi.org/10.1105/tpc.13.5.1231

Safi, A., Medici, A., Szponarski, W., Ruffel, S., Lacombe, B., & Krouk, G. (2017). The world according to GARP transcription factors. *Current Opinion in Plant Biology*, *39*, 159–167. https://doi.org/10.1016/j.pbi.2017.07.006

Schindelin, J., Arganda-Carreras, I., Frise, E., Kaynig, V., Longair, M., Pietzsch, T., Preibisch, S., Rueden, C., Saalfeld, S., Schmid, B., Tinevez, J. Y., White, D. J., Hartenstein, V., Eliceiri, K., Tomancak, P., & Cardona, A. (2012). Fiji: An open-source platform for biological-image analysis. *Nature Methods*, *9*(7), 676–682. https://doi.org/10.1038/NMETH.2019

Shibata, K. (1957). Spectroscopic studies on chlorophyll formation in intact leaves. *Journal of Biochemistry*, *44*(3), 147–173. https://doi.org/10.1093/oxfordjournals.jbchem.a126741

Shimada, T. L., Shimada, T., & Hara-Nishimura, I. (2010). A rapid and non-destructive screenable marker, FAST, for identifying transformed seeds of Arabidopsis thaliana. *Plant Journal*, *61*(3), 519–528. https://doi.org/10.1111/j.1365-313X.2009.04060.x

Shkolnik-Inbar, D., Adler, G., & Bar-Zvi, D. (2013). ABI4 downregulates expression of the sodium transporter HKT1;1 in Arabidopsis roots and affects salt tolerance. *Plant Journal*, *73*(6), 993–1005. https://doi.org/10.1111/tpj.12091

Shkolnik-Inbar, D., & Bar-Zvi, D. (2010). ABI4 mediates abscisic acid and cytokinin inhibition of lateral root formation by reducing polar auxin transport in Arabidopsis. *Plant Cell*, *22*(11), 3560–3573. https://doi.org/10.1105/tpc.110.074641

Shu, K., Chen, Q., Wu, Y., Liu, R., Zhang, H., Wang, S., Tang, S., Yang, W., & Xie, Q. (2016). ABSCISIC ACID-INSENSITIVE 4 negatively regulates flowering through directly promoting Arabidopsis *FLOWERING LOCUS C* transcription. *Journal of Experimental Botany*, *67*(1), 195–205. https://doi.org/10.1093/jxb/erv459

Shu, K., Zhang, H., Wang, S., Chen, M., Wu, Y., Tang, S., Liu, C., Feng, Y., Cao, X., & Xie, Q. (2013). ABI4 regulates primary seed dormancy by regulating the biogenesis of abscisic acid and gibberellins in Arabidopsis. *PLoS Genetics*, *9*(6). https://doi.org/10.1371/journal.pgen.1003577

Song, P., Yang, Z., Wang, H., Wan, F., Kang, D., Zheng, W., Gong, Z., & Li, J. (2024). Regulation of cryptochrome-mediated blue light signaling by the ABI4–PIF4 module. *Journal of Integrative Plant Biology*, *66*(11), 2412–2430. https://doi.org/10.1111/JIPB.13769

Song, Y., Feng, L., Alyafei, M. A. M., Jaleel, A., & Ren, M. (2021). Function of chloroplasts in plant stress responses. *International Journal of Molecular Sciences*, *22*(24). https://doi.org/10.3390/ijms222413464

Song, Y., Jiang, Y., Kuai, B., & Li, L. (2018). Circadian clock-associated 1 inhibits leaf senescence in Arabidopsis. *Frontiers in Plant Science*, *9*. https://doi.org/10.3389/fpls.2018.00280

Steffens, A., Jaegle, B., Tresch, A., Hülskamp, M., & Jakoby, M. (2014). Processing-body movement in Arabidopsis depends on an interaction between myosins and DECAPPING PROTEIN1. *Plant Physiology*, *164*(4), 1879–1892. https://doi.org/10.1104/PP.113.233031

Stephenson, P. G., Fankhauser, C., & Terry, M. J. (2009). PIF3 is a repressor of chloroplast development. *Proceedings of the National Academy of Sciences of*

the United States of America, *106*(18), 7654–7659. https://doi.org/10.1073/PNAS.0811684106

Sun, T., Hazra, A., Lui, A., Zeng, S., Wang, X., Rao, S., Owens, L. A., Fei, Z., Zhao, Y., Mazourek, M., Giovannoni, J. G., & Li, L. (2025). GLKs directly regulate carotenoid biosynthesis via interacting with GBFs in plants. *New Phytologist*, *246*(2), 645–665. https://doi.org/10.1111/NPH.20457

Sun, T., Li, L., Huang, X. Q., Chen, W. C., Kong, M. J., Zhou, C. F., Zhuang, Z., & Lu, S. (2019). ORANGE represses chloroplast biogenesis in etiolated Arabidopsis cotyledons via interaction with TCP14. *The Plant Cell*, *31*(12), 2996–3014. https://doi.org/10.1105/TPC.18.00290

Sun, X., Feng, P., Xu, X., Guo, H., Ma, J., Chi, W., Lin, R., Lu, C., & Zhang, L. (2011). A chloroplast envelope-bound PHD transcription factor mediates chloroplast signals to the nucleus. *Nature Communications*, *2*(1), 1–10. https://doi.org/10.1038/ncomms1486

Susek, R. E., Ausubel, F. M., & Chory, J. (1993). Signal transduction mutants of Arabidopsis uncouple nuclear CAB and RBCS gene expression from chloroplast development. *Cell*, *74*(5), 787–799. https://doi.org/10.1016/0092-8674(93)90459-4

Susila, H., Nasim, Z., Gawarecka, K., Jung, J.-Y., Jin, S., Youn, G., & Ahn, J. H. (2023). Chloroplasts prevent precocious flowering through a GOLDEN2-LIKE–B-BOX DOMAIN PROTEIN module. *Plant Communications*, *4*(3). https://doi.org/10.1016/j.xplc.2023.100515

Tachibana, R., Abe, S., Marugami, M., Yamagami, A., Akema, R., Ohashi, T., Nishida, K., Nosaki, S., Miyakawa, T., Tanokura, M., Kim, J. M., Seki, M., Inaba, T., Matsui, M., Ifuku, K., Kushiro, T., Asami, T., & Nakano, T. (2024). BPG4 regulates chloroplast development and homeostasis by suppressing GLK transcription factors and involving light and brassinosteroid signaling. *Nature Communications*, *15*(1), 1–20. https://doi.org/10.1038/s41467-023-44492-5

Tachibana, R., Akema, R., Yoshihara, A., Ujihara, C., Nishida, K., Ri, S., Yamagami, A., Miyakawa, T., Kobayashi, K., Tanaka, R., & Nakano, T. (2025). Dark-inducible

BGH2 suppresses GLK transcription factors and maintains plastid homeostasis to promote light adaptation. *Plant Cell*, *37*(8). https://doi.org/10.1093/PLCELL/KOAF180

Tamai, H., Iwabuchi, M., & Meshi, T. (2002). Arabidopsis GARP transcriptional activators interact with the Pro-rich activation domain shared by G-box-binding bZIP factors. *Plant Cell Physiol*, *43*(1), 99–107.

Tano, D. W., Kozlowska, M. A., Easter, R. A., & Woodson, J. D. (2023). Multiple pathways mediate chloroplast singlet oxygen stress signaling. *Plant Molecular Biology*, *111*(1–2), 167–187. https://doi.org/10.1007/S11103-022-01319-Z

Tokumaru, M., Adachi, F., Toda, M., Ito-Inaba, Y., Yazu, F., Hirosawa, Y., Sakakibara, Y., Suiko, M., Kakizaki, T., & Inaba, T. (2017). Ubiquitin-proteasome dependent regulation of the GOLDEN2-LIKE 1 transcription factor in response to plastid signals. *Plant Physiology*, *173*(1), 524–535. https://doi.org/10.1104/pp.16.01546

Triantaphylidès, C., Krischke, M., Hoeberichts, F. A., Ksas, B., Gresser, G., Havaux, M., Van Breusegem, F., & Mueller, M. J. (2008). Singlet oxygen is the major reactive oxygen species involved in photooxidative damage to plants. *Plant Physiology*, *148*(2), 960–968. https://doi.org/10.1104/PP.108.125690

Trojanowski, J., Frank, L., Rademacher, A., Mücke, N., Grigaitis, P., & Rippe, K. (2022). Transcription activation is enhanced by multivalent interactions independent of phase separation. *Molecular Cell*, *82*(10), 1878–1893. https://doi.org/10.1016/j.molcel.2022.04.017

Tu, X., Ren, S., Shen, W., Li, J., Li, Y., Li, C., Li, Y., Zong, Z., Xie, W., Grierson, D., Fei, Z., Giovannoni, J., Li, P., & Zhong, S. (2022). Limited conservation in cross-species comparison of GLK transcription factor binding suggested wide-spread cistrome divergence. *Nature Communications*, *13*(1). https://doi.org/10.1038/s41467-022-35438-4

Van Oosten, J. M., Gerbaud, A., Huijser, C., Dijkwel, P. P., Chua, N. H., & Smeekens, S. C. M. (1997). An Arabidopsis mutant showing reduced feedback inhibition of photosynthesis. *Plant Journal*, *12*(5), 1011–1020. https://doi.org/10.1046/j.1365-313X.1997.12051011.x

Vinti, G., Fourrier, N., Bowyer, J. R., & López-Juez, E. (2005). Arabidopsis *cue* mutants with defective plastids are impaired primarily in the photocontrol of expression of photosynthesis-associated nuclear genes. *Plant Molecular Biology*, *57*(3), 343–357. https://doi.org/10.1007/S11103-004-7867-8

Voinnet, O., Pinto, Y. M., & Baulcombe, D. C. (1999). Suppression of gene silencing: A general strategy used by diverse DNA and RNA viruses of plants. *Proceedings of the National Academy of Sciences of the United States of America*, *96*(24), 14147–14152. https://doi.org/10.1073/pnas.96.24.14147

Wade Harper, J., Adami, G. R., Wei, N., Keyomarsi, K., & Elledge, S. J. (1993). The p21 Cdk-interacting protein Cip1 is a potent inhibitor of G1 cyclin-dependent kinases. *Cell*, *75*(4), 805–816. https://doi.org/10.1016/0092-8674(93)90499-G

Wagner, D., Przybyla, D., Op Den Camp, R., Kim, C., Landgraf, F., Keun, P. L., Würsch, M., Laloi, C., Nater, M., Hideg, E., & Apel, K. (2004). The genetic basis of singlet oxygen-induced stress response of *Arabidopsis thaliana*. *Science*, *306*(5699), 1183–1185. https://doi.org/10.1126/SCIENCE.1103178

Wang, L., Leister, D., Guan, L., Zheng, Y., Schneider, K., Lehmann, M., Apel, K., & Kleine, T. (2020). The Arabidopsis SAFEGUARD1 suppresses singlet oxygen-induced stress responses by protecting grana margins. *Proceedings of the National Academy of Sciences of the United States of America*, *117*(12), 6918–6927. https://doi.org/10.1073/PNAS.1918640117

Wang, L., Tian, Y., Shi, W., Yu, P., Hu, Y., Lv, J., Fu, C., Fan, M., & Bai, M. Y. (2020). The miR396-GRFs module mediates the prevention of photo-oxidative damage by brassinosteroids during seedling de-etiolation in Arabidopsis. *The Plant Cell*, *32*(8), 2525–2542. https://doi.org/10.1105/TPC.20.00057

Wang, M., Lee, J., Choi, B., Park, Y., Sim, H. J., Kim, H., & Hwang, I. (2018). Physiological and molecular processes associated with long duration of ABA treatment. *Frontiers in Plant Science*, *9*. https://doi.org/10.3389/fpls.2018.00176

Wang, Z., Mao, Y., Liang, L., Pedro, G. C., Zhi, L., Li, P., & Hu, X. (2024). HFR1 antagonizes ABI4 to coordinate cytosolic redox status for seed germination under

high-temperature stress. *Physiologia Plantarum*, *176*(4), e14490. https://doi.org/10.1111/PPL.14490

Waters, M. T., Moylan, E. C., & Langdale, J. A. (2008). GLK transcription factors regulate chloroplast development in a cell-autonomous manner. *Plant Journal*, *56*(3), 432–444. https://doi.org/10.1111/j.1365-313X.2008.03616.x

Waters, M. T., Wang, P., Korkaric, M., Capper, R. G., Saunders, N. J., & Langdale, J. A. (2009). GLK transcription factors coordinate expression of the photosynthetic apparatus in Arabidopsis. *Plant Cell*, *21*(4), 1109–1128. https://doi.org/10.1105/tpc.108.065250

Wickham, Hadley. (2009). ggplot2 : Elegant graphics for data analysis. In *Journal of Statistical Software* (Issue July). Springer.

Woodson, J. D., Perez-Ruiz, J. M., & Chory, J. (2011). Heme synthesis by plastid ferrochelatase I regulates nuclear gene expression in plants. *Current Biology*, *21*(10), 897–903. https://doi.org/10.1016/j.cub.2011.04.004

Xian, B., Rehmani, M. S., Fan, Y., Luo, X., Zhang, R., Xu, J., Wei, S., Wang, L., He, J., Fu, A., & Shu, K. (2024). The ABI4-RGL2 module serves as a double agent to mediate the antagonistic crosstalk between ABA and GA signals. *New Phytologist*, *241*(6), 2464–2479. https://doi.org/10.1111/NPH.19533

Xu, X., Chi, W., Sun, X., Feng, P., Guo, H., Li, J., Lin, R., Lu, C., Wang, H., Leister, D., & Zhang, L. (2016). Convergence of light and chloroplast signals for de-etiolation through ABI4-HY5 and COP1. *Nature Plants*, *2*(6). https://doi.org/10.1038/NPLANTS.2016.66

Yamamoto, H., Kurumiya, S., Ohashi, R., & Fujita, Y. (2011). Functional evaluation of a nitrogenase-like protochlorophyllide reductase encoded by the chloroplast DNA of *Physcomitrella patens* in the cyanobacterium *Leptolyngbya boryana*. *Plant & Cell Physiology*, *52*(11), 1983–1993. https://doi.org/10.1093/PCP/PCR132

Yang, J., & Cheng, Q. (2004). Origin and evolution of the light-dependent protochlorophyllide oxidoreductase (LPOR) genes. *Plant Biology (Stuttgart, Germany)*, *6*(5), 537–544. https://doi.org/10.1055/S-2004-821270

Yang, Y., Yu, X., Song, L., & An, C. (2011). ABI4 activates DGAT1 expression in Arabidopsis seedlings during nitrogen deficiency. *Plant Physiology*, *156*(2), 873–883. https://doi.org/10.1104/PP.111.175950

Yeh, S. Y., Lin, H. H., Chang, Y. M., Chang, Y. L., Chang, C. K., Huang, Y. C., Ho, Y. W., Lin, C. Y., Zheng, J. Z., Jane, W. N., Ng, C. Y., Lu, M. Y., Lai, I. L., To, K. Y., Li, W. H., & Ku, M. S. B. (2022). Maize Golden2-like transcription factors boost rice chloroplast development, photosynthesis, and grain yield. *Plant Physiology*, *188*(1), 442–459. https://doi.org/10.1093/plphys/kiab511

Yu, B., Gruber, M. Y., Wei, S., Zhou, R., Hegedus, D., Khachatourians, G. G., & Hannoufa, A. (2016). Global gene expression and secondary metabolite changes in Arabidopsis thaliana ABI4 over-expression lines. *Botany*, *94*(8), 615–634. https://doi.org/10.1139/cjb-2016-0043

Yu, X., Li, L., Zola, J., Aluru, M., Ye, H., Foudree, A., Guo, H., Anderson, S., Aluru, S., Liu, P., Rodermel, S., & Yin, Y. (2011). A brassinosteroid transcriptional network revealed by genome-wide identification of BESI target genes in Arabidopsis thaliana. *Plant Journal*, *65*(4), 634–646. https://doi.org/10.1111/j.1365-313X.2010.04449.x

Zhang, D., Tan, W., Yang, F., Han, Q., Deng, X., Guo, H., Liu, B., Yin, Y., & Lin, H. (2021). A BIN2-GLK1 signaling module integrates brassinosteroid and light signaling to repress chloroplast development in the dark. *Developmental Cell*, *56*(3), 310–324. https://doi.org/10.1016/j.devcel.2020.12.001

Zhang, T., Zhang, R., Zeng, X. Y., Lee, S., Ye, L. H., Tian, S. L., Zhang, Y. J., Busch, W., Zhou, W. Bin, Zhu, X. G., & Wang, P. (2024). GLK transcription factors accompany ELONGATED HYPOCOTYL5 to orchestrate light-induced seedling development in Arabidopsis. *Plant Physiology*, *194*(4), 2400–2421. https://doi.org/10.1093/PLPHYS/KIAE002

Zhang, Z. W., Feng, L. Y., Cheng, J., Tang, H., Xu, F., Zhu, F., Zhao, Z. Y., Yuan, M., Chen, Y. E., Wang, J. H., Yuan, S., & Lin, H. H. (2013). The roles of two transcription factors, ABI4 and CBFA, in ABA and plastid signalling and stress responses. *Plant Molecular Biology*, *83*(4–5), 445–458. https://doi.org/10.1007/s11103-013-0102-8

Zhang, Z. W., Fu, Y. F., Yang, X. Y., Yuan, M., Zheng, X. J., Luo, X. F., Zhang, M. Y., Xie, L. B., Shu, K., Reinbothe, S., Reinbothe, C., Wu, F., Feng, L. Y., Du, J. B., Wang, C. Q., Gao, X. S., Chen, Y. E., Zhang, Y. Y., Li, Y., … Yuan, S. (2023). Singlet oxygen induces cell wall thickening and stomatal density reducing by transcriptome reprogramming. *Journal of Biological Chemistry*, *299*(12). https://doi.org/10.1016/J.JBC.2023.105481

Zhao, H. L., Chang, T. G., Xiao, Y., & Zhu, X. G. (2021). Potential metabolic mechanisms for inhibited chloroplast nitrogen assimilation under high CO2. *Plant Physiology*, *187*(3), 1812–1833. https://doi.org/10.1093/plphys/kiab345

Zhong, S., Shi, H., Xue, C., Wei, N., Guo, H., & Deng, X. W. (2014). Ethylene-orchestrated circuitry coordinates a seedling's response to soil cover and etiolated growth. *Proceedings of the National Academy of Sciences of the United States of America*, *111*(11), 3913–3920. https://doi.org/10.1073/PNAS.1402491111

Zhong, S., Zhao, M., Shi, T., Shi, H., An, F., Zhao, Q., & Guo, H. (2009). EIN3/EIL1 cooperate with PIF1 to prevent photo-oxidation and to promote greening of Arabidopsis seedlings. *Proceedings of the National Academy of Sciences of the United States of America*, *106*(50), 21431–21436. https://doi.org/10.1073/PNAS.0907670106

Zhou, M., Zhang, J., Shen, J., Zhou, H., Zhao, D., Gotor, C., Romero, L. C., Fu, L., Li, Z., Yang, J., Shen, W., Yuan, X., & Xie, Y. (2021). Hydrogen sulfide-linked persulfidation of ABI4 controls ABA responses through the transactivation of MAPKKK18 in Arabidopsis. *Molecular Plant*, *14*(6), 921–936. https://doi.org/10.1016/j.molp.2021.03.007

Zubo, Y. O., Blakley, I. C., Franco-Zorrilla, J. M., Yamburenko, M. V., Solano, R., Kieber, J. J., Loraine, A. E., & Schaller, G. E. (2018). Coordination of chloroplast development through the action of the GNC and GLK transcription factor families. *Plant Physiology*, *178*(1), 130–147. https://doi.org/10.1104/pp.18.00414

6. Supplement

The following figures show the dCAPS results, and independent repeats of some of the assays in the main text.

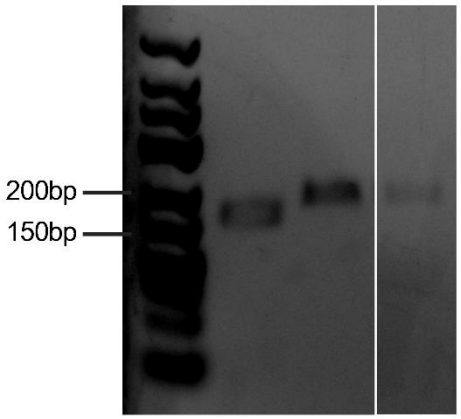

Figure S1. Verification of the *glk1 glk2 abi4-1* triple mutant by dCAPS
Samples were ran on a 3 % agarose gel at 100 V for 25 min. From left to right: GeneRuler low range DNA ladder; sample with *Col-0* gDNA; sample with *abi4-1* gDNA; sample with homozygous *glk1 glk2 abi4-1* gDNA. The *Col-0* fragment is predicted to be 25 bp smaller than the *abi4-1* fragment.

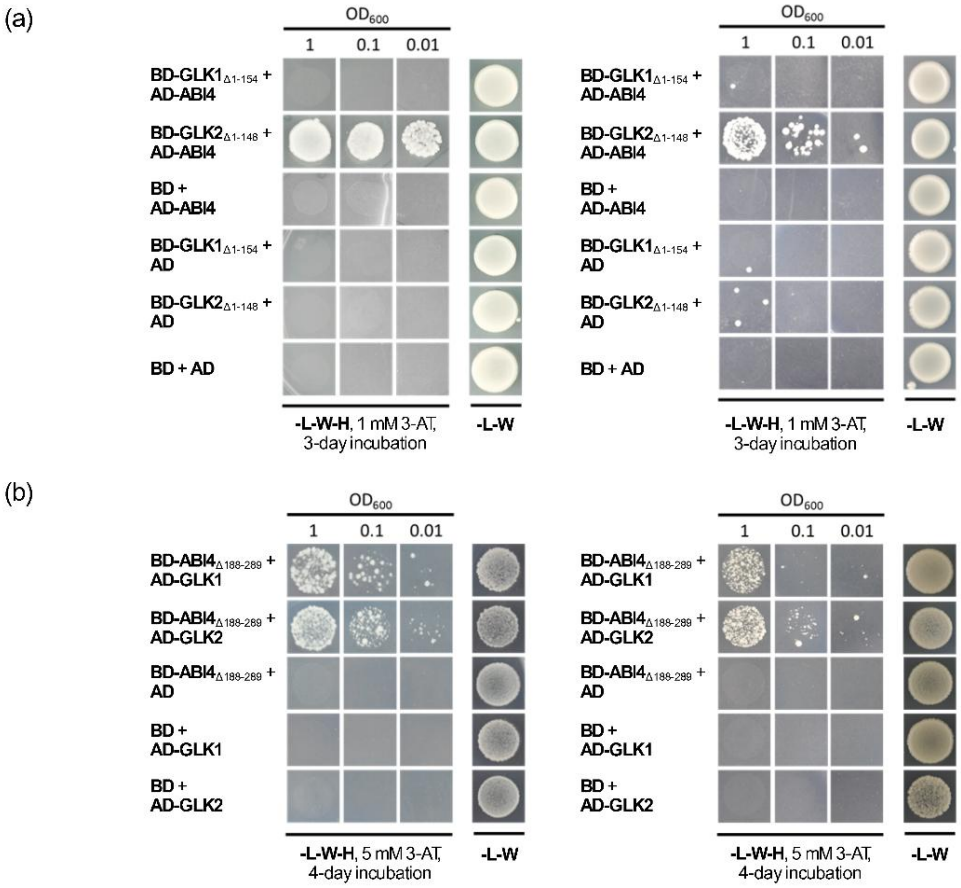

Figure S2. ABI4 physically interacts with GLK1 and GLK2 in Y2H
(a) GLK2$_{\Delta 1\text{-}154}$ interacts with ABI4. **(b)** ABI4$_{\Delta 188\text{-}289}$ interacts with full-length GLK1 and GLK2.

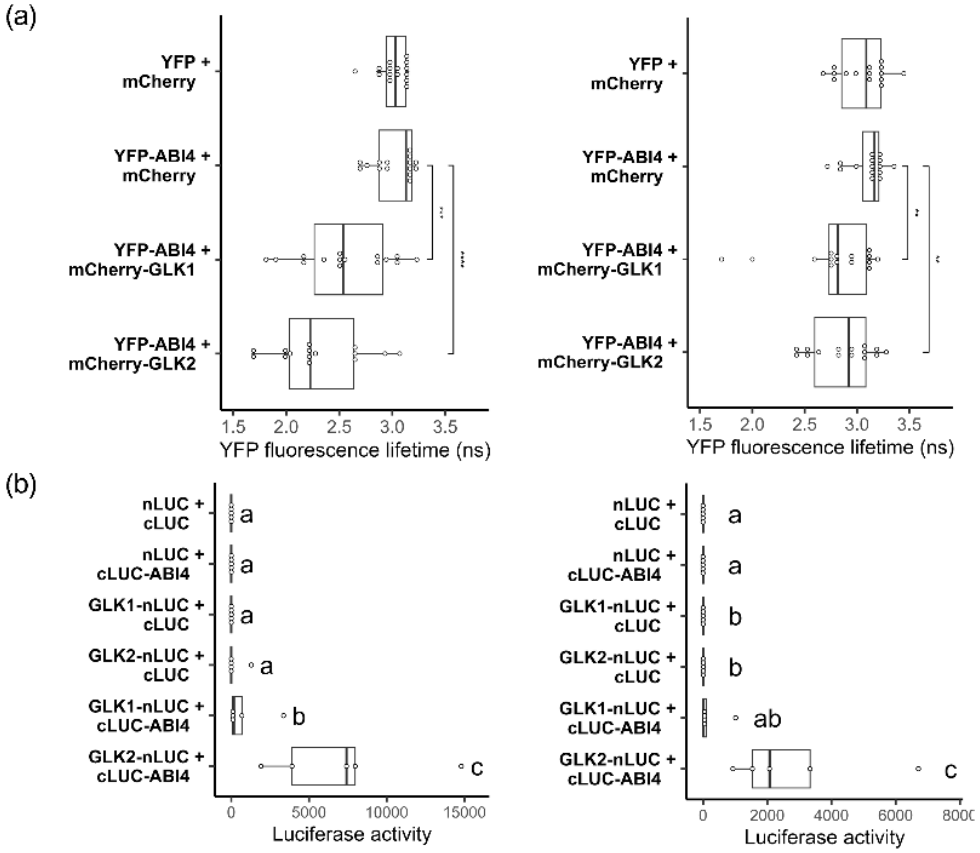

Figure S3. ABI4 physically interacts with GLK1 and GLK2 *in planta*
Data on (a) FRET-FLIM assays in bombarded leek epidermal cells and in (b) luciferase complementation assays in transfected tobacco

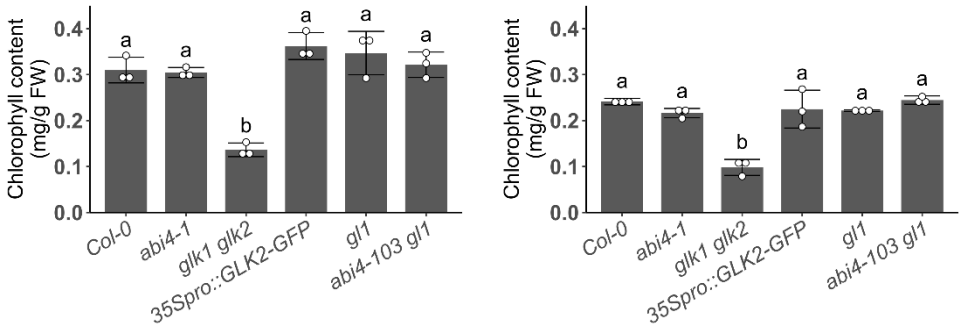

Figure S4. Chlorophyll content is not altered in light-grown *abi4* mutants

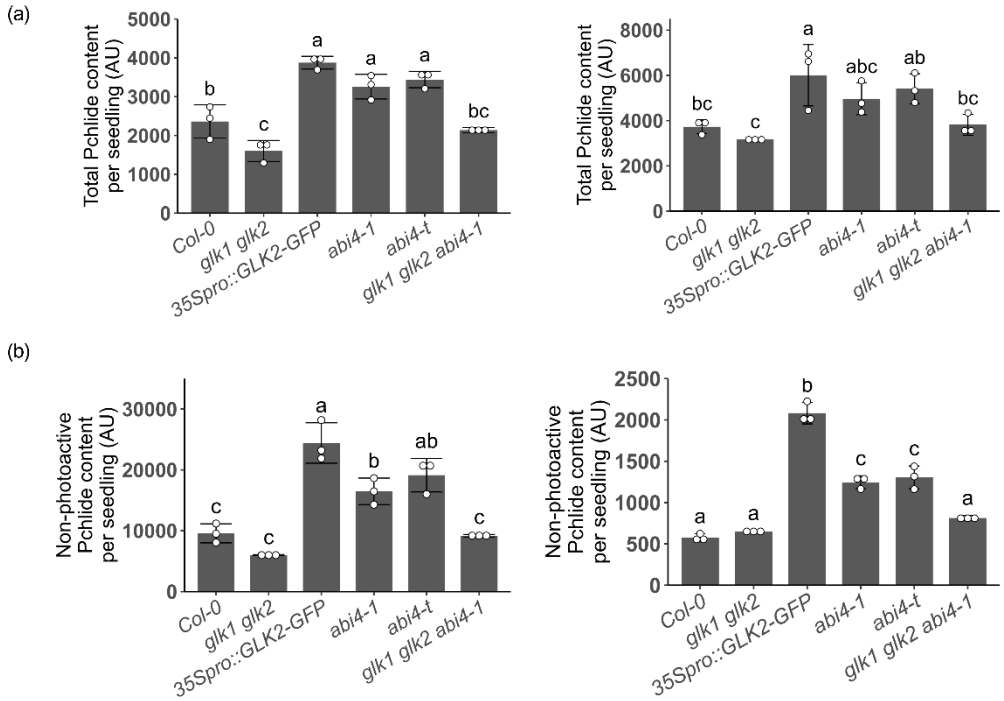

Figure S5. Etiolated *abi4* mutants overaccumulate Pchlide (a) and cannot efficiently convert all Pchlide into Chlide (b), and these phenotypes are dependent on *GLK1* and *GLK2*.

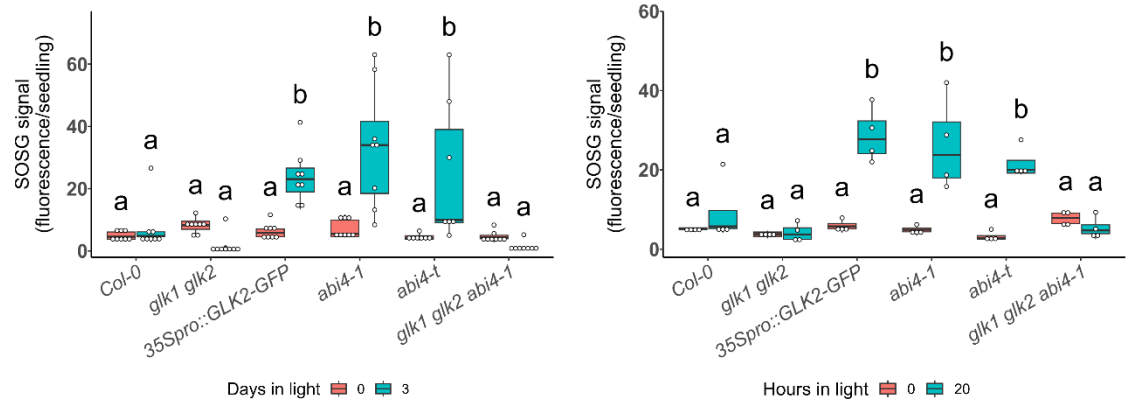

Figure S6. Etiolated, then light-exposed *abi4* mutant and *35Spro*::*GLK2-GFP* seedlings show high singlet oxygen ($^1O_2$) accumulation

Singlet Oxygen Sensor Green fluorescence (SOSG, dectecting $^1O_2$) in 5-day-old etiolated seedlings before (0 d Wc) and after exposure to 100 µmol m^{-2} s^{-1} constant white light for 3 days (left pane, n=8) or 20 hours (right pane, n=4). SOSG fluorescence per seedling in cotyledons of seedlings were quantified.

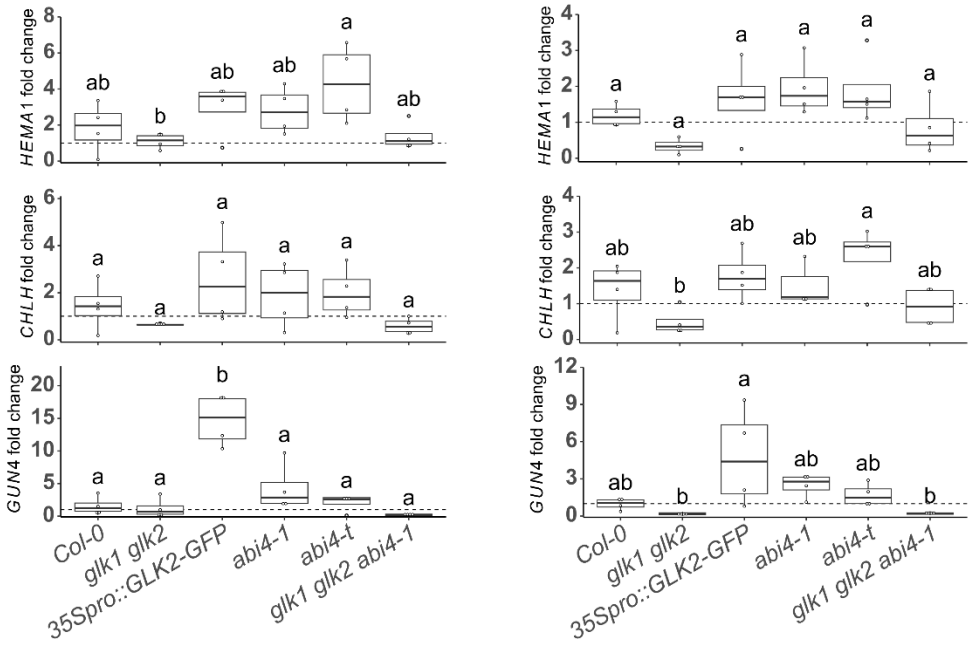

Figure S7. Transcript levels of *HEMA1*, *CHLH* and *GUN4* may explain the Pchlide overaccumulation in etiolated *abi4* mutant seedlings

Seedlings were grown on MS agar plates without sucrose for 5 days, and the transcript levels were quantified using RT-qPCR. Mean transcript level in *Col-0* was set to 1 (indicated by the dashed line).

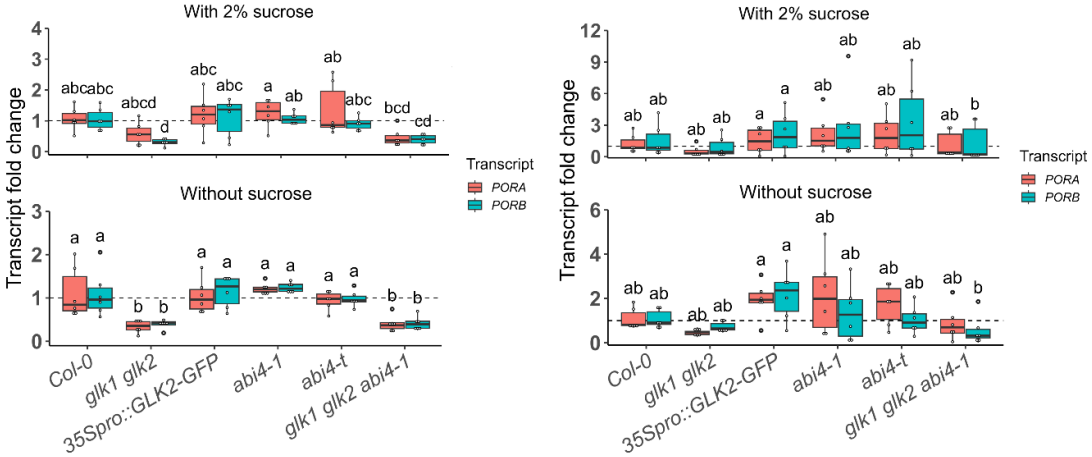

Figure S8. Transcript levels of *PORA* and *PORB* cannot explain the inefficient Pchlide photoreduction in etiolated *abi4* mutant seedlings exposed to light

Seedlings were grown on MS agar plates either with or without sucrose for 5 days, and the transcript levels were quantified using RT-qPCR. Mean transcript level in *Col-0* was set to 1 (indicated by the dashed line).

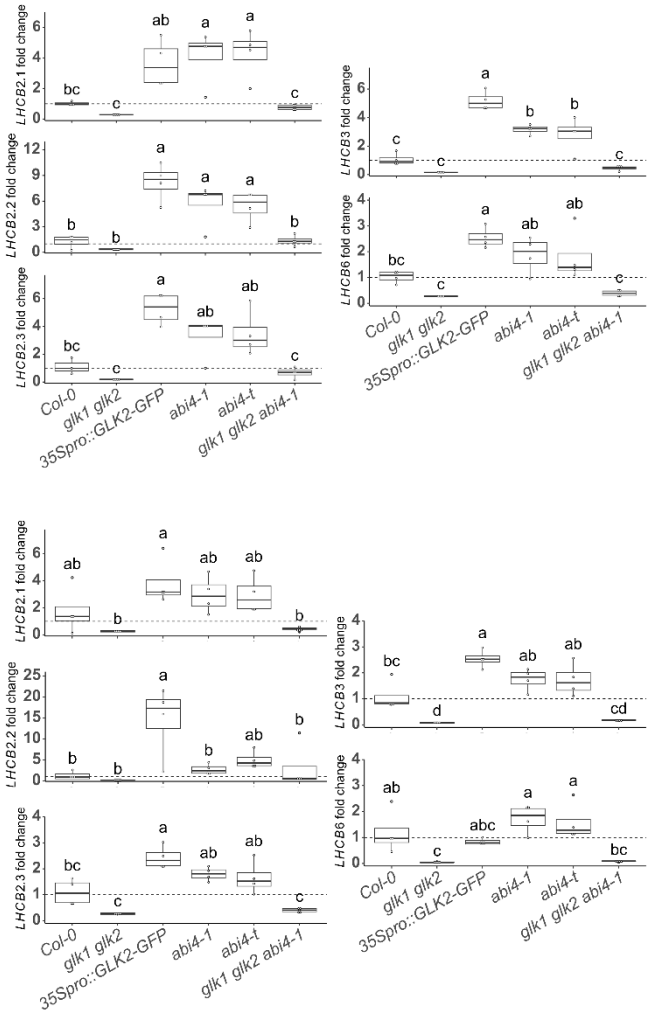

Figure S9. Transcript levels of *LHCB*s may contribute to the photobleaching in light-exposed etiolated *abi4* mutant seedlings

Seedlings were grown on MS agar plates without sucrose for 5 days, and the transcript levels were quantified using RT-qPCR. Mean transcript level in *Col-0* was set to 1 (indicated by the dashed line).

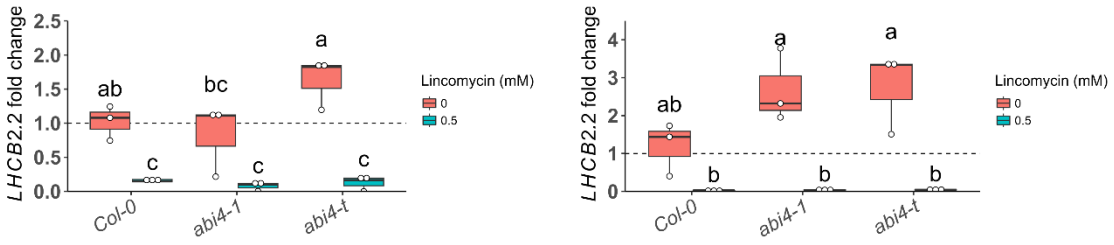

Figure S10. Transcript accumulation of *LHCB2.2* is not insensitive to the plastid inhibitor lincomycin in light-grown *abi4* mutant seedlings

Seedlings were grown on MS agar plates without sucrose under 100 µmol m^{-2} s^{-1} constant white light for 5 days, and the transcript levels were quantified using RT-qPCR. Mean transcript level in *Col-0* without lincomycin was set to 1 (indicated by the dashed line).

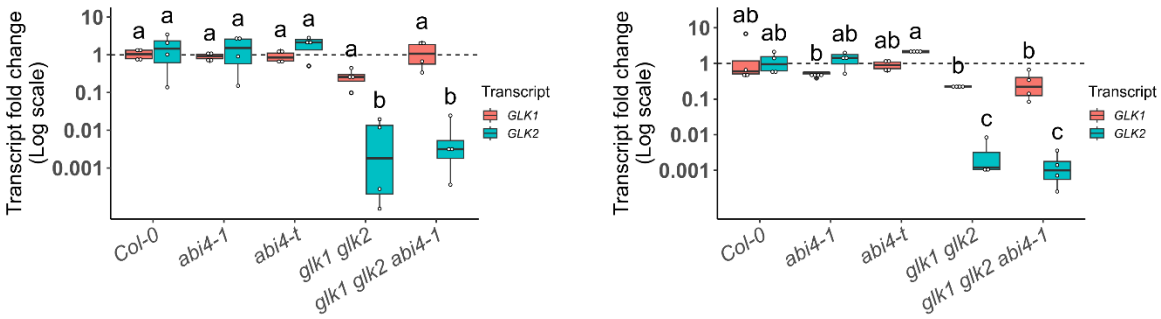

Figure S11. *GLK1* and *GLK2* transcript levels are not changed by *abi4* mutations in 5-day-old etiolated seedlings

Seedlings were grown on MS agar plates without sucrose, and the transcript levels were quantified using RT-qPCR. Mean transcript level in *Col-0* was set to 1 (indicated by the dashed line).